STUDY OF TOTAL ELECTRON CONTENT FROM GPS FREQUENCY BAND SATELLITES AT THE EQUATORIAL MAGNETIC LATITUDE STATION, CHUMPHON, THAILAND

PRASERT KENPANKHO

A THESIS SUBMITTED IN FULFILLMENT

OF THE REQUIREMENT FOR THE DEGREE OF

DOCTOR OF ENGINEERING IN ELECTRICAL ENGINEERING

FACULTY OF ENGINEERING

KING MONGKUT'S INSTITUTE OF TECHNOLOGY LADKRABANG

2014

KMITL-2014-EN-D-018-073

Thesis Title	Study of Total Electron Content from GPS Frequency Band Satellites at the Equatorial Magnetic Latitude Station, Chumphon, Thailand
Student	Mr. Prasert Kenpankho
Student ID.	51060037
Degree	Doctor of Engineering
Program	Electrical Engineering
Year	2014
Thesis Advisor	Assoc. Prof. Dr. Pornchai Supnithi

ABSTRACT

This thesis presents an analysis of the total electron content (TEC) from Global Positioning System (GPS) frequency band satellites at the equatorial magnetic latitude station, Chumphon, Thailand, where the phenomenon of the disturbed ionosphere occurs. The objectives of this thesis are to find and analyze the TEC derived from GPS satellites, GPS receiver bias for a single station, GPS delay time, the rate of TEC index, the peak electron density in the F-region, and the ionospheric slab thickness. This thesis focuses on a single station for the diurnal and seasonal variations of TEC and the period of study is during 2004-2013, corresponding to the low and high solar activities. Another important objective of this research is to reduce the complexity of GPS receiver bias estimation and the TEC computation time by proposing is two methods, the median cut and Lagrange interpolation. The benefit of this thesis is to improve the TEC estimation in the International Reference Ionosphere (IRI) model over the equatorial latitude region.

หัวข้อวิทยานิพนธ์	**การศึกษาปริมาณอิเล็กตรอนรวมในชั้นบรรยากาศไอโอโนสเฟียร์จากดาวเทียมย่านความถี่จีพีเอส บริเวณเส้นศูนย์สูตรแม่เหล็ก ณ จังหวัดชุมพร ประเทศไทย**
นักศึกษา	**นายประเสริฐ เดนพันค้อ**
รหัสประจำตัว	51060037
ปริญญา	**วิศวกรรมศาสตรดุษฎีบัณฑิต**
สาขาวิชา	**วิศวกรรมไฟฟ้า**
พ.ศ.	2557
อาจารย์ที่ปรึกษาวิทยานิพนธ์	**รศ.ดร.พรชัย ทรัพย์นิธิ**

บทคัดย่อ

วิทยานิพนธ์ฉบับนี้ นำเสนอผลการศึกษาปริมาณอิเล็กตรอนรวมที่วัดได้จากสัญญาณดาวเทียมย่านความถี่จีพีเอส บริเวณเส้นศูนย์สูตรแม่เหล็ก ณ จังหวัดชุมพร ประเทศไทย ซึ่งมีปรากฏการณ์ปริมาณอิเล็กตรอนสูง และมีการเปลี่ยนแปลงจำนวนอิเล็กตรอนตลอดเวลา วัตถุประสงค์ของวิทยานิพนธ์นี้คือการค้นหาและวิเคราะห์ปริมาณอิเล็กตรอนรวม ค่าชดเชยของเครื่องรับสัญญาณจีพีเอสสำหรับสถานีเดียว การหน่วงเวลาของสัญญาณดาวเทียมจีพีเอส อัตราการเปลี่ยนแปลงปริมาณอิเล็กตรอนรวม ค่าสูงสุดของความหนาแน่นอิเล็กตรอนในชั้นเอฟ และความหนาของชั้นบรรยากาศไอโอโนสเฟียร์ วิทยานิพนธ์ฉบับนี้นำเสนอการเปลี่ยนแปลงของปริมาณอิเล็กตรอนรวมรายวันและรายฤดูกาลในช่วงของปี ค.ศ. 2004 ถึง ปี ค.ศ. 2013 ซึ่งครอบคลุมการเปลี่ยนแปลงของแสงจากดวงอาทิตย์ทั้งที่มีปริมาณมากและน้อย นอกจากนี้ วิทยานิพนธ์ฉบับนี้ยังมีวัตถุประสงค์ที่จะลดความซับซ้อนในการประมาณค่าชดเชยเครื่องรับสัญญาณดาวเทียมจีพีเอส และลดเวลาของการคำนวณค่าปริมาณอิเล็กตรอนรวมโดยการนำเสนอวิธีการสองวิธีคือ วิธีการใช้ค่ามัธยฐาน (Median cut) และ การประมาณค่าแบบ Lagrange ประโยชน์ที่ได้รับโดยตรงจากวิทยานิพนธ์ฉบับนี้คือการปรับปรุงการทำนายค่าปริมาณอิเล็กตรอนรวมในแบบจำลองการอ้างอิงชั้นบรรยากาศไอโอโนสเฟียร์นานาชาติ บริเวณเส้นศูนย์สูตรแม่เหล็กอีกด้วย

ACKNOWLEDGEMENT

I wish to thank my family and the following people for their assistance and support during my study. My academic supervisor Associate Professor Dr. Pornchai Supnithi at the Telecommunication Engineering Department, King Mongkut's Institute of Technology Ladkrabang (KMITL), for his technical guidance, encouragement and support over the years. My group researchers Dr. Takashi Maruyama and Dr. Takuya Tsugawa, Space Weather and Environment Informatics Laboratory, National Institute of Information and Technology (NICT) for providing me with an opportunity to pursue my research objectives. In addition, I would like to sincerely thank all Laboratory members at the Communications, Signal processing and Storage Research Group (CSSRG), KMITL, for their friendships, activities and socializations during the period of my study.

LIST OF CONTENTS

Page

LIST OF TABLES

Table Page

LIST OF FIGURES

Figure Page

CHAPTER 1

INTRODUCTION

1.1 Background

Global Positioning System (GPS) satellites have been used for the position determination on the Earth. The positional accuracy of GPS is limited due to several error sources. The major error source is the ionosphere. The ionosphere is a dispersive medium of charged particles between the GPS satellites and the user on Earth. These dispersive ionized media play an important role in the various applications of GPS because the ionosphere directly influences the radio waves propagating from the satellite to the receiver as shown in Figure 1.1. The ionosphere is utilized as a transmitter of radio frequency communication signals. The radio wave communication is significantly influenced by the ionospheric properties such as the total electron content (TEC), the peak electron density in the F2-region (*Nm*F2), and the slab thickness. GPS signals are useful for the analysis of TEC. Although the International Reference Ionosphere (IRI) model can predict the TEC values at all regions of Earth, it has been known that TEC prediction errors of the IRI model in the equatorial and low-latitude regions exist. The analysis (Ma and Maruyama, 2003) of TEC in this region is the focus of this thesis.

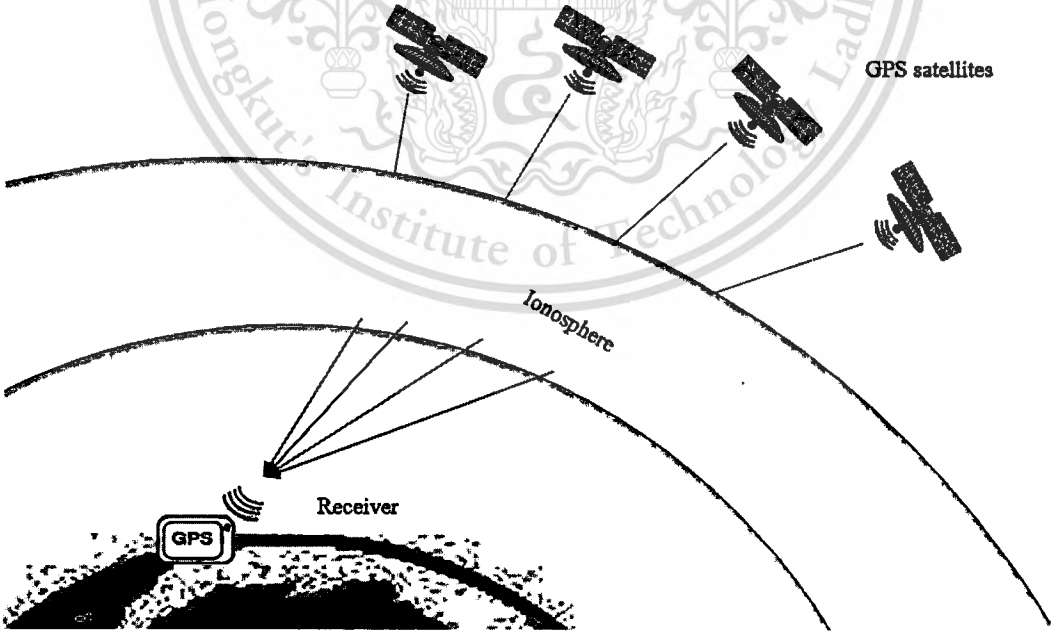

Figure 1.1 The GPS system through the ionosphere.

The selected ionospheric location for this thesis is the Chumphon station. The reason why we use Chumphon station is because the station is near the equatorial ionization anomaly (EIA) region. EIA is a phenomenon of the anomalous ionosphere at equatorial magnetic and low latitudes. In addition, Chumphon station is a part of the South East Asia Low Latitude Ionosphere Observation Network (SEALION). SEALION network stations observe and monitor the ionospheric variation in the Asia Pacific region near the magnetic equator.

1.2 Objectives of research

In this thesis, the GPS signals are as a special tool for studying the ionosphere. The objectives of this research are to analyze the TEC from GPS satellites, the comparison of TEC, the rate of TEC index, the GPS delay time, the peak electron density in the F-region, and the ionospheric slab thickness at the equatorial magnetic latitude station, Chumphon, Thailand.

1.3 Scope of study

This study focuses on a single station for the diurnal and seasonal variations of TEC, the variation of rate of TEC index, the variation of GPS delay time, the variation of the peak electron density in F-region, and the variation of the ionospheric slab thickness at the equatorial magnetic latitude station, Chumphon, Thailand. The study of TEC from the GPS is complexity and needed many periods of times. We focus on the daily, monthly, seasonal, and yearly variation of TEC. Due to the TEC characteristics and the solar cycle with decreasing and increasing phases to the Earth, the periods during 2004-2013 is chosen for the ionospheric study.

1.4 Benefits of research

The benefits of this research are to improve the TEC estimation in the International Reference Ionosphere (IRI) model over the equatorial latitude region and to understand the TEC characteristics at the equatorial latitude region over Chumphon, Thailand.

1.5 Contributions of research

The complexity part of the TEC computation is the calculation of GPS receiver bias. In this thesis, the contributions of this research are two methods of GPS receiver bias estimations. Those two methods are the median cut and Lagrange interpolation which are used for TEC computation on the study of TEC from GPS at the equatorial magnetic latitude region. The median cut is for reducing the complexity of GPS receiver estimation of TEC computation. Lagrange interpolation is for saving the times in finding the GPS receiver bias and TEC. In addition, new ionospheric data analysis in comparison with the IRI model is shown.

1.6 Literature reviews

The ionospheric studies are found in the literature that report comparisons of TEC obtained by different techniques at different locations and comparisons of TEC measurements with predictions of models such as the IRI models (Bilitza et al., 1998; Belehaki et al., 2003, 2004; Gulyaeva et al., 2002; Huang and Reinisch, 2001; Jakowski et al., 1998; Jodogne et al., 2004; Mosert et al., 2004; Oru's et al., 2003; Sethi et al.,2001).

For the equatorial latitude region, the availability of TEC measurement data is required for the development of ionospheric models such as the International Reference Ionosphere (IRI) (Bilitza, 2001; Bilitza and Rinisch, 2008). Adohi et al. (2008) investigated the equatorial night-time behavior for the F-layer from ionogram at Korhogo, Ivory Coast in 1995, declining solar flux period, according to the magnetic activity. Bremer (2008) studied the trend of the critical frequency of the E and F layers and found that the values are slightly dependent on the longitudes with an indication of the variation at the mid latitude regions. Forbes et al. (2000) investigated the variability of the ionosphere and observed that the TEC increased as the magnetic activity increases from lower to higher latitudes. Rabiu et al. (2007) examined the variability of the equatorial ionosphere inferred from the geomagnetic field measurement and made the statement that the daytime magnitude of the solar daily variation in the magnetic field is greater than the nighttime magnitudes for all months.

Measurements of the ionospheric TEC are useful for determining the delay of a radio signal transmitted from a GPS satellite to a ground receiver (Davies, 1980; Goodwin et al., 1995). In this study, TEC monitoring improved by GPS satellites has been used to investigate the variation in the ionospheric slab thickness according to diurnal, seasonal, and solar activity variations in the

equatorial ionization anomaly (EIA) region. The ionospheric slab thickness is defined as the ratio of TEC to the maximum electron density of the F-region (*Nm*F2), proportional to the square of the F2-layer critical frequency (*fo*F2). Ionospheric slab thickness may also be regarded as the depth of an imaginary ionosphere that has the same TEC as the actual ionosphere and a uniform electron density is equal to the maximum electron density of the actual ionosphere (Chuo, 2007).

The GPS receiver biases are estimated by various researchers. For a single station, a GPS receiver bias is estimated by two methods that can be found in the literature. The first group of studies estimates GPS receiver bias by using a polynomial of coordinates in Earth-Sun reference system. The polynomial coefficients and biases being the unknowns, the observations form a linear system of equations that is solved by the least squares method (Lanyi and Roth, 1988; Coco et al., 1991; Jakowski et al., 1996; Warnant, 1997; Lin, 2001; Kee and Yun, 2002; Otsuka et al., 2002; Chen et al., 2004). In the second group of studies, the trial receiver biases are used in TEC computation then the receiver bias that minimizes the standard deviation is chosen as the receiver bias value for that GPS station (Ma and Maruyama, 2003; Zhang et al., 2003). However, both of the two methods have to be used off-line.

CHAPTER 2

IONOSHPERE

In this chapter, the structure of ionosphere, the ionospheric measurement, the ionospheric parameters, the ionospheric models and the variation of ionospheric are explained. In addition, the information on Chumphon ionospheric station and the importance of this station are described.

The ionosphere is a part of the upper atmosphere comprising portions of the mesosphere, thermosphere and exosphere. It is ionized by solar radiation and plays an important part in atmospheric electricity. It has practical importance because, among other functions, it influences radio propagation to distant places on the Earth. In Figure 2.1, the structure of the neutral atmosphere consists of troposphere, stratosphere, mesosphere, thermosphere, and exosphere. For the structure of the ionized atmosphere, there are troposphere, stratosphere, and ionosphere.

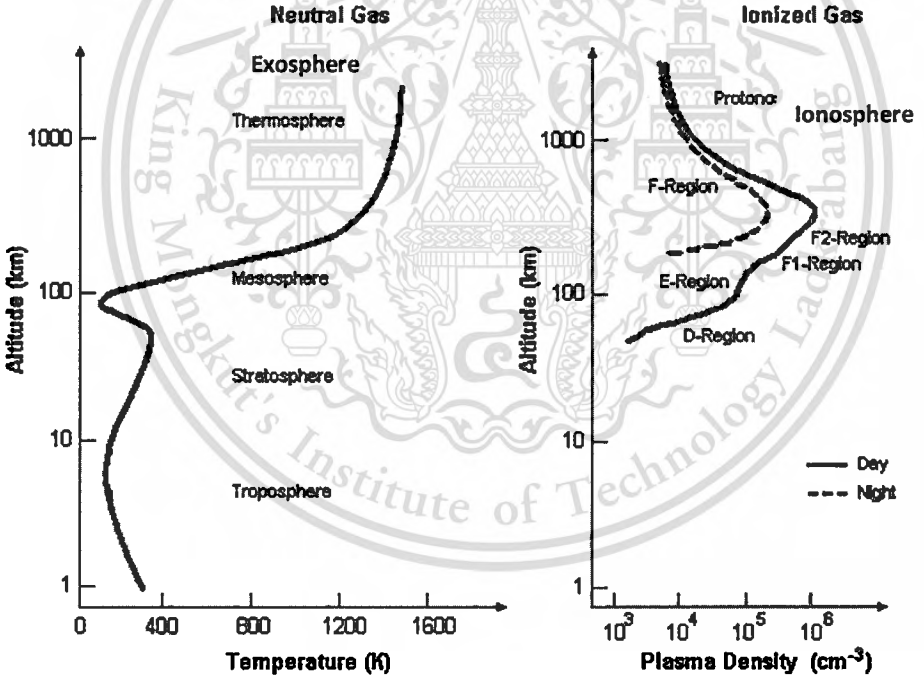

Figure 2.1 The structure of neutral and ionized atmosphere layers. Adapted from the formation of the earth's ionospheric regions, in *The Earth's Ionosphere*, retrieved January 10, 2014, from http://utd500.utdallas.edu/ionosphere.htm.

2.1 Structure of the ionosphere

The ionosphere is a region of the upper atmosphere in which the density of free electrons is large enough to have an effect on the propagation of radio waves (Davies, 1980). The ionosphere is 60-1500 kilometers (km) above the Earth's surface and forms the transition region between the neutral atmosphere and the fully ionized magnetospheric plasma. The ionosphere is constituted of free electrons and ions which are produced during interaction of extreme ultra violet (EUV) and X-ray radiation with upper atmosphere neutral gas during ionization, a process involving the stripping of electrons from neutral atoms in the atmosphere to form positively charged ions and negatively charged electrons. The total number of free ions and electrons in the ionosphere is determined by the rate at which specific species of ions recombine with electrons to form neutral atoms, a process called recombination.

In the ionosphere, there are two types of recombinations which are radiative recombination and dissociative recombination. For radiative combination, the electrons combine directly with ions, converting them into neutral atoms and emitting a photon to conserve energy and momentum. The dissociative recombination is a two-step process. In the first step, positive ions interact with neutral molecules, replacing one of the atoms in the molecule and forming a neutral atom and a positively charged molecular ion. In the second stage, electrons combine with the newly formed molecular ion, forming two neutral atoms. The dissociative recombination rate is faster than the radiative recombination, resulting in much shorter lifetime for molecular ions than for atomic ions (Bremer, 2008). Due to molecular ions' short lifespan, when their productions are rapidly reduced at night, rapid recombination quickly reduces the plasma concentration. Daytime ionization involving UV radiation is called the photoionization. Because different gas atoms and molecules are more abundant in some regions of the neutral atmosphere than others, ionization and recombination of the different species result in differing electron densities concentrated at different regions of the ionosphere (Forbes et al., 2000).

Figure 2.2 shows the ionosphere layers where the electrons and ions of thermal energy are present, as a result of ionization of the neutral atmospheric constituents by electromagnetic and corpuscular radiation. At daytime, there are four layers in the ionosphere including D-layer, E-layer, and F1 and F2-layers. At nighttime, the ionosphere merges the four layers into three layers by replacing the F1 and F2-layers with the F-layer located higher in altitude.

The lower boundary of the ionosphere coincides with the region where the most penetrating radiations produce free electron and ion pairs in numbers sufficient to affect the

propagation of radio waves in the D-region. The upper boundary of the ionosphere is next to the earth upper atmosphere with the condition of the solar wind. At the nighttime, the ionosphere can extend to greater distances, representing the solar wind shadow.

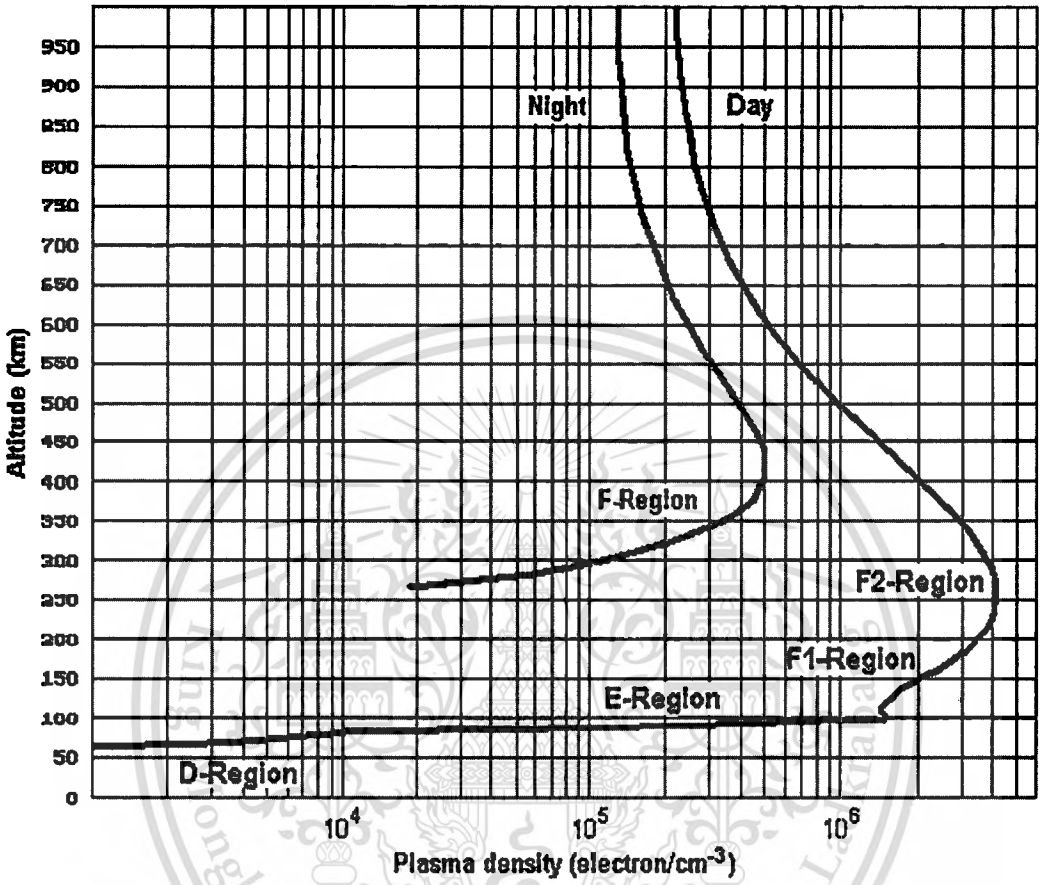

Figure 2.2 The ionosphere layers in daytime and nighttime. Reprinted from Astrosurf, in *HF Propagation tutorial*, retrieved January 10, 2014, from http://www.astrosurf.com/luxorion/Radio/.

2.1.1 D-layer

The D-layer is 60 km to 90 km above the surface of the Earth. Ionization here is due to hydrogen radiation at a wavelength of 121.5 nanometers (nm) ionizing nitric oxide (NO). In addition, the high solar activity hard X-rays (wavelength < 1nm) may ionize (N_2, O_2). During the night, cosmic rays produce a residual amount of ionization. Recombination is high in the D-layer, the net ionization effect is low, but loss of wave energy is great due to frequent collisions of the electrons. As a result, high-frequency (HF) radio waves are not reflected by the D-layer but suffer

a loss of energy. This is the main reason for absorption of HF radio waves, particularly at 10 MHz and below, with progressively smaller absorption as the frequency gets higher. The absorption is small at night but large about midday. The layer reduces greatly after sunset; a small part remains due to galactic cosmic rays. A common example of the D-layer in action is the disappearance of distant AM broadcast band stations in the daytime (Aggson et al., 1995).

During solar proton events, ionization can reach unusually high levels in the D-region over high and polar latitudes. Such very rare events are known as Polar Cap Absorption (or PCA) events, because the increased ionization significantly enhances the absorption of radio signals passing through the region. In fact, absorption levels can increase by many tens of dB during intense events, which is enough to absorb most transpolar HF radio signal transmissions. Such events typically last less than 24 to 48 hours.

2.1.2 E-layer

The E layer is the middle layer, 90 km to 120 km above the surface of the Earth. Ionization is due to soft X-ray (1-10 nm) and far ultraviolet (UV) solar radiation ionization of molecularoxygen (O_2). Normally, at oblique incidence, this layer can only reflect radio waves having frequencies lower than about 10 MHz and may contribute a bit to absorption on frequencies above. However, during intense Sporadic E events, the E_s -layer can reflect frequencies up to 50 MHz and higher. The vertical structure of the E-layer is primarily determined by the competing effects of ionization and recombination. At nighttime, the E-layer rapidly disappears because the primary source of ionization is no longer present. After sunset, an increase in the height of the E layer maximum increases the range to which radio waves can travel by reflection from the layer.

The E_s -layer (sporadic E-layer) is characterized by small, thin clouds of intense ionization, which can support reflection of radio waves, rarely up to 225 MHz. Sporadic-E events may last for just a few minutes to several hours. Sporadic E propagation makes radio amateurs very excited, as propagation paths that are generally unreachable can open up. There are multiple causes of sporadic-E that are still being pursued by researchers. This propagation occurs most frequently during the summer months when high signal levels may be reached. The skip distances are generally around 1,000 km. Distances for one hop propagation can be close to 900 km or up to 2,500 km. Double-hop reception over 3,500 km is possible (Gulyaeva et al., 2002).

2.1.3 F1-layer

The F1-layer is 120 km to 200 km above the Earth's surface. It disappears at nighttime when it combines with the F2-layer to form the nighttime F-layer. Ionization of atomic oxygen (O) by He emission or by Lyman continuum lines, probably accompanied by N2 ionization which disappears after sunset. Most of the ionization is in the molecular form and disappears by the dissociative recombination.

2.1.4 F2-layer

The F2-layer begins at 200 km and peaks at about 300 km, in daytime. The F2 layer's height and electron density are highly variable and large daily, seasonal and sunspot-cycle variations are combined with general erratic behavior. Ionization is due to extreme ultraviolet radiation (EUV) (10-100 nm) solar radiation of atomic oxygen (O). The ionosphere's highest electron density values are present in the F2-layer.

2.2 Ionospheric measurement

In the ionospheric measurements, an ionosonde is a special radar for the examination of the ionosphere. Figure 2.3 shows the block diagram of the ionosonde system that is installed at Chumphon station. The ionosonde system consists of:

(1) Two antennas, one for a high frequency (HF) transmitter which can automatically tunable over a wide range 2–30 MHz and another for a tracking HF receiver which can automatically track the frequency of the transmitter.

(2) Low pass filter and power amplifier circuits with a suitable radiation pattern which transmits well vertically upwards and is efficient over the whole frequency range used.

(3) A GPS antenna which is used for synchronous signal.

(4) A personal computer set for data recording

(5) Connecting components such as coaxial cable, RS232, and 25-pin cable.

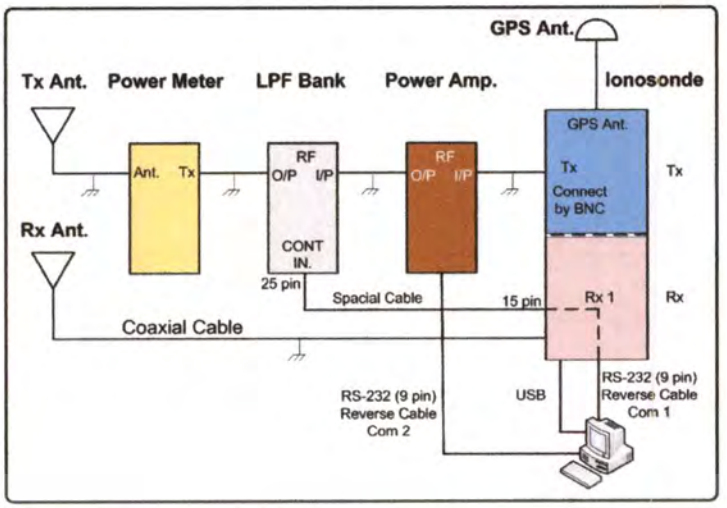

Figure 2.3 The ionosonde block diagram used at the Chumphon station. Reprinted from "The variation of critical frequency of E layer over the magnetic equatorial region, Chumphon, Thailand." by Wongcharoen et al., 2013, *IRI2013 Workshop,* Poland.

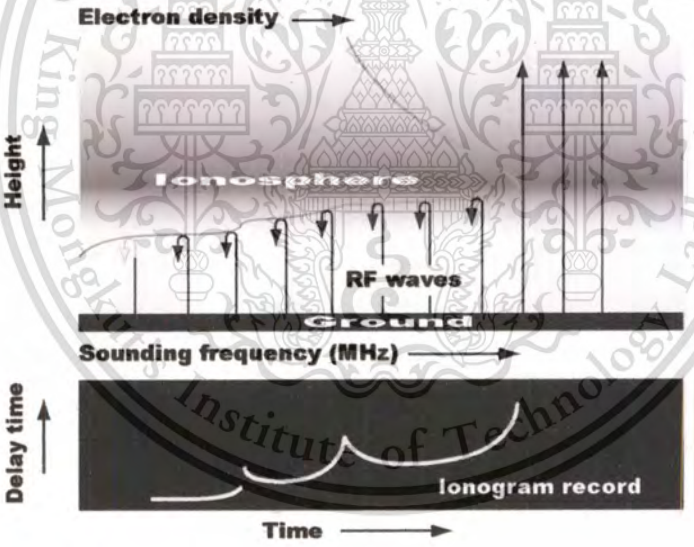

Figure 2.4 Ionospheric observation technique (ionosonde). Reprinted from "Ionosphere study" by Takashi Maruyama, 2010, *Science of Space Environment course*, KMITL, Thailand.

In Figure 2.4, the transmitter sweeps all or parts of the HF frequency range, transmitting short pulses. These pulses are reflected at various layers of the ionosphere, at heights of 80–500 km, and their echos are received by the receiver and analyzed by the control system. The result is

displayed in the form of an ionogram, a graph of reflection height (actually time between transmission and reception of pulse) versus carrier frequency.

Figure 2.5 shows an ionogram which records the ionospheric parameters as follow.

1) Minimum frequency for E-layer or F-layer echoes (fmin)
2) E-layer exceeding critical frequency (fxE)
3) E-layer critical frequency (foE)
4) E-layer virtual height (h'E)
5) Sporadic E-layer critical frequency (foEs)
6) Sporadic E -layer exceeding critical frequency (fxEs)
7) Sporadic E -layer virtual height (h'Es)
8) F1-layer critical frequency (foF1)
9) F1-layer exceeding critical frequency (fxF1)
10) F1-layer virtual height (h'F1)
11) F2-layer critical frequency (foF2)
12) F2-layer exceeding critical frequency (fxF2)
13) F2-layer virtual height (h'F2)

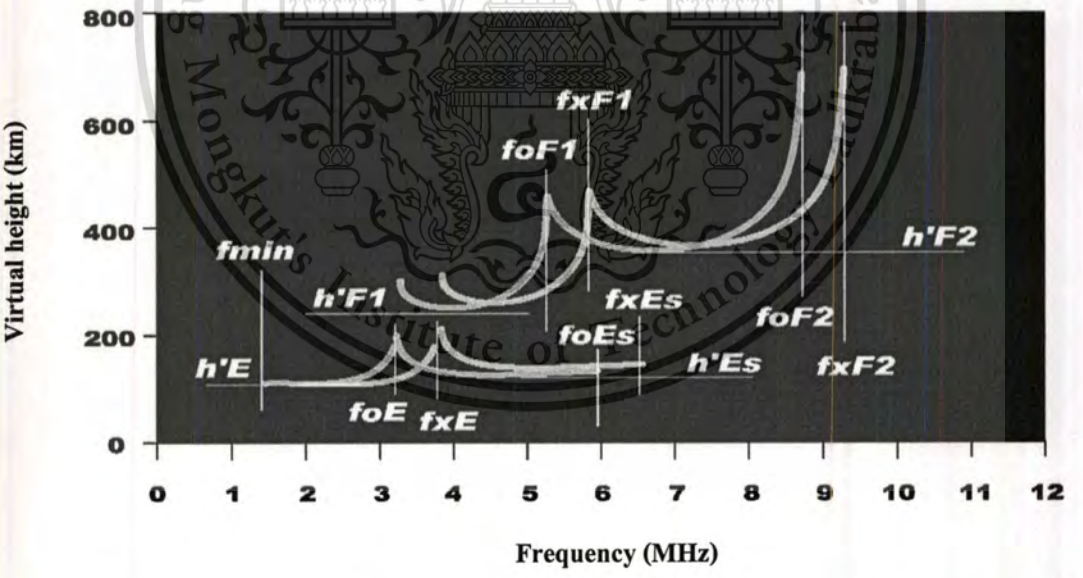

Figure 2.5 The ionospheric parameters on the ionogram. Reprinted from "Ionosphere study" by Takashi Maruyama, 2010, *Science of Space Environment course,* KMITL, Thailand.

2.3 Parameters relevant to the ionosphere

The definitions of ionospheric parameters and concepts relevant to this study are presented as follow.

2.3.1 Total electron content (TEC)

The TEC is the total electron content along a signal ray path between satellite and receiver which is assumed to include all the electrons in a column with a cross section of 1 m^2 and extends from receiver to the satellite. TEC is measured in TEC units with 1 TECU = 10^{16} electrons.m^{-2}.

Using the approximation for refractive index, the amount of group delay (Δt) imposed on a radio signal of frequency (f) is given by

$$\Delta t = \frac{e^2}{8\pi^2 m \varepsilon_0 c f^2} \int_s n ds \tag{2.1}$$

where e is the elementary charge (1.6022×10^{-19} C), m is the static electron mass (1.6605×10^{-31} kg), ε_0 is the permittivity of free space (8.8542×10^{-12} F/m), c is the light speed in vacuum (2.9979×10^{8} m/s), n is the electron density, as

$$\Delta t = \frac{A}{cf^2} TEC \tag{2.2}$$

where $A = \frac{e^2}{8\pi^2 m \varepsilon_0}$ and $TEC = \int_s n ds$.

2.3.2 F2-layer critical frequency (*fo*F2)

The parameter *fo*F2 is measured from the frequency modulated continuous wave (FMCW) ionosonde through the ionograms recorded at a cadence of 15 minutes.

The ionogram in Figure 2.6 was recorded in 2006 at Chumphon station. The recorded date was on 03 September 2006 at 07:45 local time. The ionogram indicated the line positions of the F2-layer critical frequency (*fo*F2), F2-layer exceeding critical frequency (*fx*F2), and the F-layer virtual height. The x-axis is frequency in Hz, while the y-axis is the height in km. According to the ionogram, foF2 is about 6 MHz, fxF2 is about 7 MHz, and h'F is about 200 km.

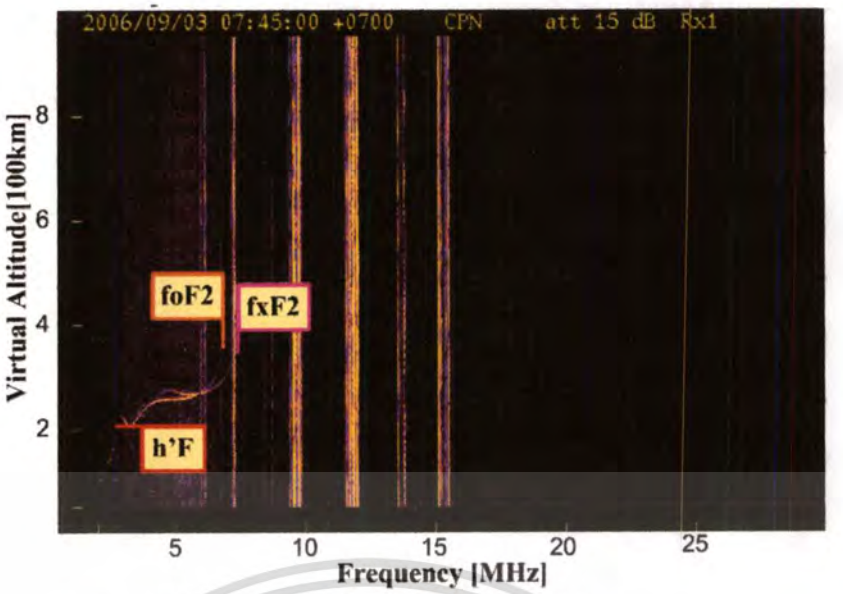

Figure 2.6 The example of an ionogram recorded at Chumphon station.

2.3.3 The peak electron density in the F2-region (*Nm*F2)

The parameter *Nm*F2 is the peak electron density in the F2-region (electron/m^3), computed using the expression (Goodwin et al., 1995).

$$NmF2 = 1.24 \times 10^{10} \left(foF2 \right)^2, \tag{2.3}$$

where *fo*F2 is in MHz, and *Nm*F2 is in m^{-3}.

2.3.4 Ionospheric slab thickness

Ionospheric slab thickness or slab thickness (τ) is defined as the ratio of TEC to the maximum electron density of the F-region (*Nm*F2), proportional to the square of the F2-layer critical frequency (*fo*F2) (Kenpankho et al., 2011). Ionospheric slab thickness may also be regarded as the depth of an imaginary ionosphere that has the same TEC as the actual ionosphere and a uniform electron density that is equal to the maximum electron density of the actual ionosphere (Chuo, 2007). The parameter TEC and *Nm*F2 can be used to compute the variation of slab thickness in kilometers (Goodwin et al., 1995). The slab thickness can be calculated from

$$\tau = \frac{TEC}{NmF2}, \tag{2.4}$$

where *TEC* is in TECU (10^{16} electrons/m^2) and *NmF2* is in 1/m^3.

2.4 Ionospheric Models

2.4.1 Chapman function

Chapman function is generally used to describe seasonal, local time, and latitudinal variations of electron density and are given by (Rishbeth and Garriott, 1969)

$$N(z) = \frac{N_e(z)}{NmF2}, \tag{2.5}$$

where $N_e(z)$, the electron density which applies at a solar zenith angle of χ is

$$N(z, \chi) = e^{\frac{1}{2}\left[1 - z - e^{-z \sec \chi}\right]} \tag{2.6}$$

and $NmF2$ is the peak electron density in the F2-region and z is the normalized height given by

$$z = \frac{h'}{H}, \tag{2.7}$$

where h' is the distance above the F2 peak and H is the scale height

$$H = \frac{kT}{mg}, \tag{2.8}$$

where k is the Boltzmann's constant, T is Kelvin temperature, m is the molecular mass of gas, and g is the gravitational acceleration.

2.4.2 Thin shell model

To make the geographic mapping of TEC measurements, the thin shell model is used as a spherical ionosphere located at some shell height (H). A simple elevation mapping function is applied to convert the slant TEC measurement to vertical TEC values. The vertical TEC measurement is then assigned to the geographic location at the Ionospheric Pierce Point (IPP). Different models use different shell heights which approximately correspond to the F2 peak density height ($hmF2$), about 450 km above the Earth.

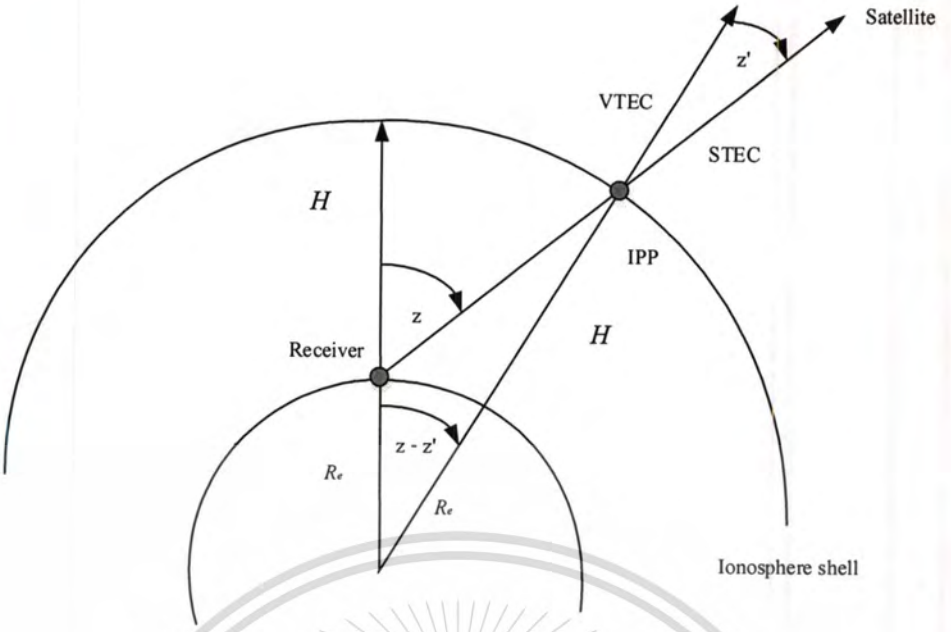

Figure 2.7 Geometry of slant to vertical TEC (VTEC) mapping function

Assuming the ionospheric shell height, H, corresponds to typical F2 peak density height. VTEC is mapped at the geographic location of the IPP, distinct from the receiver location as shown in Figure 2.7. The elevation mapping function to convert slant to vertical TEC measurements is given by

$$STEC = \frac{VTEC}{\cos z'}, \tag{2.9}$$

and

$$\sin z' = \frac{R_e}{R_e + H} \sin z, \tag{2.10}$$

where z is the satellite zenith angle and R_e is the Earth equatorial radius (6378.134 km).

2.5 Ionospheric variation

The ionosphere is the upper atmosphere which is as the main ionization energy source. The ionosphere naturally varies with time of day, season and geographic position. The following significant variations are shortly described.

2.5.1 Diurnal variation

The day-night variation is dependent on the Earth's rotation. Nighttime electron densities are much lower than daytime values, because of higher recombination rates in the absence of a radiation source. Daytime electron densities typically reach their peak at two hours past local noon due to the Earth's atmosphere lagging two hours behind the solid Earth's rotation.

2.5.2 Seasonal variation

At different times of year, the Sun is vertically above different geographic locations. At equinox noon (March 21, Sep 23), the Sun is vertically above observers at the equator and vertically above observers at the Tropics of Capricon and Cancer on solstice dates (21 December, 21 June). As vertical illumination from the Sun results in higher ionization rates, higher electron density concentrations are observed at these locations than at other locations.

The ionosphere variable investigation is conducted in order to understand the variations and effects of seasons on local times. The data and analysis method are classified into 3 seasons including equinox (March, April, September, and October), summer (May, June, July, and August), and winter (January, February, November, and December) (Kenpankho et al., 2011).

2.5.3 Latitudinal variation

Similar to diurnal and seasonal variation, the Sun's position relative to the atmosphere plays a significant role in latitudinal variation of ionospheric densities. The solar zenith angle which is the angle measured from an observer's local position vertical to the Sun, determines the intensity of ionization where locations with small zenith angles are exposed to higher radiation rates.

The latitudinal variation is divided in to 4 latitudes including equatorial latitude, low-latitude, mid-latitude, and high latitude. The equatorial latitude is about 0 degree. The low latitude is 0 degrees to 30 degrees. The mid-latitude is 30 degrees to 60 degrees. The high-latitude is 60 degrees to 90 degrees (Kenpankho et al., 2011).

2.5.4 Solar activity variation

Solar activity variation is the change in the amount of radiation emitted by the Sun and in its spectral distribution over thousand years. These variations have periodic components, the main one being approximately 11-year solar cycle (or sunspot cycle). The changes also have a periodic fluctuation. In recent decades, solar activity has been measured by satellites, while before that it was estimated using proxy variables. Scientists studying climate change are interested in understanding the effects of variations in the total and spectral solar irradiance on Earth and its climate.

2.6 Chumphon station

Chumphon station is located at longitude 99.30°E, latitude 10.70°N, and magnetic latitude 3.00°N. The station is established at King Mongkut's Institute of Technology Ladkrabang, Chumphon campus, Chumphon, Thailand. The facilities of Chumphon station consist of the ionosonde system, GPS receiver measurement, and network equipment. Figure 2.8 (a) shows the geography of Chumphon station and the ionosonde antenna is shown in Figure 2.8 (b).

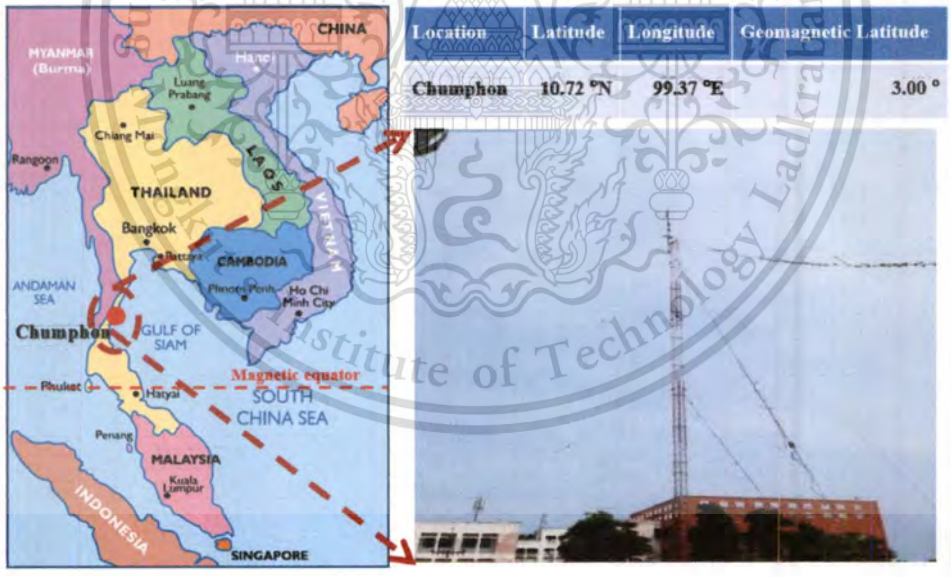

(a) (b)

Figure 2.8 Chumphon station. Reprinted from "The variation of critical frequency of E layer over the magnetic equatorial region, Chumphon, Thailand." by Wongcharoen et al., 2013, *IRI2013 Workshop,* Poland.

Chumphon station is a part of the South East Asia Low Latitude Ionosphere Observation Network (SEALION) which is a joint project among the following institutions and countries: National Institute of Information and Communications Technology (NICT), Japan, King Mongkut's Institute of Technology Ladkrabang (KMITL), Thailand, Chiang Mai University (CMU), Thailand, National Institute of Aeronautics and Space (LAPAN), Indonesia, Hanoi Institute of Geophysics (HIG), Vietnamese Academy of Science and Technology, Vietnam, Center for Space Science and Applied Research (CSSAR), Chinese Academy of Sciences, China, and Kyoto University, Japan. These stations observe and monitor the ionospheric variation in the Asia Pacific region near the magnetic equator.

Chumphon station is near the equatorial ionization anomaly (EIA) which is a phenomenon of the F region in ionosphere at low latitudes. It is characterized by an electron density trough at the magnetic equator, and a dual band of enhanced electron density at about 15 degrees north and south of the trough. The EIA was discovered by Appleton (1954) and it has repeatedly been reviewed in the literature (Stenning, 1992; Walker et al., 1994).

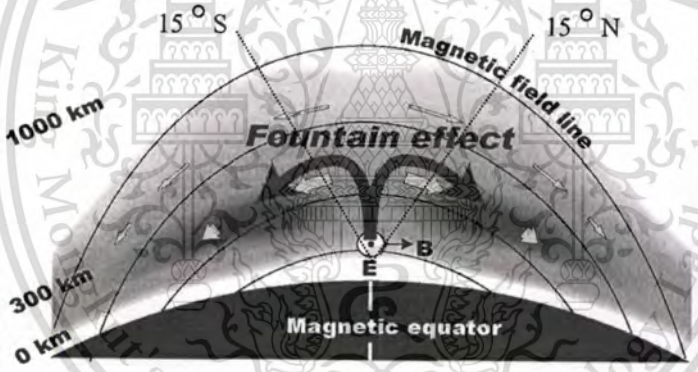

Figure 2.9 EIA phenomenon called as "Fountain effect" at magnetic equator. Reprinted from "Ionosphere study" by Takashi Maruyama, 2010, *Science of Space Environment course,* KMITL, Thailand.

The formation of the EIA is the result of the diurnal variation of the zonal electric field, which primarily points eastward during the day. With the horizontal geomagnetic field at equatorial latitudes, the plasma is lifted up by vertical E x B drift. Once transported to higher altitudes, the plasma diffuses downward along the geomagnetic field lines into both hemispheres due to gravitational and pressure gradient forces (Millward et al., 2001; Namgaladze et al., 1991; Richmond et al., 1992; Schunk et al., 2005).

CHAPTER 3

GPS TECHNOLOGY

In Chapter 3, the knowledge of Global Positioning System (GPS) is given including the GPS principle, the GPS receivers and data format, and the GPS group delay and phase advance.

3.1 GPS principle

The GPS is a space-based satellite navigation system that provides location and time information in all weather, anywhere on the Earth, where there is an unobstructed line of sight to four or more GPS satellites. The GPS project was developed in 1973. It is maintained by the United States government and is freely accessible to anyone with a GPS receiver. The GPS system provides critical capabilities to military, civil and commercial users around the world. Moreover, GPS is the backbone for modernizing the global air traffic system.

For the understanding of GPS technology, this thesis divides the information into the segments of the GPS system, GPS constellation, GPS determination on user position, the transmitting frequency, and GPS code structures which are described in following sections.

3.1.1 Segments of the GPS system

The GPS system can be comprised of three segments: the control segment, the space segment, and the user segment. In Figure 3.1, the space segment contains all the GPS satellites. The user segment can be considered the base of receivers and their processing. The control segment consists of five control stations, including a master control station. These control stations are separated in longitude around the Earth. The master control station is located at Falcon Air Force Base, Colorado Springs, Colorado, The United States of America. The control operations are maintained at all times. The main purpose of the control stations is to monitor the performance of the GPS satellites. The data collected from the GPS satellites by the control stations will be sent to the master control station for processing. The master control station is responsible for all aspects of constellation control and command. The operation objectives are

(1) Monitor GPS satellites performance in support of all performance standards.

(2) Generate and upload the navigation data to the GPS satellites to sustain performance standards.

(3) Promptly detect and respond to GPS satellites failure to minimize the impact.

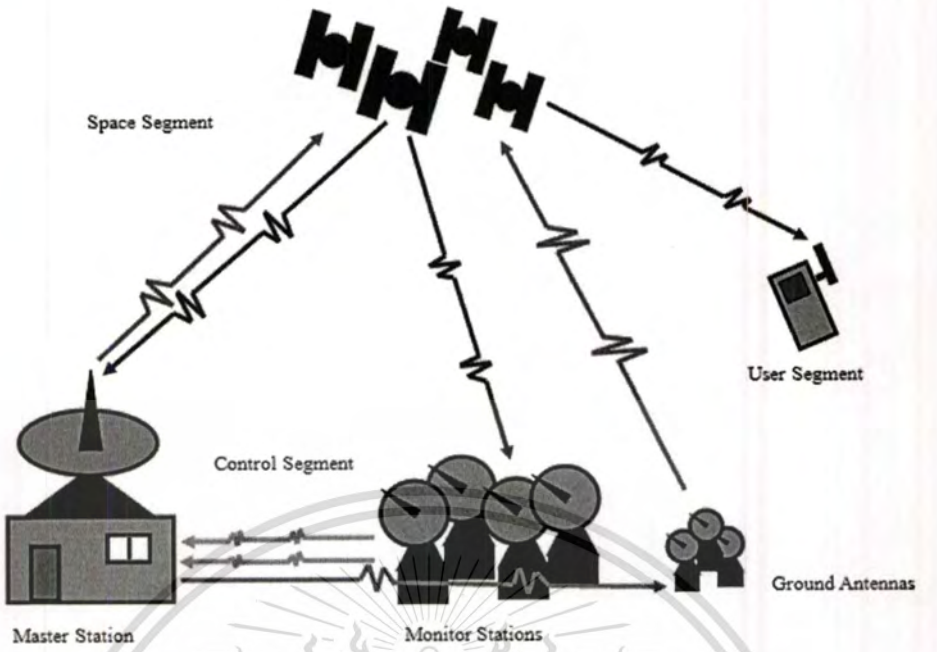

Figure 3.1 Three segments of GPS system. Reprinted from GPS, in *Indigo Information System*, retrieved January 14, 2014, from http://www.indigoinform.com/solngps.aspx.

3.1.2 GPS constellation

There is a total of 24 GPS satellites which can be divided into six orbits and each orbit has four satellites as shown in Figure 3.2. Each orbit makes a 55-degree angle with the equator, which is referred to as the inclination angle. The orbits are separated by 60 degrees to cover the complete 360 degrees. The radius of the satellite orbit is 26,560 km and it rotates around the earth twice in a sidereal day. Table 3.1 lists all these parameters.

Figure 3.2 The GPS constellation. Reprinted from What is GPS?, in *European Southern Observatory*, retrieved January 14, 2014, from http://www.eso.org/public/outreach/eduoff/.

Table 3.1 Characteristics of GPS satellites

Parameters	Values
Number of satellites	24
Number of orbital planes	6
Number of satellites per orbit	4
Orbital inclination	55 ^{o}
Orbital radius	26560 km
Period	11 hrs 57 min 57.26 sec

3.1.3 GPS determination on user position

The position of a certain point in space can be found from distances measured from this point to some known positions in space. In Figure 3.3, the user position is on the x-axis; this is a one dimensional case. If the satellite position S_1 and the distance to the satellite x_1 are both known, the user position can be at two places, either to the left or right of S_1. In order to determine the user position, the distance to another satellite with known position must be measured. In Figure 3.3, the positions of S_2 and x_2 uniquely determine the user position U.

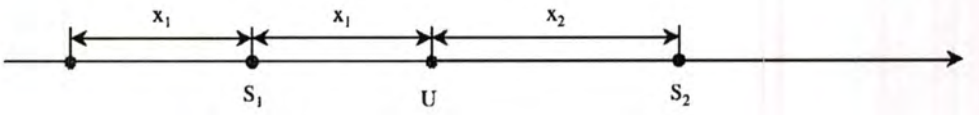

Figure 3.3 One dimensional case for user position.

Figure 3.4 shows a two-dimensional case. In order to determine the user position, three satellites and three distances are required. The trace of a point with constant distance to a fixed point is a circle in the two-dimensional case. Two satellites and two distances give two possible solutions because two circles intersect at two points. A third circle is needed to uniquely determine the user position. For similar reasons, one might decide that in a three-dimensional case four satellites and four distances are needed. The equal-distance trace to a fixed point is a sphere in a three-dimensional case. Two spheres intersect to make a circle. This circle intersects another sphere to produce two points. In order to determine which point is the user position, one more satellite is needed.

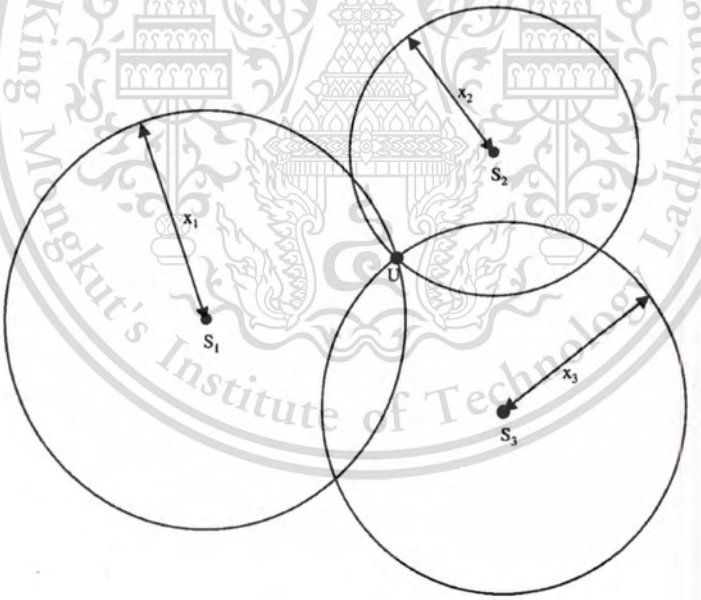

Figure 3.4 Two-dimensional user position.

In GPS, the position of the satellite is known from the ephemeris data transmitted by the satellites. The distance from the receiver to the satellite can be measured. Therefore, the position of the receiver can be determined. Since the user position is usually close to the surface of the earth, it can be uniquely determined. Therefore, the general statement is that four satellites can be used to determine a user position, even though the measured distance has a bias error.

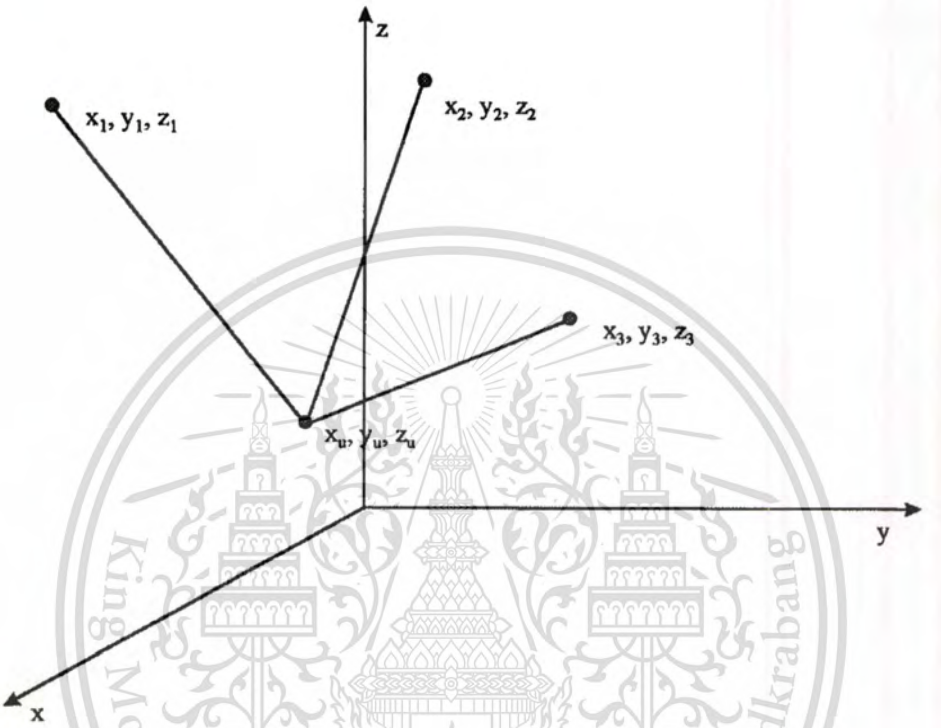

Figure 3.5 The use of three known positions to determine one unknown position.

In Figure 3.5, there are three known points at locations (x_1, y_1, z_1), (x_2, y_2, z_2), and (x_3, y_3, z_3), and an unknown point at (x_u, y_u, z_u). If the distances between the three known points to the unknown point can be measured as ρ_1, ρ_2, and ρ_3, these distances can be written as

$$\begin{aligned}\rho_1 &= \sqrt{(x_1 - x_u)^2 + (y_1 - y_u)^2 + (z_1 - z_u)^2}\,, \\ \rho_2 &= \sqrt{(x_2 - x_u)^2 + (y_2 - y_u)^2 + (z_2 - z_u)^2}\,, \\ \rho_3 &= \sqrt{(x_3 - x_u)^2 + (y_3 - y_u)^2 + (z_3 - z_u)^2}\end{aligned} \tag{3.1}$$

The GPS constellation is schematically shown in Figure 3.6 for October 13, 2012 at 12:00 UT. Each orbital plane, numbered from one to six, contains nominally four or effectively up to five satellites, identified by plane or slot and PRN numbers. The longitude and latitude lines are indicated by the dashed line. To optimize global satellite visibility, the satellites are not equally spaced within the orbital planes.

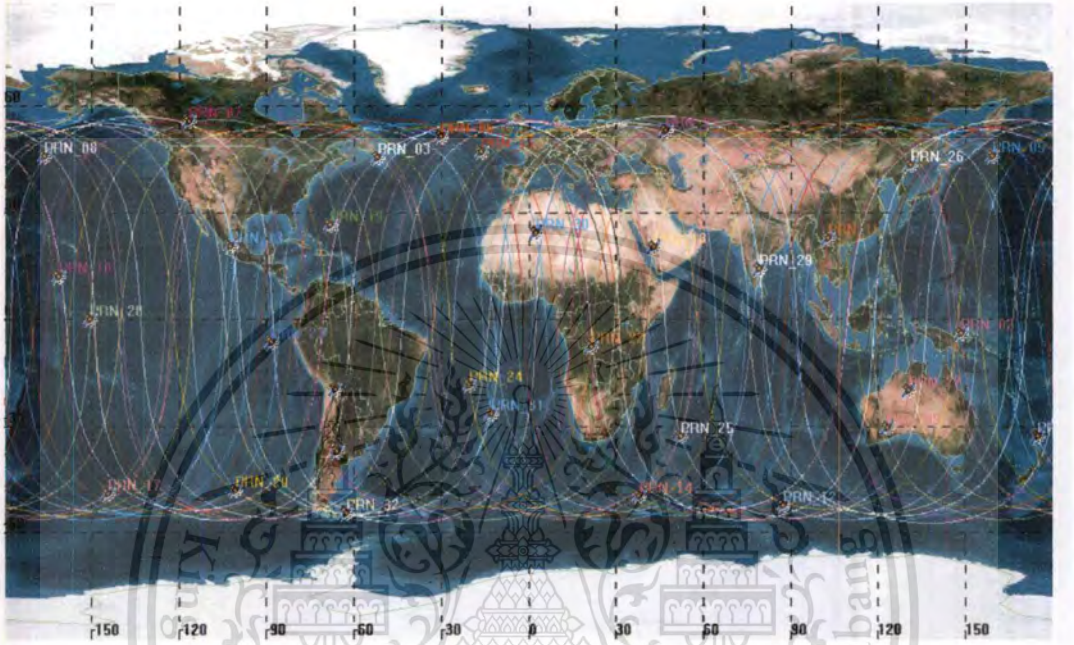

Figure 3.6 Sub satellite trajectories of all GPS satellites on October 13, 2013

3.1.4 Transmitting frequency

The GPS signal contains two frequency components: f_1 and f_2. The center frequency of f_1 is at 1575.42 MHz and f_2 is at 1227.6 MHz. These frequencies are coherent with a 10.23 MHz clock. These two frequencies can be related to the clock frequency as

$$f_1 = 1575.42 \text{ MHz} = 154 \times 10.23 \text{ MHz}$$

$$f_2 = 1227.6 \text{ MHz} = 120 \times 10.23 \text{ MHz}$$

Table 3.2 shows the GPS frequencies and code usages which the f_1 carrier is modulated by both the C/A and P(Y) codes, while the f_2 carrier is only modulated by the P(Y) code. The C/A code, for civilian use, transmits data at 1.023 million chips per second, whereas the P(Y) code, for U.S. military use, transmits at 10.23 million chips per second.

Table 3.2 GPS frequencies and code usages. Adapted from GPS and GLONASS Satellite Identification, in *GLONASS Overview*, retrieved January 15, 2014, from http://www.novatel.com/assets/Documents/Papers/GLONASSOverview.pdf.

<table>
<tr><th>Band</th><th>Frequency (MHz)</th><th>Phase</th><th>Original Usage</th><th>Modernized Usage</th></tr>
<tr><td rowspan="2">f_1</td><td rowspan="2">1575.42 (10.23×154)</td><td>In-Phase (I)</td><td colspan="2">Encrypted Precision P(Y) code</td></tr>
<tr><td>Quadrature-Phase (Q)</td><td>Coarse-acquisition (C/A) code</td><td>C/A, L1 Civilian (L1C), and Military (M) code</td></tr>
<tr><td rowspan="2">f_2</td><td rowspan="2">1227.60 (10.23×120)</td><td>In-Phase (I)</td><td colspan="2">Encrypted Precision P(Y) code</td></tr>
<tr><td>Quadrature-Phase (Q)</td><td>Unmodulated carrier</td><td>L2 Civilian (L2C) code and Military (M) code</td></tr>
</table>

3.1.5 GPS code structures

This section presents the GPS code structures including the coarse or clear /acquisition (C/A) and the precision (P(Y)) codes.

(1) P(Y) code

The P(Y) code is bi-phase signal modulated at 10.23 MHz. P(Y) code can be encrypted as a so-called P(Y) code which is only available to military equipment with a proper decryption key. The chip length is about 97.8 ns (1/10.23 MHz). The code is generated from two pseudorandom noise (PRN) codes with the same chip rate. One PRN sequence has 15,345,000 chips, which has a period of 1.5 seconds, the other one has 15,345,037 chips, and the difference is 37 chips. The two numbers, 15,345,000 and 15,345,037, are relative prime, which means there are no common factors between them. Therefore, the code length generated by these two codes is 23,017,555.5 (1.5 × 15,345,037) seconds, which is slightly longer than 38 weeks. However, the actual length of the P code is 1 week as the code is reset every week. This 38-week-long code can be divided into 37 different P(Y) codes and each satellite can use a different portion of the code.

There are a total of 32 satellite identification numbers although only 24 of them are in the orbit. Five of the P(Y) code signals are reserved for other uses such as ground transmission. In order to perform acquisition on the signal, the time of the week must be known very accurately.

(2) C/A code

The C/A code is a bi-phase modulated signal with a chip rate of 1.023 MHz. Therefore, the null-to-null bandwidth of the main lobe of the spectrum is 2.046 MHz. Each chip is about 977.5 ns (1/1.023 MHz) long. The transmitting bandwidth of the GPS satellite in the L1 frequency is approximately 20 MHz to accommodate the P(Y) code signal; therefore, the C/A code transmitted contains the main lobe and several side lobes. The total code period contains 1,023 chips. With a chip rate of 1.023 MHz, 1,023 chips last 1 ms; therefore, the C/A code is 1 ms long.

3.2 GPS receiver and data format

3.2.1 GPS receiver

In this section, currently, there are many products of GPS receivers which are produced by many companies. Most modern GPS receiver designs are digital receivers. There are some differences on models, functions and prices but there are generally working in the same concepts of GPS receiver. So, the GPS receiver which is only used for this thesis would be described.

At the Chumphon station, the GPS receiver is produced by JAVAD GNSS Inc. Block diagram of a digital GPS receiver is shown in Figure 3.7. The GPS radio frequency (RF) signals of all GPS satellites in view are received by a RHCP (right hand circularly polarized) antenna with nearly above the local horizon gain coverage. These RF signals are amplified by a low noise preamplifier (preamp), which effectively sets the noise figure of the receiver. These amplified and signal conditioned RF signals are then down-converted to an inter-medium frequency (IF) using signal mixing frequencies from local oscillators (LOs). The LOs are derived from the reference oscillator by the frequency synthesizer dependent on the frequency plan of the receiver design. One LO per down converter stage is required. The LO signal mixing process generates both upper and lower sidebands of the GPS signals, so the lower sidebands are selected and the upper sidebands and leak through signals are rejected by a postmixer bandpass filter. The signal Dopplers and the PRN codes are preserved after the mixing process. Only the carrier frequency is lowered, but the Doppler remains referenced to the original L-band signal.

The A/D conversion process and automatic gain control (AGC) functions take place at IF. The IF must be high enough to provide a single-sided bandwidth that will support the PRN code

chipping frequency. An antialiasing IF filter must suppress the stopband noise to levels that are acceptably low when this noise is aliased into the GPS signal passband by the A/D conversion process. The signals from all GPS satellites in view are buried in thermal noise at IF. At this point the digitized IF signals are ready to be processed by each of the N digital receiver channels. No demodulation has taken place, only signal gain and conditioning plus A/D conversion into the digital IF. This digitized IF signal will be processed by a set of channels which will normally implemented on digital receiver channel. A receiver channel may be assigned to a single satellite or multiple channels using multiplexing depending upon the availability of hardware resources.

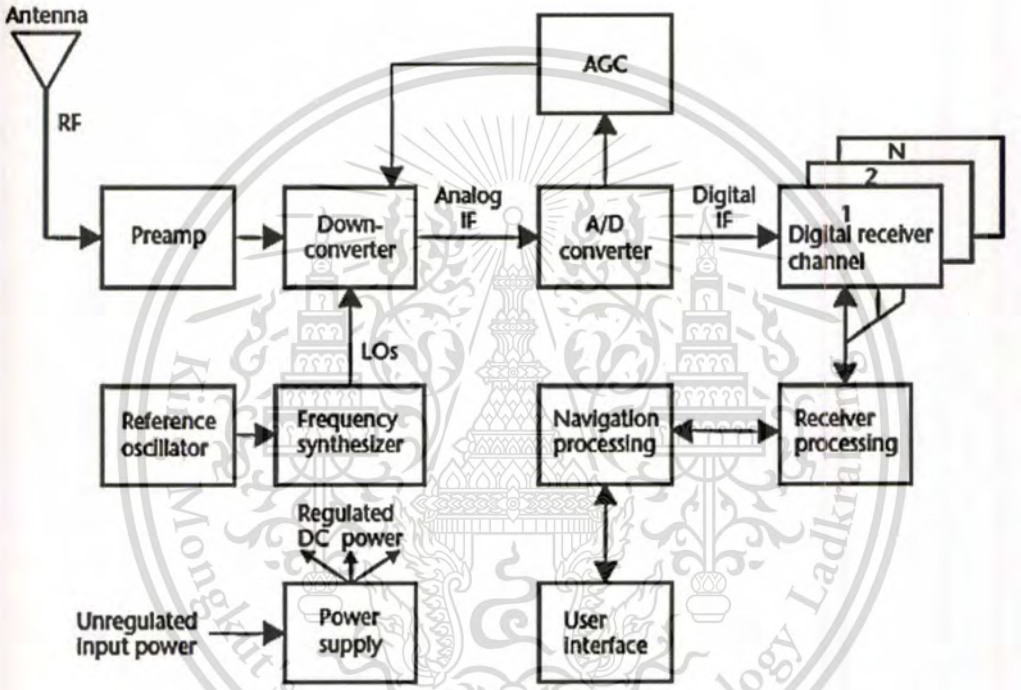

Figure 3.7 The digital GPS receiver block diagram. Adapted from GNSS receiver operator's manual, in *JAVAD Delta GNSS manual*, retrieved January 17, 2014, from http://www.javad.com/downloads/javadgnss/manuals/hardware/Delta_Operators_Manual.pdf.

3.2.2 RINEX format

The Receiver Independent Exchange (RINEX) format was developed by the Astronomical Institute of the University of Berne for the exchange of the GPS data to be collected during the first large European GPS campaign EUREF 89, which involved more than 60 GPS receivers of 4 different manufacturers. The original RINEX presented at and accepted by the 5th International Geodetic Symposium on Satellite Positioning in Las Cruces, 1989 (Gurtner et al. 1989).

In this thesis, the RINEX format version 2 is used for obtaining the GPS data file at Chumphon station. The RINEX format consists of three ASCII file types:

1. Observation data file
2. Navigation message file
3. Meteorological data file

All file types consist of a header section and a data section. The header section contains global information for the entire file and is placed at the beginning of the file. The header section contains header labels in columns 61-80 for each line contained in the header section.

The RINEX format has been optimized for minimum space requirements independent from the number of different observation types of a specific receiver or satellite system by indicating in the header the types of observations to be stored for this receiver and the satellite systems having been observed. In computer systems allowing variable record lengths the observation records may be kept as short as possible. There is no maximum record length limitation for the observation records.

Each observation file and each meteorological data file generally contain the data from one site and one session. If data from more than one receiver have to be exchanged, it would not be economical to include the identical satellite messages collected by the different receivers several times. Therefore the navigation message file from one receiver may be exchanged or a composite navigation message file created containing non-redundant information from several receivers in order to make the most complete file (Gurtner et al. 1989).

The example of observation file from Chumphon station is shown in Figure 3.8. There are seven parameters in RINEX observation file including C1, P1, P2, L1, L2, D1, and D2. L1 and L2 are the phase measurements on L1 and L2 frequencies of GPS signals, respectively. C1 is pseudoranges using C/A-Code on L1 frequency. P1 and P2 are pseudoranges using P-Code on L1 and L2 frequencies, in orderly. D1 and D2 are Doppler frequencies on L1 and L2 frequencies.

```
     2.10           OBSERVATION DATA    G (GPS)             RINEX VERSION / TYPE
JPS2RIN 1.09 lnx    RUN BY              24-FEB-09 17:58     PGM / RUN BY / DATE
build August 24, 2001 (c) Topcon Positioning Systems        COMMENT
RUN BY;COMMENT;MARKER NAME;MARKER NUMBER;OBSERVER;AGENCY;    COMMENT
ANT #;ANT TYPE - You can set in profile.                     COMMENT
./CPN_20090122000000.jps                                     COMMENT
CPN_20090122000000_1213                                      MARKER NAME

OBSERVER            AGENCY                                   MARKER NUMBER
MT312331213         JPS LEGACY          2.0 Jan,20,2000 pl4 OBSERVER / AGENCY
CPN_20050101000000  -Unknown-                               REC # / TYPE / VERS
 -1020874.1161  6183762.5892  1179096.1746                  ANT # / TYPE
       0.0000        0.0000        0.0000                  APPROX POSITION XYZ
    1     1                                                 ANTENNA: DELTA H/E/N
  2009     1     22     0     0    0.0000000     GPS        WAVELENGTH FACT L1/2
  2009     1     22    23    59   30.0000000     GPS         TIME OF FIRST OBS
   30.000                                                    TIME OF LAST OBS
   28                                                        INTERVAL
    7    C1    P1    P2    L1    L2    D1    D2            # OF SATELLITES
 G 1  1071  1063  1063  1071  1063  1071  1063              # / TYPES OF OBSERV
 G 3   745   691   691   745   691   745   691              PRN / # OF OBS
 G 4  1000   930   930  1000   930  1000   930              PRN / # OF OBS
 G 5  1210  1109  1109  1210  1109  1210  1109              PRN / # OF OBS
 G 6   996   919   919   996   919   996   919              PRN / # OF OBS
 G 7  1080  1057  1057  1080  1057  1080  1057              PRN / # OF OBS
 G 8   725   693   693   725   693   725   693              PRN / # OF OBS
```

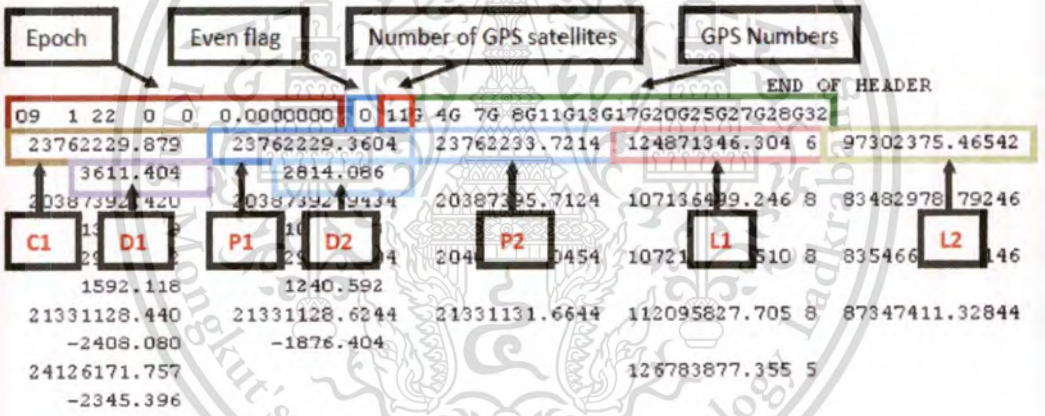

Figure 3.8 The RINEX observation file.

In the RINEX observation file, Figure 3.9 shows the loss of lock and signal strength of GPS signal which can be also recorded by putting the code number at the L1 and L2. LL1 and LL2 are for the loss of lock on L1, L2 frequencies, respectively, which the data indicates followings 0: OK, 1: Cycle slip, 4: Anti spoofing, and blank: Not known. SL1 is the signal strength on L1 frequency and SL2 is the signal strength for L2 frequency. There are 1-9 interval levels on the signal strength. The maximum signal strength is 9 and the minimum signal strength is 1. The 0 or Blank value is unknown signal strength.

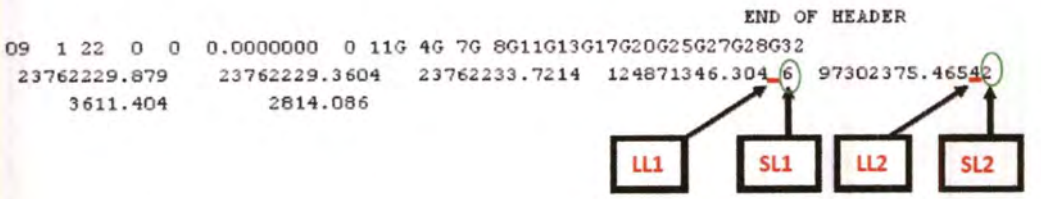

Figure 3.9 The loss of lock and signal strength of GPS signals.

The RINEX navigation file is shown in Figure 3.10. The RINEX navigation file is broadcast to users as part of the GPS signal in the navigation message. The RINEX navigation file includes the following parameters as in Table 3.3:

Table 3.3 The parameters in a RINEX navigation file.

Parameters	Descriptions
Prn	GPS PRN number
M_0	mean anomaly
$\sqrt{a}$	sqrt(semi-major axis)
Δn	variation of mea angular velocity
e	eccentricity
ω	argument of perigee
Ω	right ascension
$\dot{\Omega}$	rate of right ascension
i_0	inclination
i	rate of inclination
t_{oe}	time of ephemeris
IODE	issue of data ephemeris
IODC	issue of data clock
Cus, Crs, Cic, Crs, Cus, Cis	correction coefficients
af0, af1, af2	GPS clock bias, clock drift, clock drift rate

```
     2.10           N:  GPS NAV DATA                         RINEX VERSION / TYPE
JPS2RIN 1.09 lnx    RUN BY              24-FEB-09 17:58      PGM / RUN BY / DATE
build August 24, 2001 (c) Topcon Positioning Systems         COMMENT
     .1211D-07  -.7451D-08  -.5960D-07   .1192D-06           ION ALPHA
     .1167D+06  -.2458D+06  -.6554D+05   .1114D+07           ION BETA
    -.465661287308D-08 -.266453525910D-13   147456     1304 DELTA-UTC: A0,A1,T,W
    13                                                       LEAP SECONDS
                                                             END OF HEADER
 3 09  1  22 1 59 44.0  .732233747840D-04  .295585778076D-11  .000000000000D+00
     .106000000000D+03  .285625000000D+02  .557987528135D-08  .297871337640D+00
     .152550637722D-05  .656216021162D-02  .591948628426D-05  .515370840263D+04
     .525584000000D+06  .484287738800D-07  .216713666116D+01  .149011611938D-06
     .927097315564D+00  .247875000000D+03  .592474829355D+00 -.862393064990D-08
     .191793703263D-09  .000000000000D+00  .130300000000D+04  .000000000000D+00
     .200000000000D+01  .000000000000D+00 -.419095158577D-08  .106000000000D+03
     .525599000000D+06
16 09  1  22 1 59 44.0  .232690945268D-05 -.227373675443D-12  .000000000000D+00
     .115000000000D+03 -.136875000000D+02  .435053836024D-08 -.290859888739D+01
    -.715255737305D-06  .239433336537D-02  .100638717413D-04  .515367706871D+04
     .525584000000D+06  .335276126862D-07  .120173067204D+01 -.372529029846D-07
     .961093903499D+00  .185906250000D+03 -.121816482456D+01 -.779639617977D-08
     .246795994329D-09  .100000000000D+01  .130300000000D+04  .000000000000D+00
     .200000000000D+01  .000000000000D+00 -.977888703346D-08  .115000000000D+03
     .525599000000D+06
```

Prn	Epoch	af0	af1	af2
	IODE	Crs	Δn	M_0
	Cuc	e	Cus	$\sqrt{a}$
	t_{oe}	Cic	Ω	Cis
	i_0	Crs	ω	$\dot{\Omega}$
	i	Codes on L2	GPS week number	L2 P data flag
	GPS accuracy	GPS health	L1 and L2 correction	IODC
	Transmission time			

Figure 3.10 The RINEX navigation file.

In this thesis, the RINEX meteorological data file is not used at the Chumphon station. However, in the Figure 3.11, there is the example of RINEX meteorological data file from RINEX: The Receiver Independent Exchange Format Version 2 website which can be accessed at http://igscb.jpl.nasa.gov/igscb/data/format/rinex2.txt. In the RINEX meteorological file, PR is pressure, TD is dry temperature, and HR is relative humidity.

```
     2                    METEOROLOGICAL DATA                     RINEX VERSION / TYPE
XXRINEXM V9.9             AIUB                 3-APR-96 00:10     PGM / RUN BY / DATE
EXAMPLE OF A MET DATA FILE                                        COMMENT
A 9080                                                            MARKER NAME
     3    PR     TD     HR                                       # / TYPES OF OBSERV
PAROSCIENTIFIC          740-16B                      0.2     PR SENSOR MOD/TYPE/ACC
HAENNI                                               0.1     TD SENSOR MOD/TYPE/ACC
ROTRONIC                I-240W                       5.0     HR SENSOR MOD/TYPE/ACC
        0.0                0.0            0.0  1234.5678 PR SENSOR POS XYZ/H
                                                              END OF HEADER

 96  4  1  0  0 15  987.1   10.6   89.5
 96  4  1  0  0 30  987.2   10.9   90.0
 96  4  1  0  0 45  987.1   11.6   89.0
```

Figure 3.11 The RINEX meteorological data file. Adapted from RINEX: The RINEX meteorological data file, in *RINEX: The Receiver Independent Exchange Format Version 2*, retrieved January 19, 2014, from http://igscb.jpl.nasa.gov/igscb/data/format/rinex2.txt.

3.3 GPS group delay and phase advance

The phase v_p and group velocity v_g of the GPS signal are defined

$$v_p = \lambda f \ ,$$

and

$$v_g = -\frac{df}{d\lambda}\lambda^2 \ , \tag{3.2}$$

Therefore,

$$v_g = v_p - \lambda\frac{dv_p}{d\lambda} \ ,$$

where λ is the wavelength and f is the frequency. The ionosphere which is a dispersive medium affects the propagation of GPS signal. Therefore, the phase refractive index is impressed as

$$n_p = 1+\frac{c_2}{f^2}+\frac{c_3}{f^3}+\frac{c_4}{f^4}+...\approx 1+\frac{c_2}{f^2} \ , \tag{3.3}$$

where c_i (i =2,3,4,...) are the coefficients which do not depend on GPS frequency but on the electron density along the propagation path of GPS signal. The group refractive index is approximated by

$$n_g = 1-\frac{c_2}{f^2} \ . \tag{3.4}$$

The c_2 is estimated by Seeber (Seeber, 2003) as $c_2 = -40.28Ne[Hz^2]$. From the equation (3.3) and (3.4), it shows that $n_g > n_p$. Since the velocity is inversely proportional to the refractive index, it is evident that $v_g > v_p$. As a result, the ionosphere causes the group delay and phase advanced. Both phase advance and group delay are accounted for the ionospheric delay which causes the error on GPS observations. The details of GPS observations are presented in the next section.

CHAPTER 4

TEC COMPUTATION

In Chapter 2 and 3, the ionosphere and GPS technology are overviewed to understand the literature part of this thesis. Now, in Chapter 4, the study and investigation of TEC are described from the TEC computation including GPS TEC, IGS TEC, and IRI TEC.

4.1 GPS TEC

GPS TEC stands for the Global Positioning System Total Electron Content (GPS TEC). TEC can be derived from the delay of the traveling time of the transmitted dual-frequency GPS signals at the GPS receiver including the pseudorange and carrier phase. The distance measurement from the GPS satellites to the GPS receiver can be estimated from those observations. The accuracy of both observations depends not only on the internal system of satellite and receiver but also the environment such as ionosphere, troposphere, and multipath. The pseudorange and carrier phase at both f_1 and f_2 frequencies are measured in range as follows

$$P_1 = \rho + c(\tau^r_{p_1} - \tau^s_{p_1}) + I_{p_1} + T + \varepsilon_{p_1},$$
$$P_2 = \rho + c(\tau^r_{p_2} - \tau^s_{p_2}) + I_{p_2} + T + \varepsilon_{p_2}, \quad (4.1)$$

where, P_1 is pseudorange measured on f_1 frequency based on code, P_2 is pseudorange measured on f_2 frequency based on code, ρ is geometrical range from satellite s to receiver r, τ^r is receiver clock error, τ^s is satellite clock error, T is tropospheric delay, $I_{P_{1/2}}$ is ionospheric delay in code measurement on $L_{1/2}$, and $\varepsilon_{P_{1/2}}$ is multipath delay and other delay/error in code measurement on $L_{1/2}$.

$$L_1 = \rho - I_{p_1} + c(\tau^r_{p_1} - \tau^s_{p_1}) + T + \lambda_1 n_1 + \varepsilon_{L_1} ,$$
$$L_2 = \rho - I_{p_2} + c(\tau^r_{p_2} - \tau^s_{p_2}) + T + \lambda_2 n_2 + \varepsilon_{L_2} , \quad (4.2)$$

where, L_1 is carrier phase measured on f_1 frequency, L_2 is carrier phase measured on f_2 frequency, τ^r is receiver clock error, τ^s is satellite clock error, T is tropospheric delay, $I_{p_{1/2}}$ is ionospheric delay in code measurement on $L_{1/2}$, $\lambda_{1/2} n_{1/2}$ is integer cycle ambiguities, and $\varepsilon_{p_{1/2}}$ is multipath delay and other delay/error in code measurement on $L_{1/2}$.

The L_1, L_2, P_1, and P_2 can be extracted from the RINEX observation file which is explained in the chapter 3. The L_1, L_2, P_1, (C1 for C/A code), and P_2 values for each GPS satellites are obtained from RINEX files for every 30 seconds. Then, the slant TEC can be calculated in the next section.

4.1.1 Slant TEC (STEC)

In the GPS system, each satellite transmits signals at two frequencies, f_1 = 1575.42 MHz and f_2 = 1227.60 MHz. The GPS receiver continuously receives 4 to 12 GPS signals that will lead to the computation of the slant TEC (STEC) values. Figure 4.1 shows the directions of STEC along with the vertical TEC through the ionosphere.

Figure 4.1 The vertical TEC and slant TEC.

The STEC from a satellite to a receiver can be obtained from the difference between the pseudoranges (P_1 and P_2), and the difference between the phases L_1 and L_2 of the two frequencies (Blewitt, 1990) shown as

$$STEC_P = \frac{2(f_1 f_2)^2}{k(f_1^2 - f_2^2)}(P_2 - P_1), \tag{4.3}$$

and

$$STEC_L = \frac{2(f_1 f_2)^2}{k(f_1^2 - f_2^2)}(L_1\lambda_1 - L_2\lambda_2), \tag{4.4}$$

where k, related to the ionosphere refraction, is 80.62 (m^3/s^2), λ_1 , and λ_2 are the wavelengths corresponding to f_1 and f_2, respectively.

4.1.2 Resolving integer ambiguity and differential clock biases for STEC

A simpler approach eliminates the ambiguity-offset by means of phase leveling, which involves adjusting continuous arcs of $STEC_L$ to the mean value of the corresponding $STEC_P$ values (Mannucci et. al., 1998)

$$STEC = STEC_L + (\overline{STEC_P} - \overline{STEC_L}), \tag{4.5}$$

where $\overline{STEC_P}$ and $\overline{STEC_L}$ are the mean code and phase on STEC values.

4.1.3 Vertical TEC (VTEC)

Total electron content (TEC) is defined as the total electrons (electron/m^2) in a vertical column of 1-m^2 cross-section (Goodwin, 1995). This definition for TEC is actually the definition of the vertical TEC (VTEC) through the piercing point with the obliquity factor (Brunini et al., 2004). The VTEC, in el/m^2, can be computed from Ma and Maruyama (2003)

$$VTEC = STEC \times \cos\chi, \tag{4.6}$$

where the zenith angle χ is expressed as

$$\chi = \arcsin\left(\frac{R_E \cos\alpha}{R_E + h}\right), \tag{4.7}$$

where α is the elevation angle of the satellite, R_E is the mean radius of the Earth, and h is the height of the ionospheric layer, which is assumed to be 400 kilometers.

The STEC computed based on the carrier phase in equation (4.4) is generally less noisy than from equation (4.3), however, the ambiguity in the integer value of STEC, known as a cycle slip, often arises. The cycle slip correction can typically be made with the aid of pseudorange difference information. To obtain the VTEC, as

$$VTEC=(STEC - b_s - b_r)\times \cos\chi \ , \tag{4.8}$$

where b_s and b_r are the estimated satellite and receiver biases. The satellite bias is obtained from NICT based on the GPS Earth Observation Network (GEONET), set up by the Geographical Survey Institute (GSI) of Japan which has more than 1000 GPS receivers spreading over Japan (Miyazaki et al., 1997).

In Figure 4.2, the procedures of the VTEC computation obtained from a GPS receiver can are shown.

(1) The L1, L2, P1 (C1 for C/A code), and P2 values for each GPS satellites are obtained from RINEX observation files at every 30 seconds. In equation (4.3) and (4.4), the STEC can be rewritten as

$$STEC^m_{P,u}(n)=\frac{1}{k}\left(\frac{f_1^2 f_2^2}{f_1^2-f_2^2}\right)\left(P^m_{2,u}(n)-P^m_{1,u}(n)\right) \tag{4.9}$$

and

$$STEC^m_{L,u}(n)=\frac{1}{k}\left(\frac{f_1^2 f_2^2}{f_1^2-f_2^2}\right)\left(L^m_{1,u}(n)\lambda_1-L^m_{2,u}(n)\lambda_2\right) \tag{4.10}$$

where the subscript u denotes the receiver station index; the superscript m denotes the satellite index, and the index n denotes the time sample.

(2) Elimination the ambiguity-offset by means of phase leveling rewritten in equation (4.5) as follows

$$STEC^m_u(n)= STEC^m_{L,u}(n)+\left(\overline{STEC^m_{P,u}}(n)-\overline{STEC^m_{L,u}}(n)\right) \tag{4.11}$$

(3) For calculation the zenith angle, the satellite ephemeris data are obtained from RINEX navigation files,

(4) GPS satellite biases (b_s^m) are obtained from the IONEX files, and

(5) VTEC is computed by rewriting in equation (4.8) as

$$VTEC_u^m(n) = (STEC_u^m(n) - b_s^m - b_r) \times \cos \chi_m , \tag{4.12}$$

For this point of view, the VTEC is TEC. When TEC is obtained from GPS signals, TEC can be called GPS TEC. In the outline of VTEC computation, the GPS receiver bias (b_r) is needed to be solved. At this moment, it is not easy to find the GPS receiver bias. For finding GPS receiver bias for one day, it probably takes time in 1 hour due to try out the GPS receiver bias values. So, we use about 30 hours to find a GPS receiver bias for a month. In this thesis, we propose the methods for solving those problems in Chapter 5.

4.1.4 Ionospheric time delay from TEC

The ionospheric time delay is computed from the electron density along the propagation path of GPS signal and the carrier frequency as (Maruyama, 2001)

$$I = \frac{A}{f^2} \int N_e ds = \frac{A}{f^2} TEC \tag{4.13}$$

where $A = \frac{e^2}{8\pi^2 m \varepsilon_0}$, f is the frequency of the radio signal, e is the charge of the electron, 1.6022 x 10^{-19}, N_e is the electron density, ε_0 is the permittivity of free space, 8.8542 x 10^{-12}, m is the electron mass, 1.6605 x 10^{-31} kilograms (kg).

4.1.5 Rate of TEC index (ROTI)

Rate of TEC index (ROTI) determines the presence of amplitude and phase scintillation. ROTI is defined as the standard deviation of rate of TEC (ROT), i.e.,

$$ROTI = \sqrt{\frac{(\Delta TEC^2) - (\Delta TEC)^2}{\Delta t}} \tag{4.14}$$

where ΔTEC is a value with components composed of the change in TEC between successive samples, $(\Delta TEC^2)-(\Delta TEC)^2$ is the variance of the change in TEC between successive samples and Δt is the TEC the sampling time.

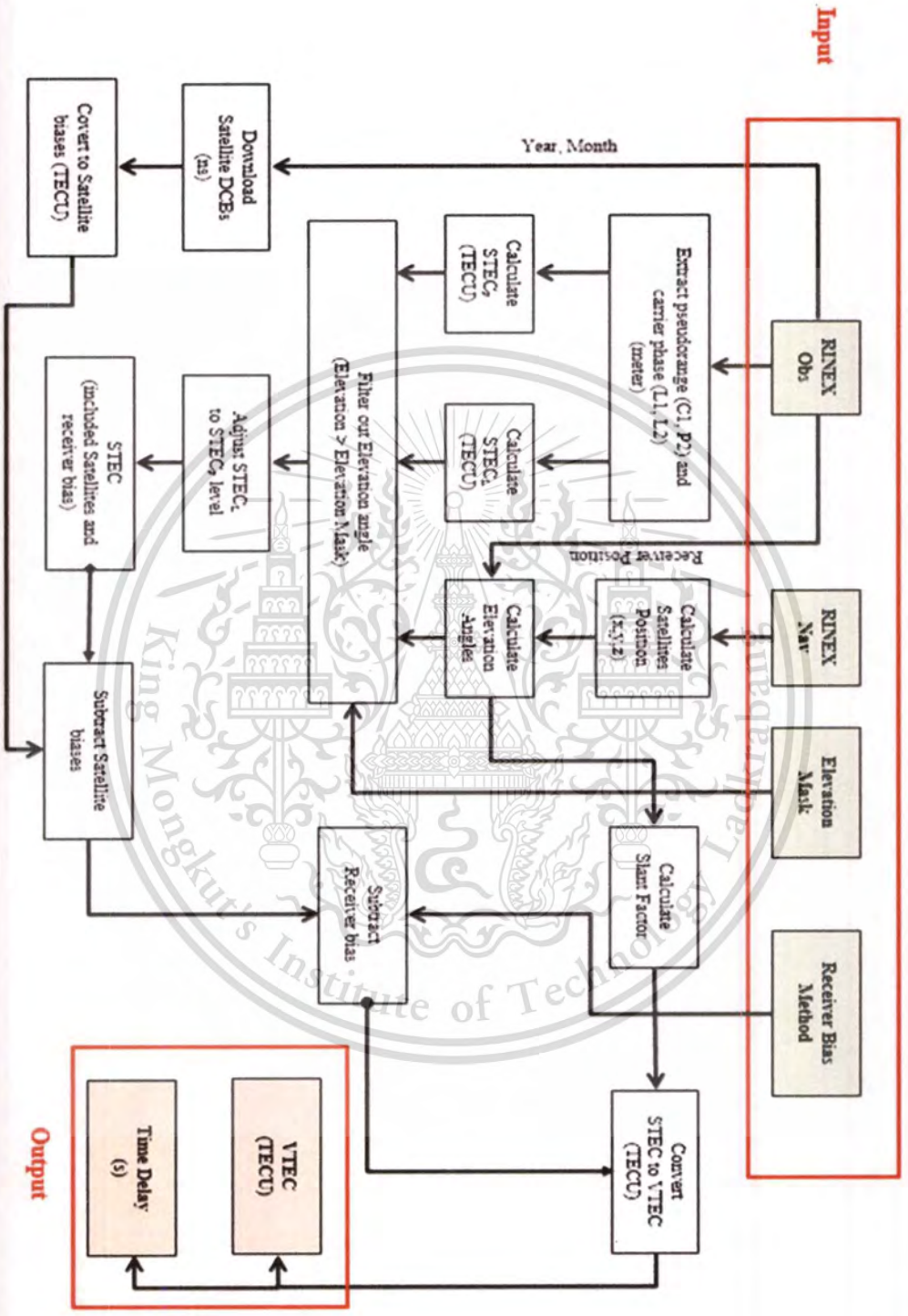

Figure 4.2 VTEC computation obtained from GPS receiver.

4.2 IGS TEC

The IGS TEC is maintained and monitored by the International GNSS service (IGS). The IGS relies on an international network of over 350 continuously operating dual-frequency GPS stations (Dow et al., 2009). The Central Bureau for the service is located at the Jet Propulsion Laboratory, which maintains the Central Bureau Information System (CBIS) and ensures access to IGS products and information. An International Governing Board oversees all aspects of the IGS. The IGS is an approved service of the International Association of Geodesy since 1994 and is recognized as a member of the Federation of Astronomical and Geophysical Data Analysis Services (FAGS) since 1996. The IGS collects, archives, and distributes GPS observation data sets. The IGS provides the TEC map data and is made available on the File Transfer Protocol. It can be access the IGS TEC data from the FTP site: ftp://igscb.jpl.nasa.gov/.

IGS TEC is the two-hour text data of global TEC maps with the different code biases in the IONEX (The IONosphere Map EXchange) format via the following FTP site: ftp://cddis.gsfc.nasa.gov/pub/gps/products/ionex/. The final TEC map data estimates are provided by three centers on the same day (COD, JPL and UPC with associated final product labels CODG, JPLG and UPCG) together with the corresponding final combined IGS values (labeled as IGSG).

```
     1.0            IONOSPHERE MAPS     MIX                 IONEX VERSION / TYPE
cmpcmb v1.2         gAGE/UPC            24-jan-06 19:32     PGM / RUN BY / DATE
ionex file containing IGS COMBINED Ionosphere maps          COMMENT
global ionosphere maps for day 009, 2006                    DESCRIPTION
IONEX file containing the COMBINED IGS TEC MAPS and DCBs    DESCRIPTION
      IONEX files of the following IAACs were combined: cod DESCRIPTION
                                                         esa DESCRIPTION
                                                         jpl DESCRIPTION
                                                         upc DESCRIPTION
Contact address (e-mail): manuel@mat.upc.es                 DESCRIPTION
  2006     1     9     0     0     0                        EPOCH OF FIRST MAP
  2006     1    10     0     0     0                        EPOCH OF LAST MAP
  7200                                                       INTERVAL
    13                                                       # OF MAPS IN FILE
  COSZ                                                       MAPPING FUNCTION
     0.0                                                     ELEVATION CUTOFF
combined TEC calculated as weighted mean of input TEC valuesOBSERVABLES USED
   310                                                       # OF STATIONS
    29                                                       # OF SATELLITES
  6371.0                                                     BASE RADIUS
     2                                                       MAP DIMENSION
   450.0 450.0   0.0                                        HGT1 / HGT2 / DHGT
    87.5 -87.5  -2.5                                        LAT1 / LAT2 / DLAT
  -180.0 180.0   5.0                                        LON1 / LON2 / DLON
```

(a)

```
     1                                                      START OF TEC MAP
2006     1     9     0     0     0                         EPOCH OF CURRENT MAP
  87.5-180.0 180.0   5.0 450.0                            LAT/LON1/LON2/DLON/H
 31   31   31   31   31   30   30   30   30   30   30   30   29   29   28   29
 28   28   28   28   28   27   28   27   28   28   28   28   28   28   29   28
 29   30   30   30   30   31   31   31   31   32   32   32   32   32   32   32
 32   32   32   32   32   32   32   32   32   32   32   31   31   31   31   31
 32   31   31   32   31   32   32   31   31
  85.0-180.0 180.0   5.0 450.0                            LAT/LON1/LON2/DLON/H
 32   32   33   32   32   32   32   31   31   30   30   30   29   28   28   27
 27   26   26   26   25   25   25   25   25   25   25   26   27   27   27   28
 28   29   29   30   31   31   31   32   33   33   33   34   34   34   34   34
 34   34   34   34   34   33   33   33   32   32   32   32   32   32   32   32
 32   33   32   32   32   32   32   32   32
  82.5-180.0 180.0   5.0 450.0                            LAT/LON1/LON2/DLON/H
 34   34   34   35   35   35   35   35   33   33   32   31   30   29   29   28
 27   26   25   25   24   23   23   22   22   22   22   22   22   23   24   25
 26   27   28   29   30   31   32   33   34   34   35   35   35   35   35   36
 35   36   35   35   34   33   33   32   32   32   31   31   31   31   32   32
 32   32   32   32   33   33   33   34   34
```

(b)

Figure 4.3 The IONEX file format. Adapted from the ionosphere map exchange format, in *IONEX file*, retrieved January 9, 2014, from ftp://cddis.gsfc.nasa.gov/pub/gps/products/ionex/.

In Figure 4.3, the example of IONEX file on January 9, 2006 is shown to calculate on the ionosphere maps (TEC map). For latitude, the TEC map starts from 87.5 °, decreases by 2.5 °, and ends at -87.5 °. In the longitude, the TEC map is from -180 ° to 180 ° by increasing at 5 °. The altitude for TEC map in the IONEX file is 450 km. The interval time for each data is 7200 seconds which is 2 hours.

In this thesis, the IONEX file is used to calculate the TEC at the Chumphon station by selecting the nearly latitude and longitude at 10 °, and 100 °, respectively as shown in Figure 4.4. The TEC result which is near Chumphon station is 210 TECU. For IONEX file, the TEC value in TECU which is divided by 10 is 21.0 TECU.

```
     1.0            IONOSPHERE MAPS     MIX                 IONEX VERSION / TYPE
cmpcmb v1.2         gAGE/UPC            24-jan-06 19:32     PGM / RUN BY / DATE
ionex file containing IGS COMBINED Ionosphere maps          COMMENT
global ionosphere maps for day 009, 2006                    DESCRIPTION
IONEX file containing the COMBINED IGS TEC MAPS and DCBs    DESCRIPTION
      IONEX files of the following IAACs were combined: cod DESCRIPTION
                                                        esa DESCRIPTION
                                                        jpl DESCRIPTION
                                                        upc DESCRIPTION
Contact address (e-mail): manuel@mat.upc.es                 DESCRIPTION
  2006     1     9     0     0     0                        EPOCH OF FIRST MAP
  2006     1    10     0     0     0                        EPOCH OF LAST MAP
  7200                                                      INTERVAL
    13                                                      # OF MAPS IN FILE
  COSZ                                                      MAPPING FUNCTION
     0.0                                                    ELEVATION CUTOFF
combined TEC calculated as weighted mean of input TEC valuesOBSERVABLES USED
   310                                                      # OF STATIONS
    29                                                      # OF SATELLITES
  6371.0                                                    BASE RADIUS
     2                                                      MAP DIMENSION
   450.0 450.0   0.0                                       HGT1 / HGT2 / DHGT
    87.5 -87.5  -2.5                                       LAT1 / LAT2 / DLAT
  -180.0 180.0   5.0                                       LON1 / LON2 / DLON
    12.5-180.0 180.0   5.0 450.0                           LAT/LON1/LON2/DLON/H
 388  396  403  402  383  340  292  240  202  182  170  156  143  131  119  110
 104  104  103  105  107  109  108  105  100   96   91   90   90   90   92   93
  90   83   76   71   67   63   59   55   54   53   51   48   46   47   47   47
  52   63   79   97  114  133  157  182  207  234  256  277  289  295  297  297
 297  295  293  295  307  328  354  376  388
   10.0-180.0 180.0   5.0 450.0                           LAT/LON1/LON2/DLON/H
 363  376  390  401  392  361  314  261  224  203  188  178  166  152  139  127
 121  121  119  119  121  123  119  112  107  104   99  100   97   94   95   95
  91   82   74   67   62   58   55   52   52   52   49   47   45   45   45   47
  52   64   81  100  118  137  160  186  210  234  254  272  282  285  286  285
 284  281  278  279  288  306  330  350  363
    7.5-180.0 180.0   5.0 450.0                           LAT/LON1/LON2/DLON/H
 336  349  366  383  384  364  327  281  247  223  209  200  190  178  166  151
 144  142  139  140  142  142  132  121  115  114  111  111  106  101   99   96
  91   82   72   64   59   56   54   53   51   50   47   46   45   45   44   46
  53   66   84  104  121  138  160  185  209  229  247  263  271  275  277  279
 278  275  271  270  276  290  309  325  336
```

Figure 4.4 The example of interpretation of TEC map at Chumphon station on January 9, 2006. Adapted from the ionosphere map exchange format, in *IONEX file*, retrieved January 9, 2014, from ftp://cddis.gsfc.nasa.gov/pub/gps/products/ionex.

4.3 IRI TEC

With the objective of establishing an international standard for the specification of ionospheric parameters based on all worldwide available data from ground-based as well as satellite observations, the International Reference Ionosphere (IRI) project was initiated by the Committee on Space Research (COSPAR) and by the International Union of Radio Science (URSI) in the late sixties (Bilitza and Rinisch, 2008). COSPAR and URSI specifically asked for an empirical IRI model to avoid the uncertainties of the evolving theoretical understanding of ionospheric processes and coupling to the regimes below and above.

TEC obtained from the IRI model is called IRI TEC. The IRI model is continually upgraded as new data and new modeling approaches become available and this process has resulted in several major milestone editions of IRI (Bilitza, 1990, 2001; Bilitza and Rawer, 1996; Bilitza and Reinisch, 2008; Rawer et al., 1978a, b, 1981) progressing from a set of tables for typical conditions, to a global model for all phases of the solar cycle. More information about the IRI project including information about the IRI Newsletter and the IRI electronic mailer can be found on the IRI homepage at http://IRI.gsfc.nasa.gov/ and http://www.irimodel.org/. The IRI-2012, a new empirical standard model of the ionosphere, is improved from the limitations of the previous IRI2001 and IRI2007 model. The most recent update is the IRI-2012 model which we can access at http://omniweb.gsfc.nasa.gov/vitmo/iri2012_vitmo.html/.

The IRI-2012 model is divided into four parts, input, optional input, output form, and desired output parameters. In Figure 4.5 and 4.6, each part can be described as

(1) The input part consists of the date and time, coordinates, and profile type and its parameters.

(2) The optional part can be input or add more data parameters such as a sunspot number, an ionospheric index, a radio flux, an upper boundary for electron content, electron density model, and F peak model.

(3) The output form is offered to three choices. The first selection is a list model data. The second selection is the create model data file in ASCII format for downloading. Third selection is the plot model data.

(4) The desired output parameters is categorized into three sections including independent variable, the IRI model parameters, and indices used by the model.

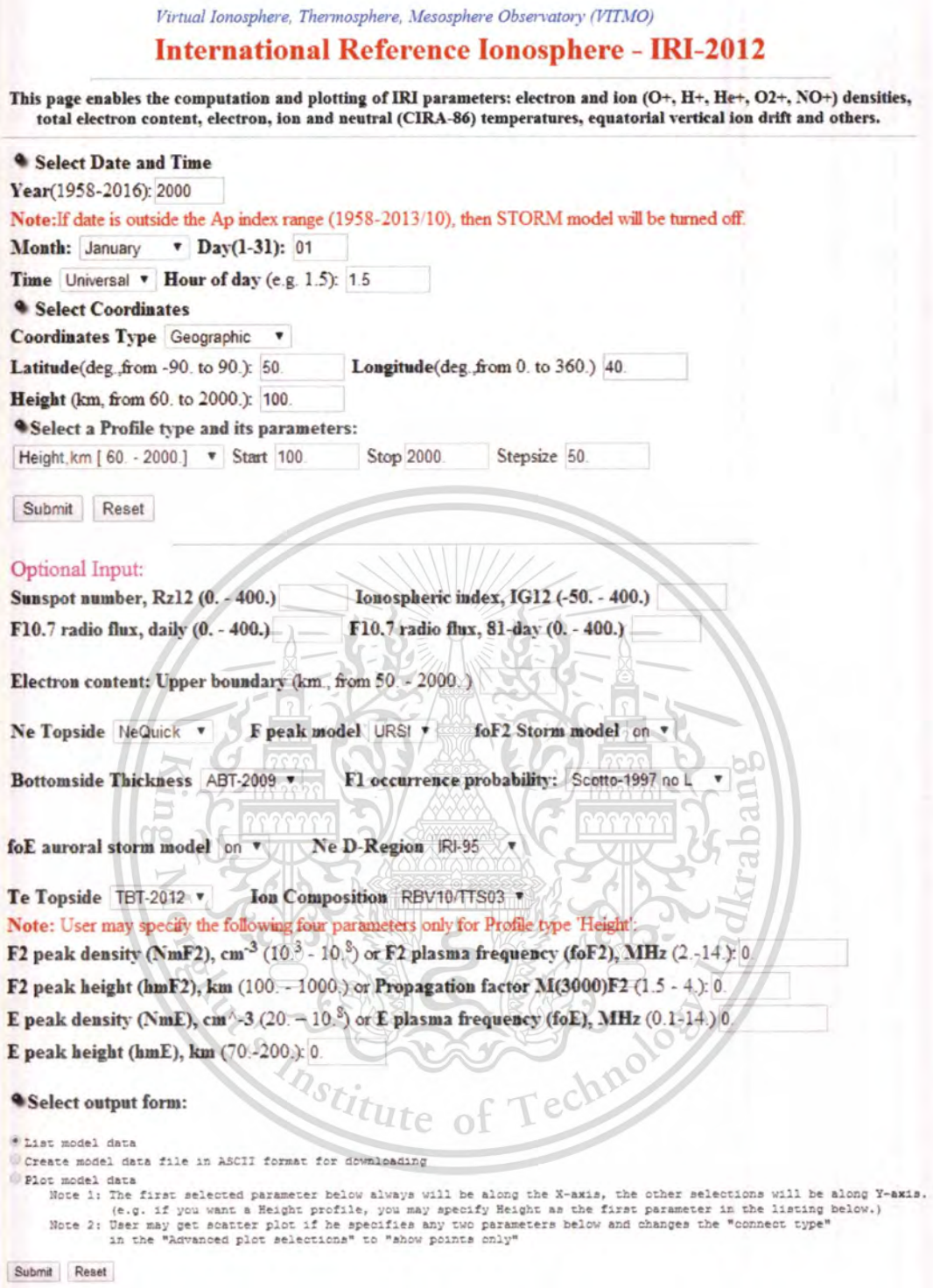

Virtual Ionosphere, Thermosphere, Mesosphere Observatory (VITMO)

International Reference Ionosphere - IRI-2012

This page enables the computation and plotting of IRI parameters: electron and ion (O+, H+, He+, O2+, NO+) densities, total electron content, electron, ion and neutral (CIRA-86) temperatures, equatorial vertical ion drift and others.

Select Date and Time

Year(1958-2016): 2000

Note:If date is outside the Ap index range (1958-2013/10), then STORM model will be turned off.

Month: January **Day(1-31):** 01

Time Universal **Hour of day** (e.g. 1.5): 1.5

Select Coordinates

Coordinates Type Geographic

Latitude(deg.,from -90. to 90.): 50. **Longitude**(deg.,from 0. to 360.) 40.

Height (km, from 60. to 2000.): 100.

Select a Profile type and its parameters:

Height,km [60. - 2000.] Start 100. Stop 2000. Stepsize 50.

Submit Reset

Optional Input:

Sunspot number, Rz12 (0. - 400.) **Ionospheric index, IG12 (-50. - 400.)**

F10.7 radio flux, daily (0. - 400.) **F10.7 radio flux, 81-day (0. - 400.)**

Electron content: Upper boundary (km, from 50. - 2000.)

Ne Topside NeQuick **F peak model** URSI **foF2 Storm model** on

Bottomside Thickness ABT-2009 **F1 occurrence probability:** Scotto-1997 no L

foE auroral storm model on **Ne D-Region** IRI-95

Te Topside TBT-2012 **Ion Composition** RBV10/TTS03

Note: User may specify the following four parameters only for Profile type 'Height':

F2 peak density (NmF2), cm^{-3} (10^3 - 10^8) or **F2 plasma frequency (foF2), MHz** (2.-14.): 0.

F2 peak height (hmF2), km (100. - 1000.) or **Propagation factor M(3000)F2** (1.5 - 4.): 0.

E peak density (NmE), cm^-3 (20. – 10^8) or **E plasma frequency (foE), MHz** (0.1-14.) 0.

E peak height (hmE), km (70.-200.): 0.

Select output form:

List model data

Create model data file in ASCII format for downloading

Plot model data

Note 1: The first selected parameter below always will be along the X-axis, the other selections will be along Y-axis. (e.g. if you want a Height profile, you may specify Height as the first parameter in the listing below.)

Note 2: User may get scatter plot if he specifies any two parameters below and changes the "connect type" in the "Advanced plot selections" to "show points only"

Submit Reset

Figure 4.5 International Reference Ionosphere – IRI-2012. Reprinted from International Reference Ionosphere, in *International Reference Ionosphere-IRI-2012*, retrieved January 12, 2014, from http://omniweb.gsfc.nasa.gov/vitmo/iri2012_vitmo.html/.

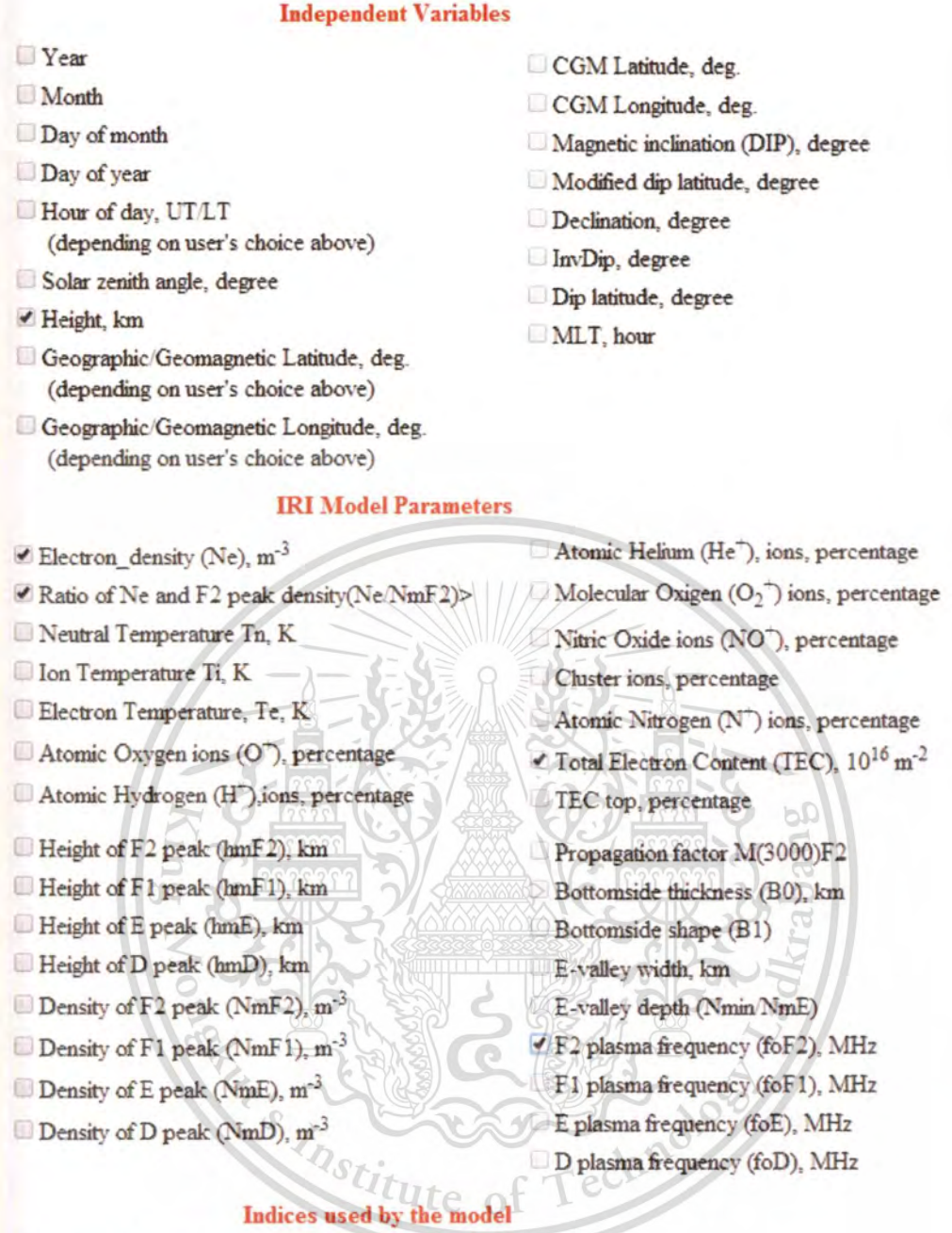

Figure 4.6 Output parameters for IRI-2012. Reprinted from International Reference Ionosphere, in *International Reference Ionosphere-IRI-2012*, retrieved January 12, 2014, from http://omniweb.gsfc.nasa.gov/vitmo/iri2012_vitmo.html/.

CHAPTER 5

GPS RECEIVER BIAS ESTIMATION

As mentioned before in Chapter 4, the current GPS receiver bias estimation methods have a high complexity. In Chapter 5, the two new methods of GPS receiver bias estimations are proposed to reduce the complexity and time of the GPS receiver bias estimation. The two methods are median cut and Lagrange interpolation which are also compared to the two current methods, polynomial and minimization of standard deviation, which are given in more details in the following sections.

5.1 Literature review on bias estimation

In the past few years, Global Positioning System (GPS) dual frequency signals have been widely used to estimate both regional and global TEC values. TEC can be derived from the delay of the traveling time of the transmitted dual-frequency GPS signals, recorded at the earth-based receivers. Yet, variation of the ionospheric refractive index with frequency is a major source of error in computation of group delay and phase advance of GPS observables. Absolute TEC can be measured from the differential delay of the GPS code on the two GPS frequencies. For both GPS precise positioning applications and for accurate TEC estimation, the effect of interfrequency satellite and receiver differential delay biases should be removed from GPS measurements (Brunini et al., 2005; Chen et al., 2004; Coco et al., 1991; Otsuka et al., 2002; Warnant, 1997). The receiver biases are also referred to as receiver instrumental bias, receiver differential bias, receiver offset, differential codebias (DCB) and interfrequency bias (IFB). The differential code biases are investigated by various researchers. Some methods are developed to obtain TEC and differential biases by considering more than one station in their computation and model TEC on the double differences of GPS recordings (Hernandez-Pajares et al., 2004; Makela et al., 2001; Sardon et al., 1994; Warnant, 1997). For single-station TEC and differential receiver bias estimates, there are two basic approaches that can be found in the literature. First group of studies models TEC by a polynomial of coordinates in Earth-Sun reference system. Both satellite and receiver biases are also included in the model. The polynomial coefficients and biases being the unknowns, the observations form a linear system of equations that is solved by least squares method (Chen et al.,

2004; Coco et al., 1991; Jakowski et al., 1996; Kee and Yun, 2002; Lanyi and Roth, 1988; Lin, 2001; Otsuka et al., 2002; Warnant, 1997). In the second group of studies, for a selected measurement time, TEC is computed from different satellites over a certain angle of elevation, and the computed TEC values are considered be close to each other. This proximity is found by calculating standard deviation of TEC obtained from all satellites. To obtain the optimum receiver bias value, trial receiver biases are used in TEC computation and the receiver bias that minimizes the standard deviation is chosen as the receiver bias value for that GPS station (Ma and Maruyama, 2003; Zhang et al., 2003). Both of the above methods can be applied to estimate differential receiver biases for a single station, yet they have to be used off-line.

Differential satellite and receiver biases can also be obtained from internet for a few number of GPS stations from International GPS Service (IGS) analysis centers, namely, the Center for Orbit Determination in Europe (CODE) University of Berne, Switzerland; Jet Propulsion Laboratory (JPL) Pasadena, CA, USA; European Space Operations Center (ESOC) of European Space Agency (ESA), Darmstadt, Germany; and gAGE/UPC of Polytechnical University of Catalonia, Barcelona, Spain. Global Ionospheric TEC maps (GIM) and interfrequency bias solutions of these analysis centers and are available at the web sites ftp://igs.ensg.ign.fr/pub/igs/iono or ftp:// cddis.gsfc.nasa.gov/gps/products/ionex/ in the form of IONosphere Map EXchange Format (IONEX) files. Most of the IGS receiver differential biases provided in the IONEX files are monthly averages of daily values and do not represent the daily variations. The algorithms to compute the receiver bias values are not clearly explained in the literature, and thus the results cannot be duplicated by other users. Also, the values provided for receiver biases in IONEX files from various centers are not always in accordance with each other (Brunini et al.,2005).

5.2 Median cut

Median cut is an algorithm to sort data of an arbitrary number of dimensions into series of sets by cutting each set of data at the median point. Median cut method is a mathematical procedure technique to identify all combinations of basic events that result in the occurrence of the top event. These basic event combinations, called median cut, are then reduced to identify those "minimal" median cut, which contain the minimum sets of events necessary and sufficient to cause of the top event. Median cut analysis is described in many texts including Henley and Kumamoto (1981). This methodology is applicable to GPS receiver bias data, regardless of size of complexity, that satisfy the following conditions.

In this thesis, the median cut method is used by the median cut algorithm to sort GPS receiver bias data of an arbitrary number of dimensions into series of sets by cutting each set of GPS receiver bias data at the median point.

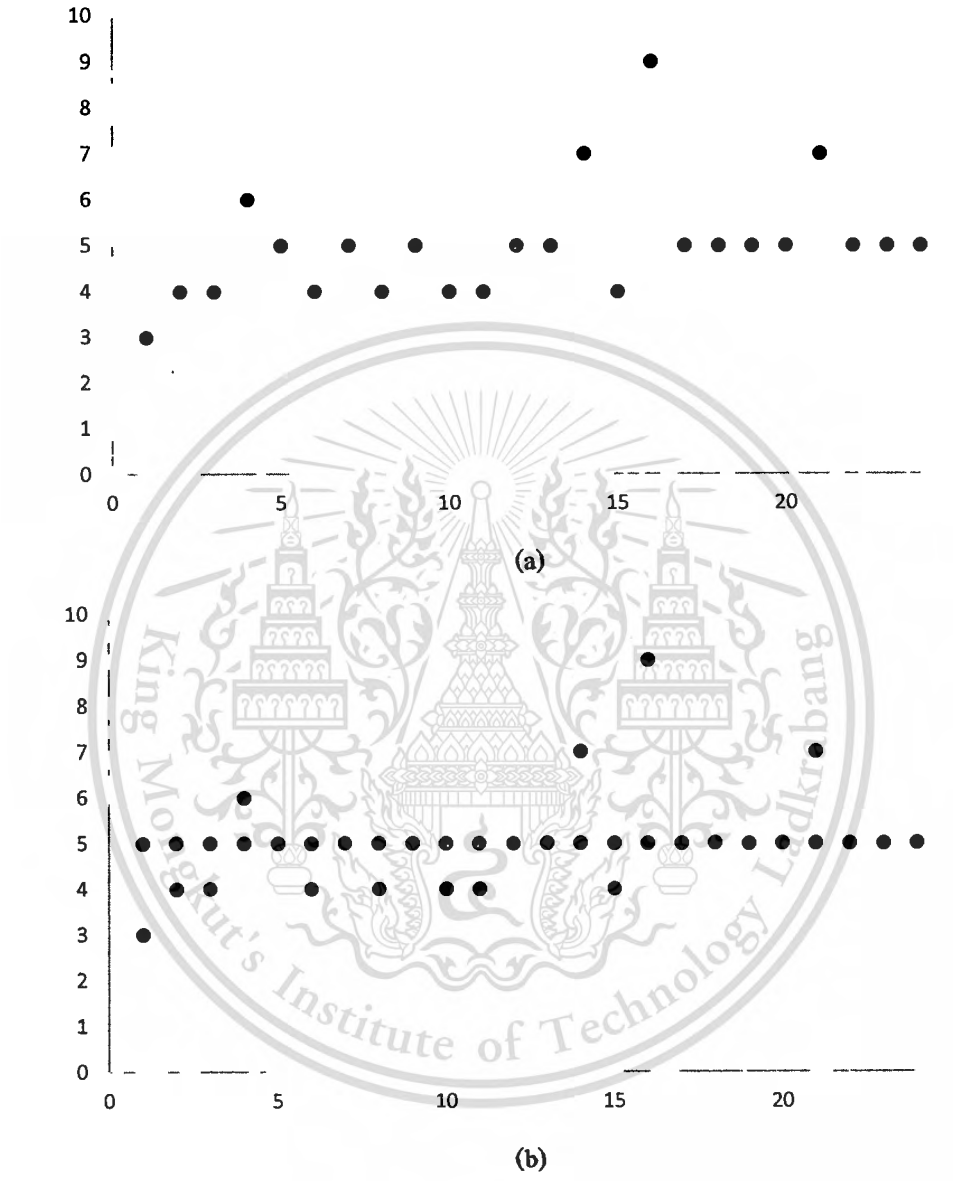

Figure 5.1 The median cut method (a) original data set and (b) median cut data.

In Figure 5.1(a), the original data set shows the data values varying between 3 to 9 points for each slots. After using the median cut in Figure 5.1(b), the data value has only one value that is 5. So, now, each data slots is given at 5 points.

5.3 Lagrange interpolation

Lagrange interpolation is the interpolation method which is used to find the derivatives and integrals of discrete functions in data. Many times, GPS receiver bias data is given only at discrete points time and bias values such as (x_0,y_0), (x_1,y_1), ..., (x_{n-1},y_{n-1}), (x_n,y_n). So, how then does one find the value of y at any other value of x? A continuous function $f(x)$ may be used to represent the $n+1$ data values with $f(x)$ passing through the $n+1$ points as Figure 5.2. Then one can find the value of y at any other value of x. A Lagrange interpolation is a common choice for an interpolating function because this interpolation is easy to find a polynomial of order n that passes through the $n+1$ data points.

The Lagrange interpolation is given by

$$f_n(x)=\sum_{i=0}^{n}L_i(x)f(x_i) \tag{5.1}$$

where n in $f_n(x)$ stands for the n^{th} order polynomial that approximates the function $y=f(x)$ given at $n+1$ data points as

$$(x_0,y_0),(x_1,y_1),.....,(x_{n-1},y_{n-1}),(x_n,y_n), \tag{5.2}$$

and

$$L_i(x)=\prod_{\substack{j=0\\ j\neq i}}^{n}\frac{x-x_j}{x_i-x_j} \tag{5.3}$$

where $L_i(x)$ is a weighting function that includes a product of $n-1$ terms with $j=i$ omitted.

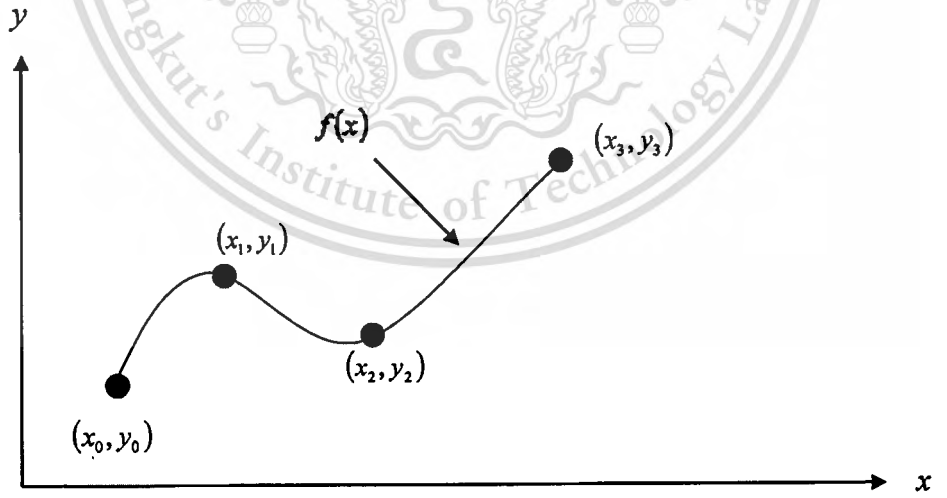

Figure 5.2 The Lagrange interpolation for the discrete points.

In this thesis, the 5th order Lagrange interpolation (Gil, Segura, and Temme, 2007; Stoer and Bulirsch, 2002) is presented for the proposed method. In the 5th order Lagrange interpolation, there are 6 points which stand for the GPS receiver biases at the first point, pre-sunrise point, noontime pint, post-sunset point, midnight point, and the last point in each days. The equation for the 5th order Lagrange polynomial interpolation is

$$y(x)=\sum_{l=0}^{5}L_l(x)y(x_l) \tag{5.4}$$

$$\begin{aligned}&=L_0(x)y(x_0)+L_1(x)y(x_1)+L_2(x)y(x_2)+L_3(x)y(x_3)\\&\quad+L_4(x)y(x_4)+L_5(x)y(x_5)\end{aligned} \tag{5.5}$$

where

$$L_0(x)=\prod_{\substack{j=0\\j\neq 0}}^{5}\frac{x-x_j}{x_0-x_j} \tag{5.6}$$

$$=\left(\frac{x-x_1}{x_0-x_1}\right)\left(\frac{x-x_2}{x_0-x_2}\right)\left(\frac{x-x_3}{x_0-x_3}\right)\left(\frac{x-x_4}{x_0-x_4}\right)\left(\frac{x-x_5}{x_0-x_5}\right) \tag{5.7}$$

$$L_1(x)=\prod_{\substack{j=0\\j\neq 1}}^{5}\frac{x-x_j}{x_1-x_j} \tag{5.8}$$

$$=\left(\frac{x-x_0}{x_1-x_0}\right)\left(\frac{x-x_2}{x_1-x_2}\right)\left(\frac{x-x_3}{x_1-x_3}\right)\left(\frac{x-x_4}{x_1-x_4}\right)\left(\frac{x-x_5}{x_1-x_5}\right) \tag{5.9}$$

$$L_2(x)=\prod_{\substack{j=0\\j\neq 2}}^{5}\frac{x-x_j}{x_2-x_j} \tag{5.10}$$

$$=\left(\frac{x-x_0}{x_2-x_0}\right)\left(\frac{x-x_1}{x_2-x_1}\right)\left(\frac{x-x_3}{x_2-x_3}\right)\left(\frac{x-x_4}{x_2-x_4}\right)\left(\frac{x-x_5}{x_2-x_5}\right) \tag{5.11}$$

$$L_3(x)=\prod_{\substack{j=0\\j\neq 3}}^{5}\frac{x-x_j}{x_3-x_j} \tag{5.12}$$

$$=\left(\frac{x-x_0}{x_3-x_0}\right)\left(\frac{x-x_1}{x_3-x_1}\right)\left(\frac{x-x_2}{x_3-x_2}\right)\left(\frac{x-x_4}{x_3-x_4}\right)\left(\frac{x-x_5}{x_3-x_5}\right) \tag{5.13}$$

$$L_4(x)=\prod_{\substack{j=0\\ j\neq 4}}^{5}\frac{x-x_j}{x_4-x_j} \tag{5.14}$$

$$=\left(\frac{x-x_0}{x_4-x_0}\right)\left(\frac{x-x_1}{x_4-x_1}\right)\left(\frac{x-x_2}{x_4-x_2}\right)\left(\frac{x-x_3}{x_4-x_3}\right)\left(\frac{x-x_5}{x_4-x_5}\right) \tag{5.15}$$

$$L_5(x)=\prod_{\substack{j=0\\ j\neq 5}}^{5}\frac{x-x_j}{x_5-x_j} \tag{5.16}$$

$$=\left(\frac{x-x_0}{x_5-x_0}\right)\left(\frac{x-x_1}{x_5-x_1}\right)\left(\frac{x-x_2}{x_5-x_2}\right)\left(\frac{x-x_3}{x_5-x_3}\right)\left(\frac{x-x_4}{x_5-x_4}\right) \tag{5.17}$$

$$\begin{aligned}y(x)=&\left(\frac{x-x_1}{x_0-x_1}\right)\left(\frac{x-x_2}{x_0-x_2}\right)\left(\frac{x-x_3}{x_0-x_3}\right)\left(\frac{x-x_4}{x_0-x_4}\right)\left(\frac{x-x_5}{x_0-x_5}\right)y(x_0)\\&+\left(\frac{x-x_0}{x_1-x_0}\right)\left(\frac{x-x_2}{x_1-x_2}\right)\left(\frac{x-x_3}{x_1-x_3}\right)\left(\frac{x-x_4}{x_1-x_4}\right)\left(\frac{x-x_5}{x_1-x_5}\right)y(x_1)\\&+\left(\frac{x-x_0}{x_2-x_0}\right)\left(\frac{x-x_1}{x_2-x_1}\right)\left(\frac{x-x_3}{x_2-x_3}\right)\left(\frac{x-x_4}{x_2-x_4}\right)\left(\frac{x-x_5}{x_2-x_5}\right)y(x_2)\\&+\left(\frac{x-x_0}{x_3-x_0}\right)\left(\frac{x-x_1}{x_3-x_1}\right)\left(\frac{x-x_2}{x_3-x_2}\right)\left(\frac{x-x_4}{x_3-x_4}\right)\left(\frac{x-x_5}{x_3-x_5}\right)y(x_3)\\&+\left(\frac{x-x_0}{x_4-x_0}\right)\left(\frac{x-x_1}{x_4-x_1}\right)\left(\frac{x-x_2}{x_4-x_2}\right)\left(\frac{x-x_3}{x_4-x_3}\right)\left(\frac{x-x_5}{x_4-x_5}\right)y(x_4)\\&+\left(\frac{x-x_0}{x_5-x_0}\right)\left(\frac{x-x_1}{x_5-x_1}\right)\left(\frac{x-x_2}{x_5-x_2}\right)\left(\frac{x-x_3}{x_5-x_3}\right)\left(\frac{x-x_4}{x_5-x_4}\right)y(x_5)\end{aligned} \tag{5.18}$$

5.4 Current GPS receiver bias estimation methods

As it is discussed in the literature, there are various GPS receiver bias estimation algorithms, and the most commonly used method can be roughly grouped into two methods.

5.4.1 Polynomial model of VTEC method

In this method, VTEC is modeled as a polynomial function that is a function of ionospheric pierce point coordinates in a coordinate system referenced to Earth-Sun axis (Lanyi and Roth, 1988). Ionospheric pierce point coordinates are provided by Lanyi and Roth (1988), using the angular definitions between the satellite and GPS receiver coordinates and ionospheric thin shell height. The slant TEC is modeled as a polynomial of angular coordinate differences as follows

$$STEC_u^m(n) = o_u^m + M(\in_m(n))(c_1 + c_2\overline{\phi}_p + c_3\overline{\theta}_p + c_4\overline{\phi}_p^2 + c_5\overline{\phi}_p\overline{\theta}_p + c_6\overline{\theta}_p^2) \tag{5.19}$$

where o_u^m denotes the sum of satellite and receiver biases where subscript u and superscript m denote receiver and satellite, respectively. The function $\in_m(n)$ can be computed from satellite-receiver geometry using satellite ephemeris data, $\overline{\phi}_p$, and $\overline{\theta}_p$ are longitude and latitude respectively, c_i, i=1,...,6 are the coefficients that form the VTEC polynomial.

Once the slant TEC is computed, the vertical TEC, *VTEC*, can be obtained using the thin shell approximation of Single Layer Ionosphere Model (SLIM) as

$$VTEC_u^m(n) = \frac{STEC_u^m(n)}{M(\in_m(n))} \tag{5.20}$$

The mapping function $M(\in_m)$ is

$$M(\in_m(n)) = \left[1 - \left(\frac{R\cos\lambda(n)}{R+h}\right)^2\right]^{-1/2} \tag{5.21}$$

where λ is the satellite elevation angle, R is the earth radius of 6,378.137 km and h is the ionospheric shell height of 428.8 km from Schaer (1999).

The polynomial coefficients and offset values can be obtained using a least squares approximation separately for nighttime and daytime measurement sessions. The satellite ephemeris data and satellite biases are widely available in IONEX files from IGS centers. For each satellite

and time index for the chosen two hour duration, equation (5.19) is formed. For example, for satellite m_1 and time index n_1, the equation (5.19) takes the form of

$$STEC_u^{m_1}(n_1) = o_u^{m_1} + M(\in_{m_1}(n_1))(VTEC_u^{m_1}(n_1)) \tag{5.22}$$

where

$$VTEC_u^{m_1}(n_1) = c_1 + c_2\overline{\phi}_p^{m_1}(n_1) + c_3\overline{\theta}_p^{m_1}(n_1) + c_4\left[\overline{\phi}_p^{m_1}(n_1)\right]^2 + c_5\overline{\phi}_p^{m_1}(n_1)\overline{\theta}_p^{m_1}(n_1) + c_6\left[\overline{\theta}_p^{m_1}(n_1)\right]^2 \tag{5.23}$$

When the equation (5.22) and (5.23) are written for M_t satellites and N_t measurement samples, M_t x N_t equations are obtained for one observation session. Then, the total bias, o_u^m, and coefficients c_1, c_2, c_3, c_4, c_5, c_6 are solved using least squares. Since the o_u^m value is different for each satellite, satellite biases obtained from IONEX files are removed from these median values to compute receiver bias. Then, the median of these receiver bias values over the 24 hour period are taken to obtain a single daily receiver bias value. The block diagram of polynomial method is used to find the GPS receiver bias as shown in Figure 5.3.

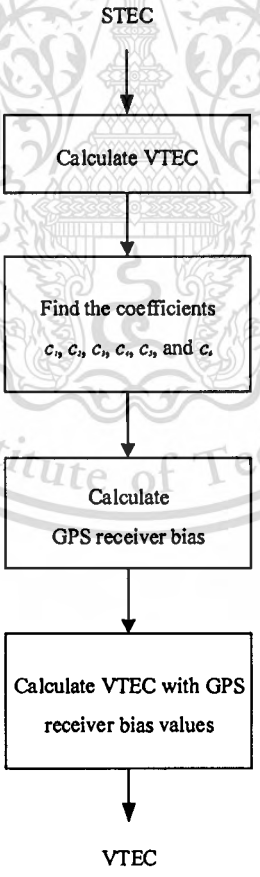

Figure 5.3 The block diagram of polynomial method for GPS receiver bias estimation.

5.4.2 Minimization of standard deviation of VTEC method

The other method for receiver bias estimation is the minimization of the standard deviation of VTEC that is computed from different satellites as discussed by Ma and Maruyama (2003). This method may be implemented for the measurements of a single receiver or a group of receivers. The minimization of standard deviation method assumes that the VTEC computed from each satellite in view should be equal since the measurement time and vertical path of satellite zenith are the same. This assumption is valid if the satellite and receiver biases are correctly removed from GPS measurements. Also, most VTEC computation techniques assume both the spatial homogeneity of ionosphere for a wide range of elevation and azimuth angles and a temporal stationarity period of at least 5 to 15 minutes (Arikan et al., 2003; Komjathy and Langley, 1996). In this method, a range of receiver bias values are applied and VTEC is calculated for each bias selection. If the correct receiver bias is selected, the standard deviation of VTEC data from each satellite with respect to the mean should be minimum (Ma and Maruyama, 2003).

The standard deviation of VTEC data for a measurement period can be computed from Ma and Maruyama (2003)

$$\sigma_{t,u} = \sum_{n=1}^{N_t} \sigma_u(n) \tag{5.24}$$

where $\sigma_{t,u}$ is a total standard deviation of TEC and

$$\sigma_u(n) = \sqrt{\frac{1}{M_t} \sum_{n=1}^{M_t} \left(VTEC_u^m(n) - \overline{VTEC_u}(n) \right)^2} \tag{5.25}$$

and M_t denotes the total number of satellites and N_t is duration of the desired measurement time interval in samples. In equation (5.24), the total standard deviation is obtained by summing the standard deviation value of each measurement samples where N_t is selected as 24 hours for this study corresponding to 2880 GPS measurements. $\overline{VTEC_u}(n)$ denotes the average of all VTEC from M_t satellites.

The minimization of standard deviation of VTEC method is applied by using trial receiver bias values starting from - 30 ns to 30 ns at the 0.001 ns steps. For each receiver bias value, VTEC and total standard deviation $\sigma_{t,u}$ are calculated using the equation (5.24) and (5.25). The receiver bias value that gives the minimum total standard deviation is the chosen receiver bias value.

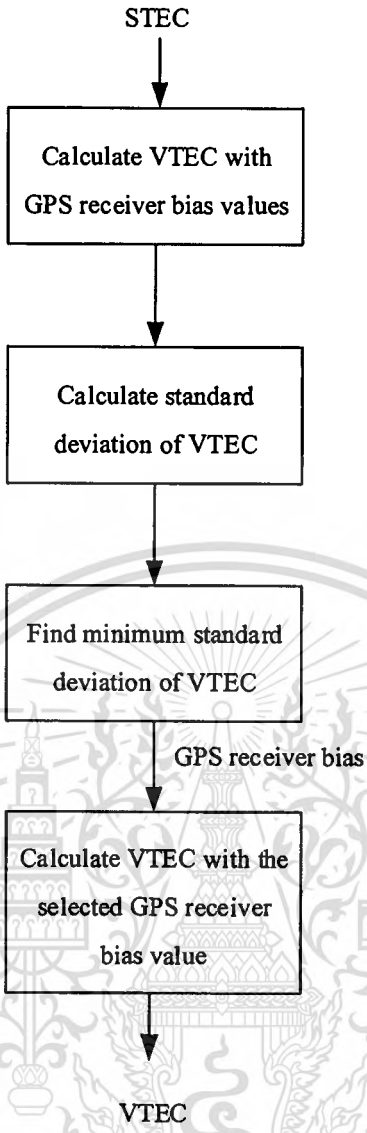

Figure 5.4 The minimization of standard deviation method for estimating the GPS receiver bias.

The block diagram of the minimization of standard deviation method is shown in Figure 5.4. The GPS receiver bias is estimated by selecting the tried out GPS receiver value which gives the minimum standard deviation of VTEC values.

5.5 Proposed GPS receiver bias methods

In this thesis, there are two problems which need to be solved on finding GPS receiver bias. One is to reduce the complexity of GPS receiver bias estimation. The other is to the GPS receiver bias estimation at the missing points. Solving those two problems, the two GPS receiver bias methods are proposed. The median cut method is for reducing the complexity of GPS receiver bias estimation method and the Lagrange interpolation method is to estimate the receiver bias for a missing point. At the preparing data set, the two methods are applied from the minimization of standard deviation of VTEC method as giving more details in section 5.3.1 and 5.3.2.

5.5.1 Median cut method for GPS receiver bias estimation

The GPS receiver bias is estimated by using the minimization of standard deviation of VTEC method. For this method, the GPS receiver bias is assumed to be consistent value in every 15 minutes. The receiver bias (b_r) is obtained from the median cut algorithm by using the median cut. The GPS receiver biases are in ns unit which are obtained from the GPS RINEX file at Chumphon station during 2004-2013. Figure 5.5 shows the block diagram of the median cut method.

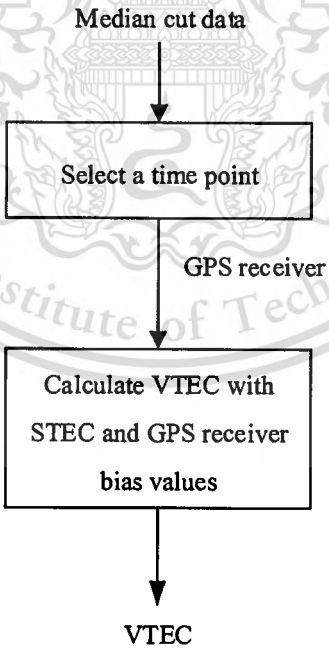

Figure 5.5 The block diagram of median cut method used to find the GPS receiver bias.

The daily median of GPS receiver bias is to be 96 points a day in 2004-2013. x is a time point for each 15 minutes and y is a median GPS receiver bias for each time point. The data structure for daily median of GPS receiver biases is constructed in Table 5.1. Then, the algorithm of median cut method is in the Table 5.1 which is used as the representative median cut data of GPS receiver bias for any days and years.

Table 5.1 Median cut data for the daily median GPS receiver bias.

x	y	x	y	y	y	x	y	x	y	x	y	x	y	x	y
1	-3	13	-3.75	25	-4.5	37	-5.75	49	-5.5	61	-5	73	-5	85	-5.25
2	-3.25	14	-4	26	-4.5	38	-5.75	50	-5.5	62	-4.75	74	-5	86	-5
3	-3	15	-4	27	-4.75	39	-5.75	51	-5.25	63	-4.75	75	-5	87	-5
4	-3.25	16	-4	28	-4.75	40	-5.75	52	-5.5	64	-4.75	76	-5.25	88	-5
5	-3.75	17	-4	29	-4.75	41	-6	53	-5.25	65	-4.75	77	-5.25	89	-5
6	-3.75	18	-4	30	-5	42	-6	54	-5.25	66	-4.75	78	-5.25	90	-5
7	-3.75	19	-4.25	31	-5	43	-6	55	-5.25	67	-4.75	79	-5.25	91	-5
8	-3.75	20	-4.25	32	-5.25	44	-5.75	56	-5	68	-4.75	80	-5.25	92	-5
9	-4	21	-4.25	33	-5.5	45	-5.75	57	-5	69	-4.75	81	-5.25	93	-5
10	-4	22	-4.5	34	-5.5	46	-5.75	58	-5	70	-4.75	82	-5.25	94	-4.75
11	-4	23	-4.5	35	-5.5	47	-5.75	59	-5	71	-4.75	83	-5.25	95	-4.75
12	-3.75	24	-4.5	36	-5.75	48	-5.5	60	-5	72	-4.75	84	-5.25	96	-4.75

From the above data structure in Table 5.1, the daily median GPS receiver is plotted against 15 minutes time point as shown in Figure 5.6.

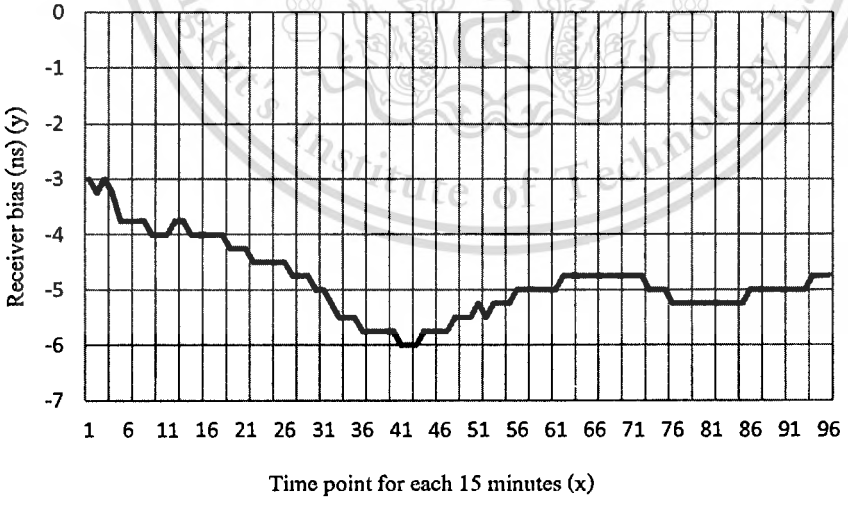

Figure 5.6 The daily median GPS receiver.

5.5.2 Lagrange interpolation method for GPS receiver bias estimation

For this method, the GPS receiver bias estimation is calculated by using the 5th order Lagrange interpolation. According to the Lagrange interpolation method, six important points for daily median GPS receiver biases are selected from the daily median 15 minute GPS receiver biases as follow

$x_0 = 1,\ y(x_0) = -3$ $x_1 = 16,\ y(x_1) = -4$ $x_2 = 43,\ y(x_2) = -6$

$x_3 = 64,\ y(x_3) = -4.75$ $x_4 = 80,\ y(x_4) = -5.25$ $x_5 = 96,\ y(x_5) = -4.75$

Then, using the equation (5.4)-(5.18) of the Lagrange interpolation method for GPS receiver bias is defined as follows

$$y(x) = -3.177179993438 + 0.167520974463x - 0.026621541654x^2 + 0.000081300189x^3 - 0.000000955941x^4 + 0.0000000038868x^5, \quad 1 \le x \le 96 \tag{5.26}$$

As an example of the Lagrange algorithm, let $x = 1$ (UTC time at 0:15) in equation (5.26), then

$$y(1) = -3.177179993438 + 0.167520974463(1) - 0.026621541654(1)^2 + 0.000081300189(1)^3 - 0.000000955941(1)^4 + 0.0000000038868(1)^5$$

$$= -3.0355$$

The estimated GPS receiver bias at 0:15 UTC is -3.0355 ns, which is close to the -3 ns at the selected point.

This method, the time is required to be selected to find the GPS receiver bias. Selected time can be outside of 15 minutes interval. For example, if the selected time is 0:01 UTC. Then, time point for finding GPS receiver bias is scaled and the result of GPS receiver bias is calculated as following. Let UTC time at 0:15 be 1, then 0:03 is

$$\frac{3}{15} \times 1 = 0.2$$

$$y(0.2) = -3.177179993438 + 0.167520974463(0.2) - 0.026621541654(0.2)^2 + 0.000081300189(0.2)^3 - 0.000000955941(0.2)^4 + 0.0000000038868(0.2)^5$$

$$= -3.1447$$

Then, the estimated GPS receiver bias at 0:03 UTC is -3.1447 ns which is used for VTEC calculation.

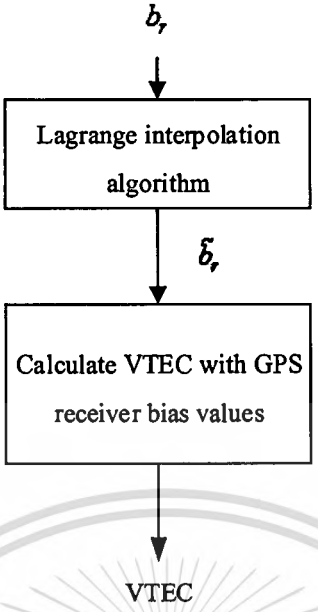

Figure 5.7 The block diagram of Lagrange interpolation method for GPS receiver bias estimation.

In Figure 5.7, the block diagram of Lagrange interpolation method is presented for estimating the GPS receiver bias. The input for this method is 96 GPS receiver bias values. This method gives more than 2880 GPS receiver bias values which depend on the interval time.

In this thesis, the two methods are not only proposed methods in this thesis, but also used for VTEC computation in Chumphon station. The advantages of two proposed method are that the complexity of finding GPS receiver bias is reduced and the time of GPS receiver bias estimation at a specified time can be achieved as well.

5.6 Comparisons and discussions

The polynomial VTEC method, and the minimization of standard deviation of VTEC method , the median cut method, and Lagrange interpolation method are calculated for a single station, Chumphon, in the equatorial region. For the comparisons, the TEC data is obtained from the RINEX file on the selected date, 21 March 2009.

The median cut method and Lagrange interpolation method are compared to the complexity of calculating time to the polynomial VTEC method and the minimization of standard deviation of VTEC method by running on a 2.6 GHz personal computer shown in Table 5.2.

Table 5.2 The results and comparisons among the polynomial VTEC method, the minimization of standard deviation of VTEC method, the median cut method, and Lagrange interpolation method on 21 March 2009

Chumphon station	Polynomial VTEC	Minimization of standard deviation	Median cut	Lagrange interpolation
Calculated time (s)	2040	2100	180	90
Number of b_r	1	96	96	>2880
Median b_r (ns)	-6.75	-6.05	-6.25	-6.55
Complexity	yes	yes	no	No

The results and comparisons among the polynomial VTEC method, the minimization of standard deviation of VTEC method, median cut method, and Lagrange interpolation method show that the calculated time for median cut method is faster than the other methods. Lagrange interpolation method gives more GPS receiver biases than others. For the median value of GPS receiver bias, polynomial VTEC method shows higher value than the others, but the minimization of standard deviation of VTEC method gives the lowest value. However, the different values of GPS receiver biases among four methods are not more than -1 ns.

CHAPTER 6

RESULTS AND DISCUSSIONS

In Chapter 6, the total electron content (TEC) and ionospheric parameters at the equatorial magnetic latitude station, Chumphon, Thailand, are studied and analyzed according to the knowledge of the ionosphere, the GPS technology, the TEC computation, and the GPS receiver bias estimation In Chapter 6, the comparisons of GPS receiver biases in different methods are investigated. The selected days are for a quiet day and a disturbed day during the year 2004-2013. However, unfortunately, the data of TEC in 2012 are missing at Chumphon station because the GPS receiver and the network system were repaired. The results for the variation of TEC, the comparisons of GPS TEC, IGS TEC, and IRI TEC, the variation of GPS delay time, the variation *of* F2-layer critical frequency, the variation of the peak electron density in the F2-region, and the variation of ionospheric slab thickness are investigated in three seasons, equinox, summer and winter for the different phases of solar activities. Then, the discussion would be given in the last section.

6.1 Results

6.1.1 The variation of GPS receiver biases

This section, we investigate the variation of GPS receiver biases on different days, a quiet day and a disturbed day during 2004-2013. By using the disturbance storm time (Dst) index described by Araujo-Pradere et al. (2004), the quiet day means the day with Dst index at more than -100 nT and the disturbed day is a day with Dst index at less than -100 nT. The Dst index can be accessed at the Geomagnetic Equatorial Dst index website via http://wdc.kugi.kyoto-u.ac.jp/dstdir/index.html.

In this thesis, we investigate and select the days according to the condition of the quiet day and the disturbed day during 2004-2013. As a result, there are a few days of the ionospheric disturbance on these periods of times. We can find the disturbed day based on a geomagnetic storm day. During the year 2004-2013, based on the Dst index at the Geomagnetic Equatorial Data center, we find that there are 26 days with Dst index at less than -100 nT. Those geomagnetic storm days are shown in Table 6.1 with the Dst index.

Table 6.1 The geomagnetic storm days with Dst index during 2004-2013.

Date	Dst (nT)	Date	Dst (nT)	Date	Dst (nT)	Date	Dst (nT)
22/01/04	-130	10/11/04	-258	15/12/06	-159	16/07/12	-102
25/07/04	-136	11/11/04	-106	6/08/11	-107	1/10/12	-119
27/07/04	-170	15/05/05	-247	26/09/11	-101	9/10/12	-105
30/08/04	-129	30/05/05	-113	25/10/11	-132	14/11/12	-108
7/11/04	-117	24/08/05	-184	8/03/12	-131	17/03/13	-132
8/11/04	-374	31/08/05	-122	24/04/12	-108		
9/11/04	-214	11/09/05	-139	15/07/12	-127		

The selected quiet day with the maximum Dst index at -2 nT is on January 1, 2010. Because of missing the data in November 2004, the chosen disturbed day with the maximum Dst index at -247 nT is on May 15, 2005. The results are shown in Table 6.2.

Table 6.2 The comparison of GPS receiver bias among the four methods during a quiet day and a disturbed day.

Chumphon station		Polynomial VTEC	Minimization of standard deviation	Median cut	Lagrange interpolation
GPS receiver bias (ns)	A quiet day January 1, 2010	-5.75	-5.65	-6.15	-6.25
	A disturbed day May 15, 2005	-4.25	-5.25	-5.15	-5.25

The results in Table 6.1 show that the GPS receiver bias values for all methods in the disturbed day are more than in the quiet day. In the quiet and disturbed days, the polynomial method gives the highest value of the GPS receiver bias at -5.75 ns and -4.25 ns, respectively, but the Lagrange interpolation shows the lowest value of GPS receiver bias at -6.85 ns and -5.25 ns, in order.

Now, we investigate more on using the GPS receiver bias for four methods into the TEC computation. The selected quiet day is on January 1, 2010 with the Dst index at -2 nT. The result of STEC including GPS receiver bias is shown in Figure 6.1. The STEC value is not smooth according to the GPS receiver bias.

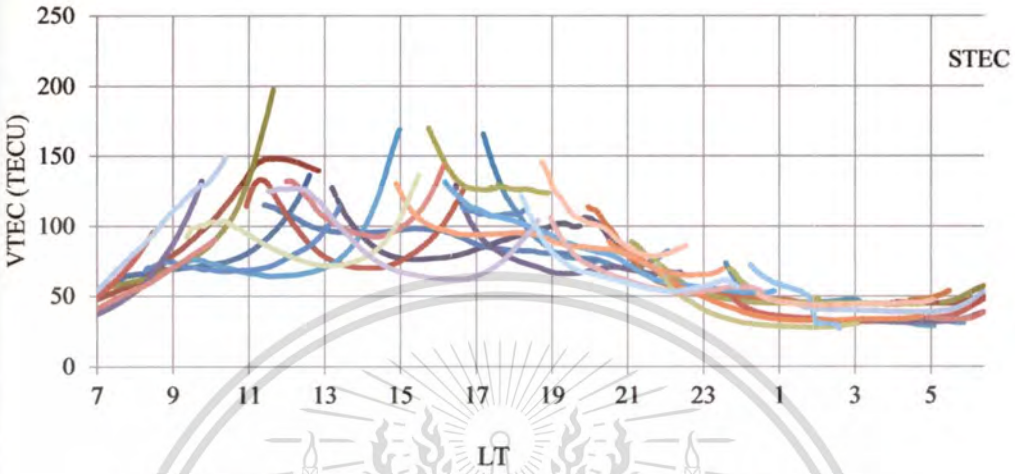

Figure 6.1 The STEC including GPS receiver bias on 1 January 2010.

Then, the polynomial VTEC method, and the minimization of standard deviation of VTEC method , the median cut method, and Lagrange interpolation method are compared to the result of TEC and the complexity of calculating time.

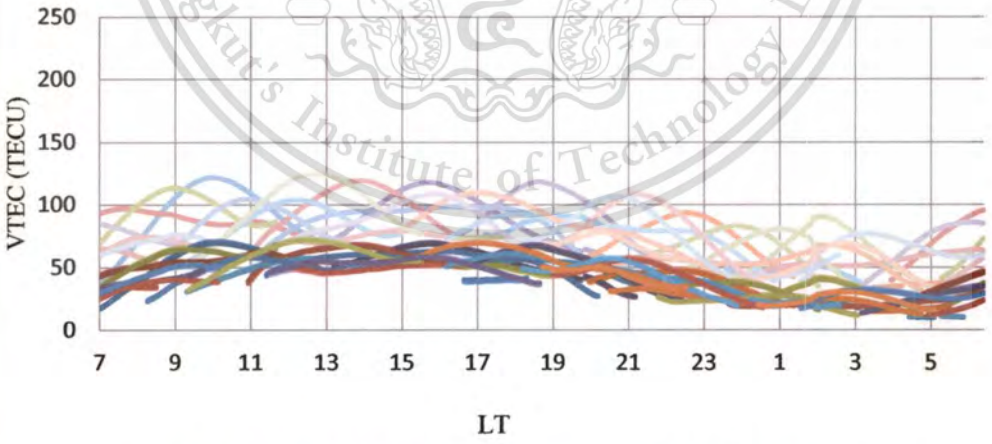

Figure 6.2 VTEC calculated by the polynomial method on 1 January 2010.

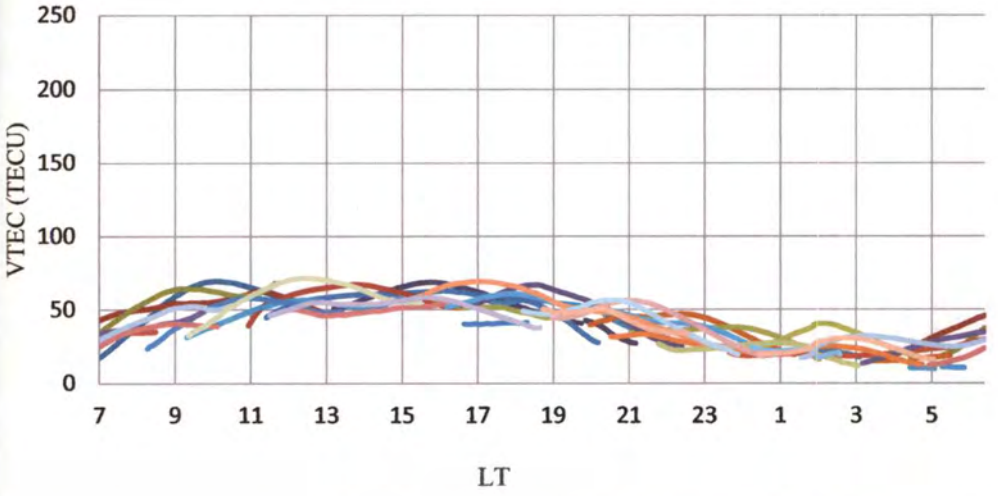

Figure 6.3 VTEC calculated by the minimization of standard deviation on 1 January 2010.

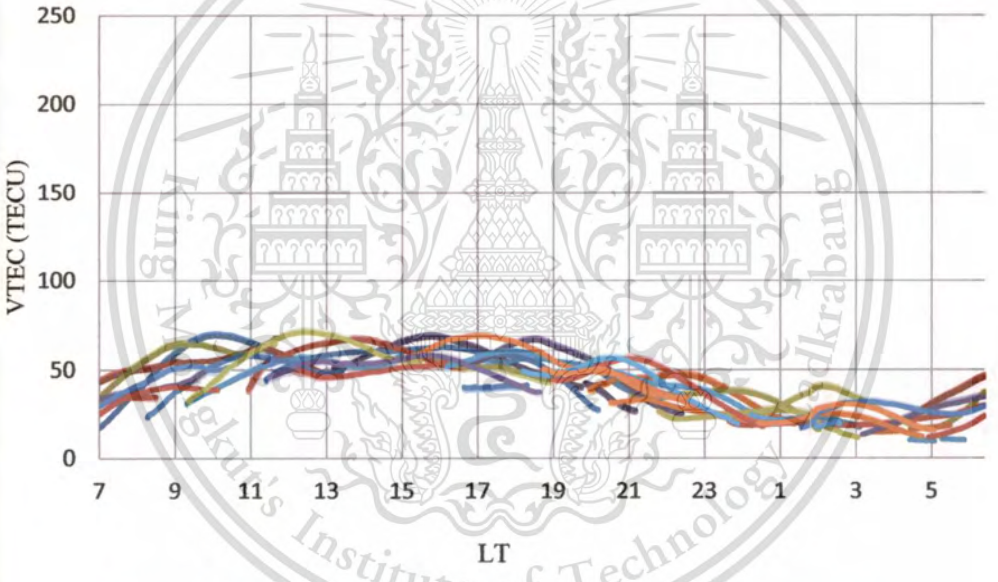

Figure 6.4 VTEC calculated by the median cut method on 1 January 2010.

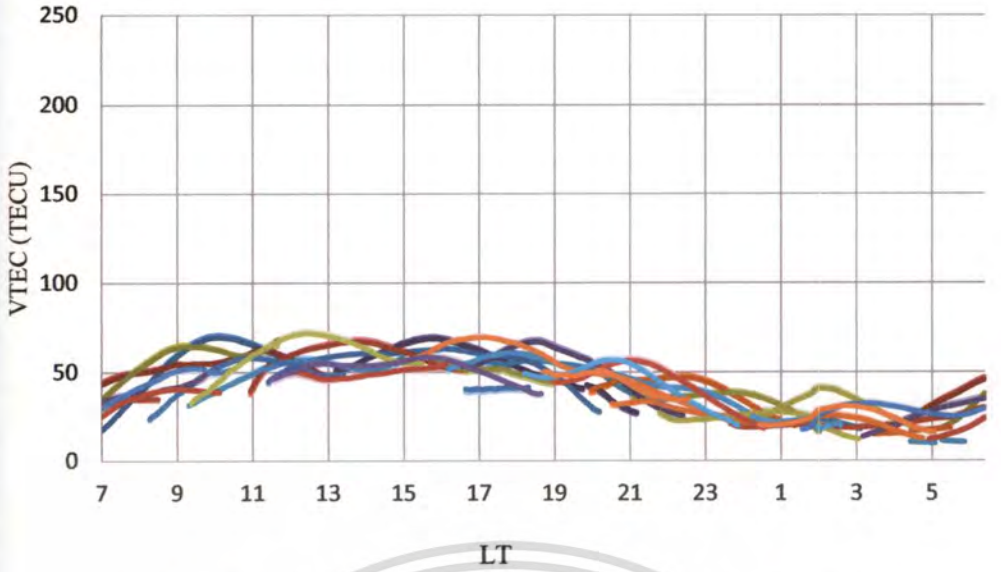

Figure 6.5 VTEC calculated by Lagrange interpolation on 1 January 2010.

As a result in Figure 6.2 to 6.5, the minimization of standard deviation of VTEC method gives the smooth curve of the VTEC and the minimum differences on the VTEC value from different GPS satellites. However, the two proposed methods, median cut and Lagrange interpolation methods give the smooth and similar VTEC to the minimization of standard deviation of VTEC method. Otherwise, the result shows that the VTEC which is obtained from the polynomial method does not give the smooth VTEC from different GPS signals.

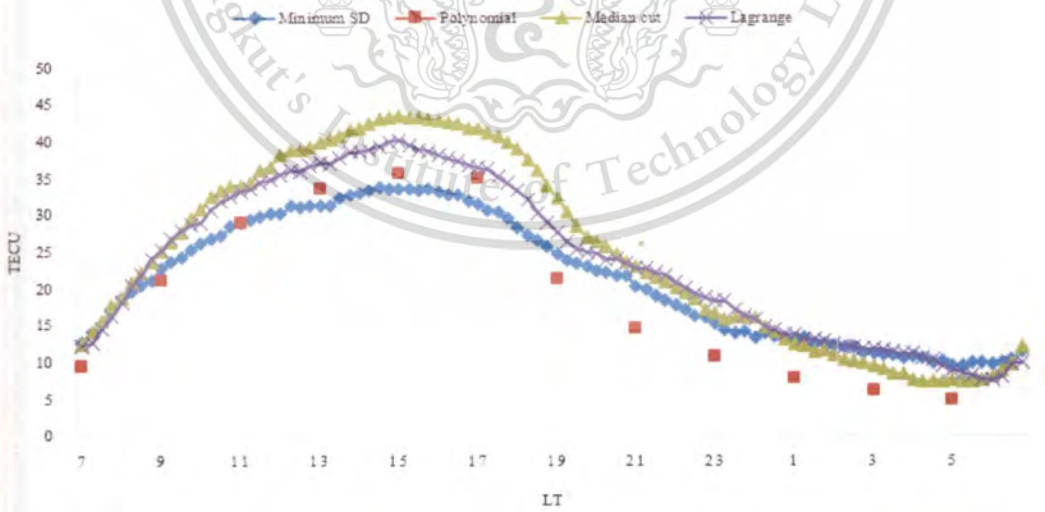

Figure 6.6 The comparisons of VTEC based on four GPS receiver bias methods at Chumphon station in 2006.

Figure 6.6 shows the investigation of the VTEC comparison used by the GPS receiver bias methods including the minimum standard deviation, the polynomial, the median cut, and the Lagrange interpolation. The comparisons among those methods in 2006 at Chumphon station show that, in daytime, the median cut gives the largest VTEC but the polynomial gives the smallest VTEC. At the noontime, the median cut method still gives the maximum values of VTEC however, the minimum standard deviation gives the minimum VTEC values. In nighttime, the polynomial give the lowest VTEC and others give closely VTEC values.

6.1.2 The variation of TEC

Figure 6.7 shows an example of the STEC values at Chumphon station on January 1, 2004. The VTEC values can be obtained with the median cut method. For a single receiver, the receiver bias is estimated to be -6.25 ns, giving the converged TEC curves with the minimum sum of standard deviation as shown in the bottom graphs of Figure 6.7.

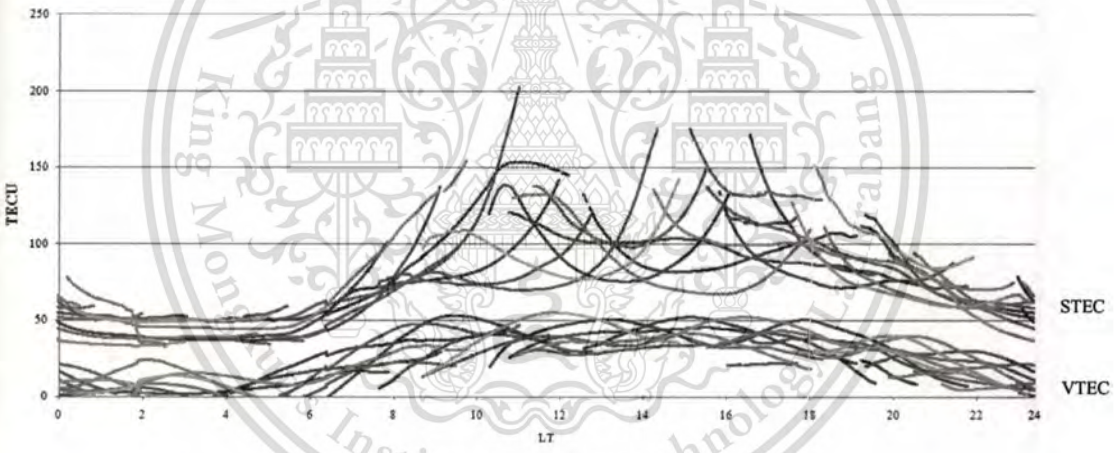

Figure 6.7 The STEC and VTEC based on GPS receiver estimation at Chumphon station, on January 1, 2010 (LT).

The diurnal variation of monthly median values of GPS-TEC measurements for equinox, summer and winter seasons is shown in Figure 6.8. The horizontal axis on each graph represents the hourly values at the local time, whereas the vertical axis on each graph shows the TEC values. It can be seen that for the diurnal variation behavior, TEC values decrease from 2004 to 2013, with the maximum values occurring at daytime hours, and the minimum values occurring at nighttime hours. The maximum TEC values in the equinox and winter are higher than those in the summer

during 2004-2013. The minimum values of TEC occur between 0300 LT and 0500 LT, while the maximum values occur between 1300 LT and 1800 LT. The largest TEC value is in the equinox and the lowest value is in summer. The monthly median values of TEC at Chumphon station for the period from 2004 to 2013 shows strong seasonal variations, with the largest daytime values occurring in equinox of 2004 and the smallest values in winter of 2008.

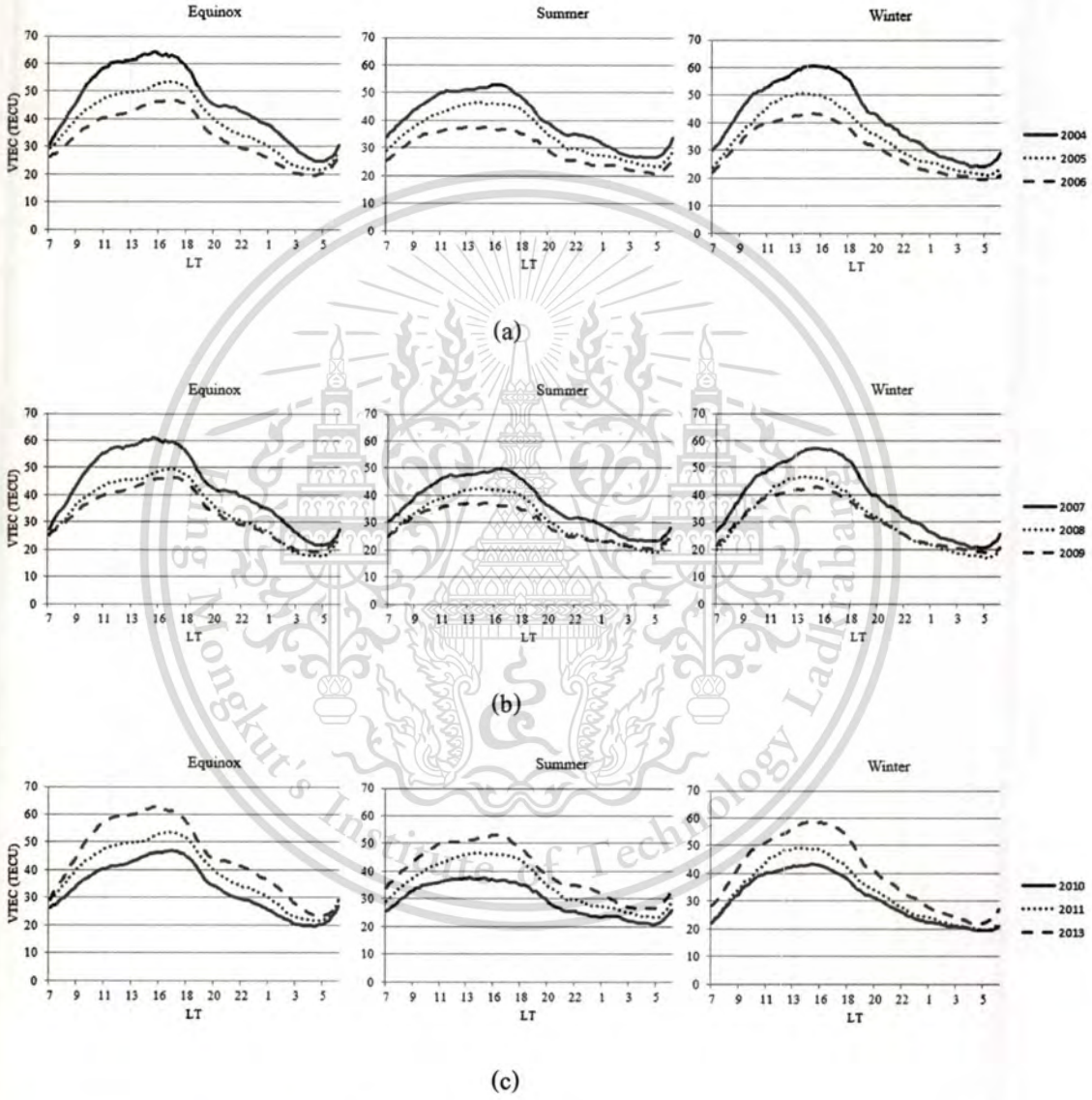

Figure 6.8 Seasonal variations of GPS-TEC measurements at Chumphon station during 2004-2013 (1 TECU = 10^{16} electrons/m^2).

6.1.3 Seasonal comparison of GPS TEC, IGS TEC and IRI TEC

In this section, we analyze the seasonal comparison of GPS TEC, IGS TEC, and IRI TEC. In this thesis, IRI 2007 model is based on the TEC derived from the ionogram, while the GPS TEC and IGS TEC data are derived from GPS data, it would be interesting to compare them with the IGS TEC obtained GIM TEC map. The IGS TEC map data is obtained at 10° N and 100° E, the location of Singapore, which is the nearest monitoring location to the Chumphon station. In Figure 5.5, there is the seasonal median TEC comparison of GPS TEC, IGS TEC and IRI-2007 TEC from 2004 to 2013. According to the high and low solar activities, the periods of study are classified into three seasons including equinox (March, April, September, and October), summer (May, June, July, and August), and winter (January, February, November, and December).

As shown in Figure 6.9, the IRI model generally underestimates the observed TEC. The underestimation is more evident at daytime than nighttime. The IRI-2007 TEC and the observed TEC are very similar during the nighttime of the equinox in 2005 and 2006. The significant difference is observed that GPS TEC is greater than IRI TEC according to the altitude (altitudes are about 20,200 kilometers and 2000 kilometers for GPS TEC and IRI TEC, respectively). In addition, Jin and Park (2007) studied the comparison of TEC at the grid point (37.5° N, 127.0° E) over South Korea, estimated from GPS and IRI-2001 TEC in different seasons; their results showed that the maximum TEC values occurred at about the noontime, between 1100 LT and 1500 LT.

The IGS TEC is generally higher than the GPS TEC for about 5 TECU during the daytime of the equinox, but it is lower than the GPS TEC at about 5 TECU during the nighttime of the winter in 2005 and 2006. The IRI-2007 TEC values follow the IGS model in the early morning more than any other time of day. The maximum difference between the GPS TEC and the IRI-2007 TEC are about 15 TECU during day time and about 5 TECU at the night time.

The maximum difference between the GPS TEC and IRI-2007 TEC during noontime indicates that the ionosphere at Chumpon or the equatorial area is expanded to cover larger TEC than other times. At equatorial latitude, there are the steepest gradients, sharp peaks and deep valleys and density crests on both sides of the equator as explained by Bilitza and Rinisch (2008). The occurrence of a prominent trough accompanied by maximum TEC values in the pre-noon and the afternoon at equatorial latitudes referred to as a noon bite-out which is a characteristic feature at an equatorial station that fall in the trough of the equatorial anomaly (Maeda, 1955; Rastogi, 1959).

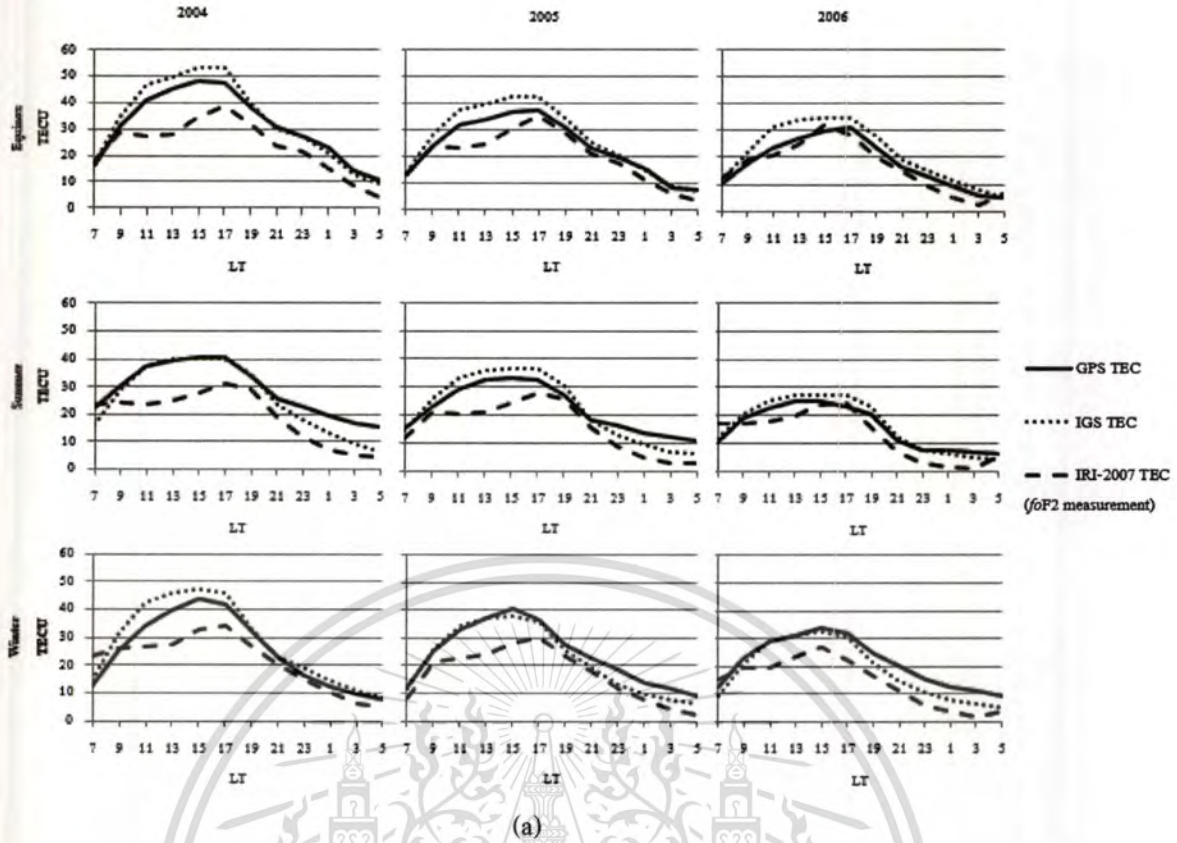

(a)

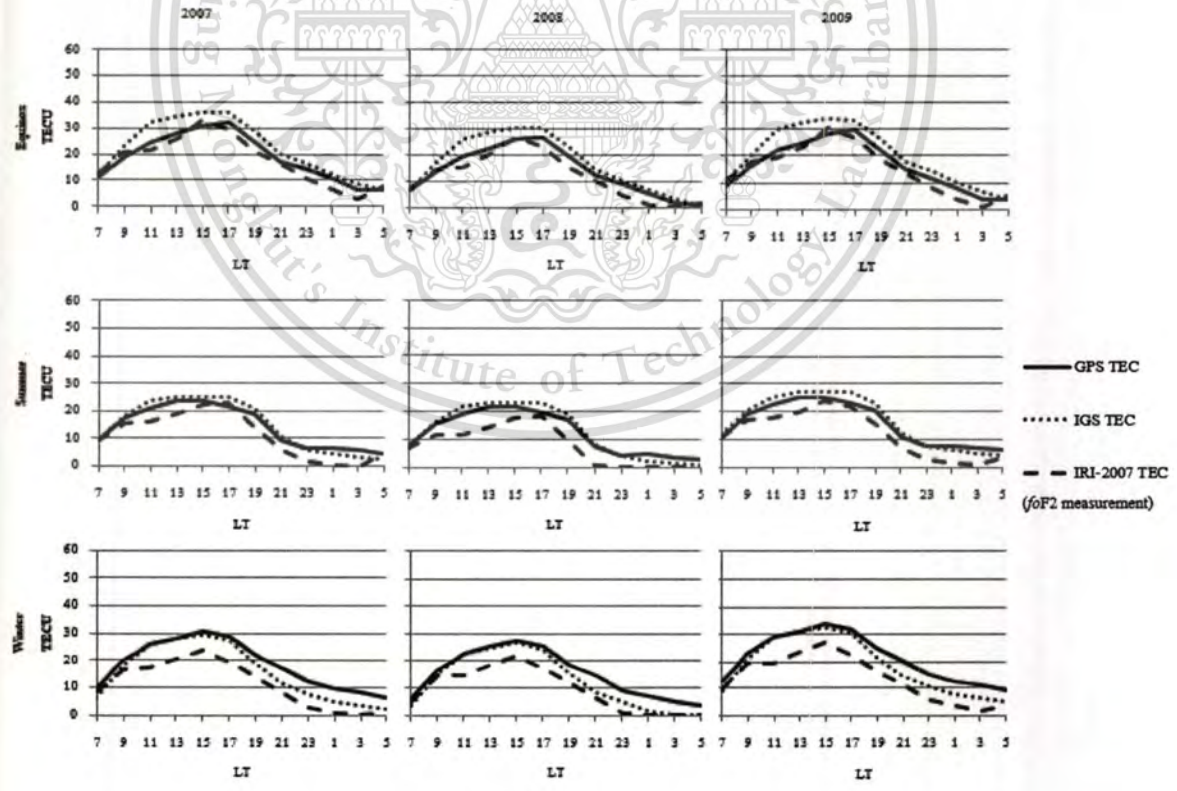

(b)

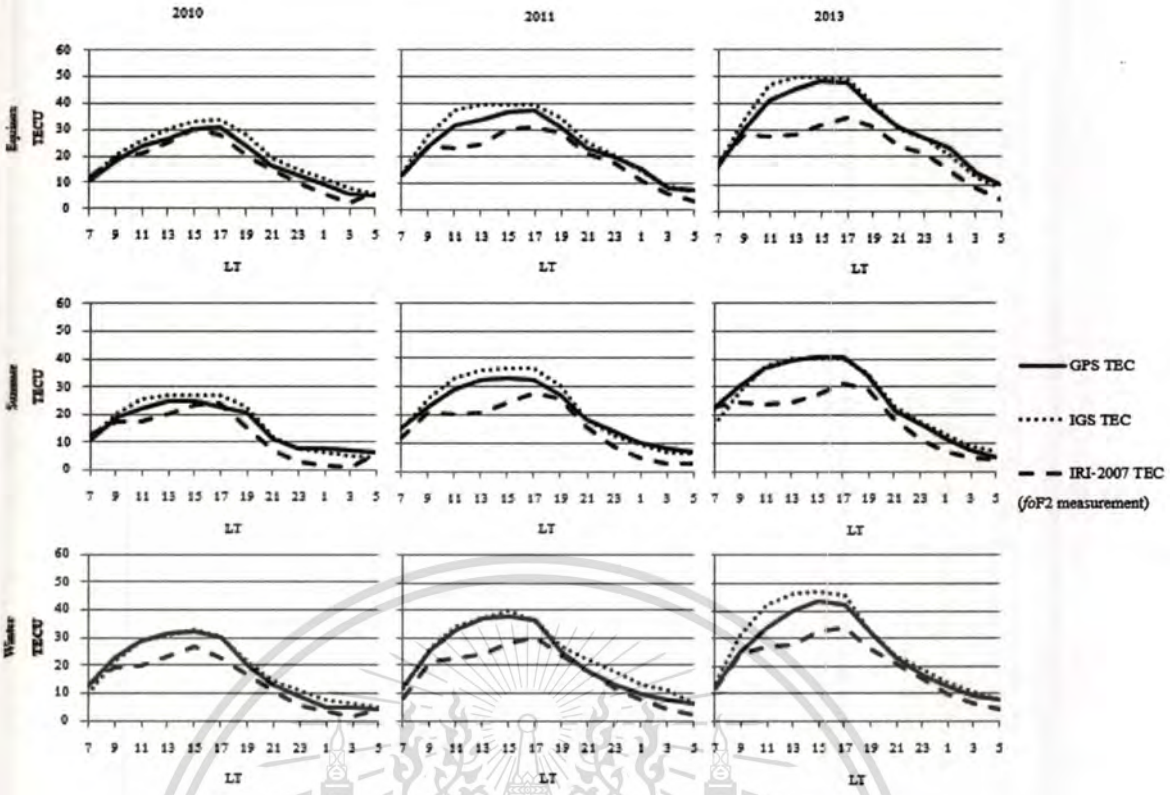

(c)

Figure 6.9 Comparison of GPS TEC, IGS TEC, and IRI TEC at Chumphon in (a) 2004-2006, (b) 2007-2009, and (c) 2010-2013.

6.1.4 The variation of rate of TEC index (ROTI)

In this thesis, the rate of TEC index (ROTI) is calculated and used for TEC monitoring specially in daily TEC and investigated the characteristics of TEC over a Chumphon station from 2004-2013. ROTI is more than 0.5 if the TEC fluctuates or the electron density at the ionosperic layer on that time is disturbed (Rabiu et al., 2007). By using the ionospheric disturbance Dst index described by Araujo-Pradere et al. (2004), we can find the disturbance day based on a geomagnetic storm day. Based on the Dst index at the Geomagnetic Equatorial Data center, those geomagnetic storm days are shown earlier in Table 6.1.

Then we can analyze the ROTI with a selected quiet day and the strongest geomagnetic storm day. The selected quiet day is on February 1, 2010 and the strongest geomagnetic days for each year excluding in November 2004 are May 15, 2005, December 15, 2006, October 25, 2011, and March 17, 2013, respectively. The results of the variation of rate of TEC index (ROTI) are shown in figure 6.10. In Figure 6.10 (a), the ROTI at Chumphon station on January 1, 2010 is

generally below 0.5. In Figure 6.10 (b), on May 15, 2005, the ROTI is above 0.5 at 13-14 LT. In Figure 6.10 (c), (d), and (e), the ROTI is lower than 0.5 for December 15, 2006, October 25, 2011, and March 17, 2013.

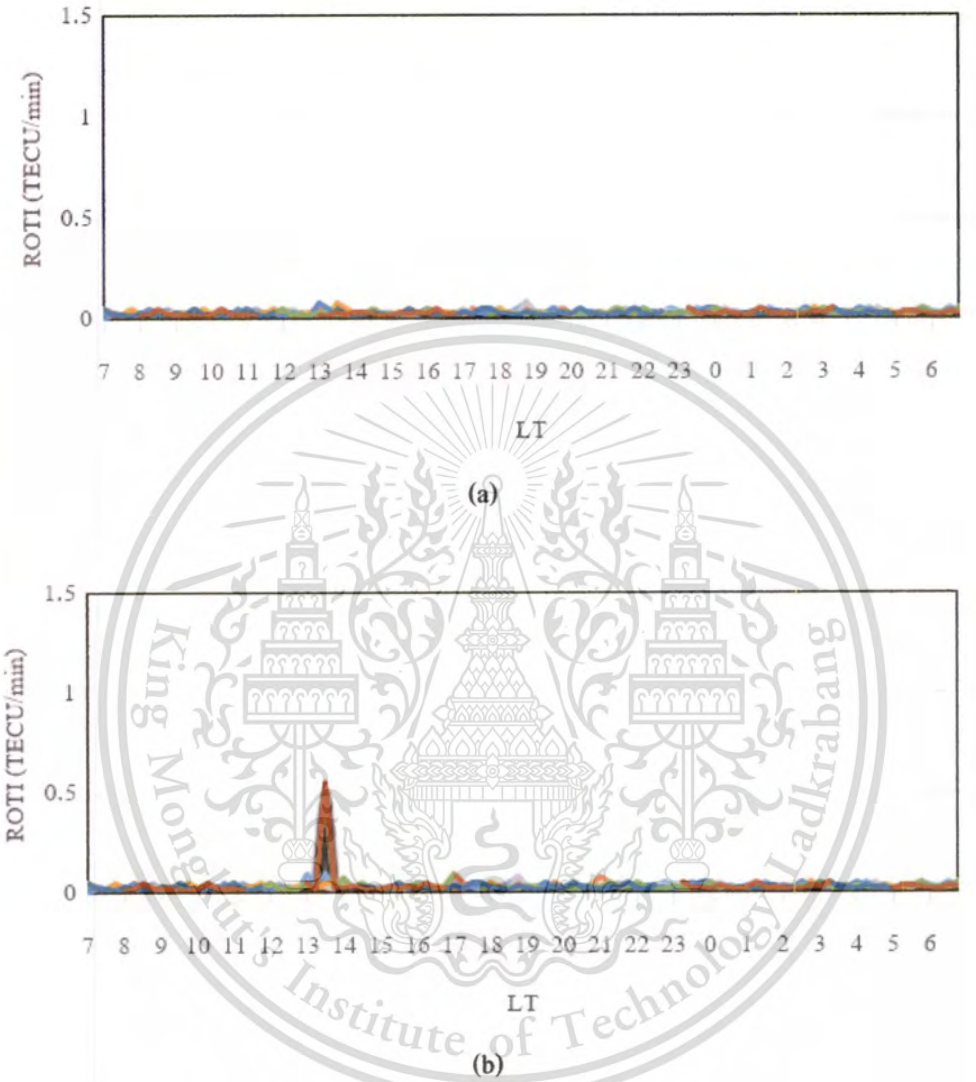

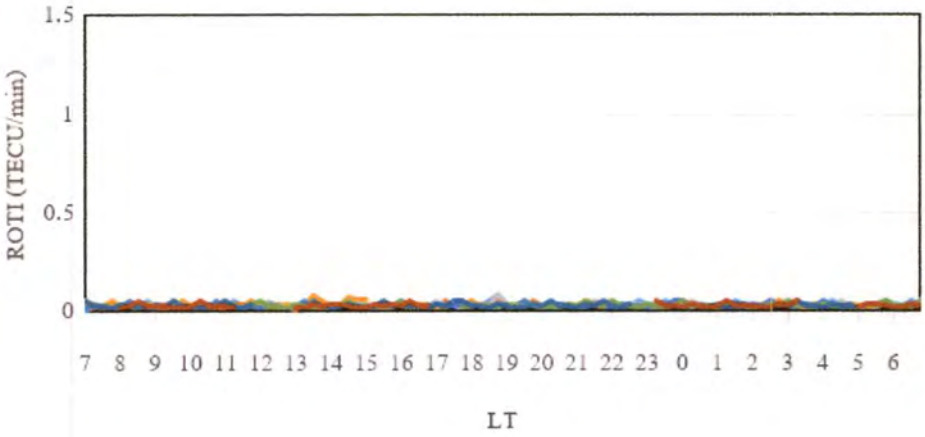

(c)

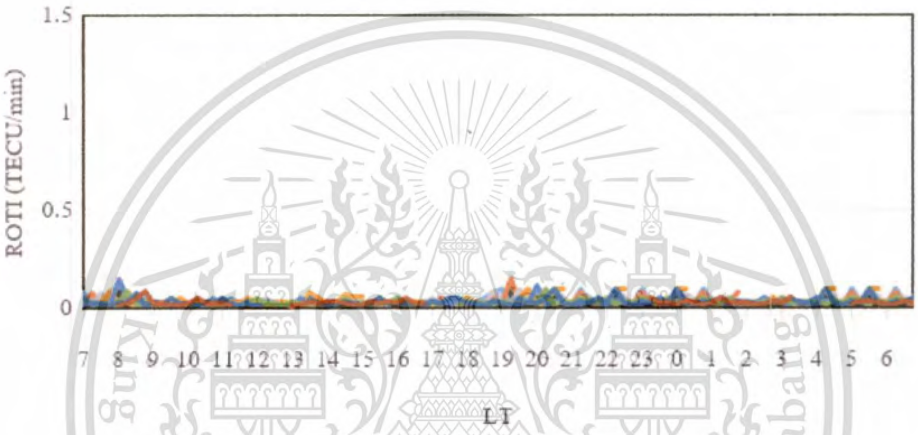

(d)

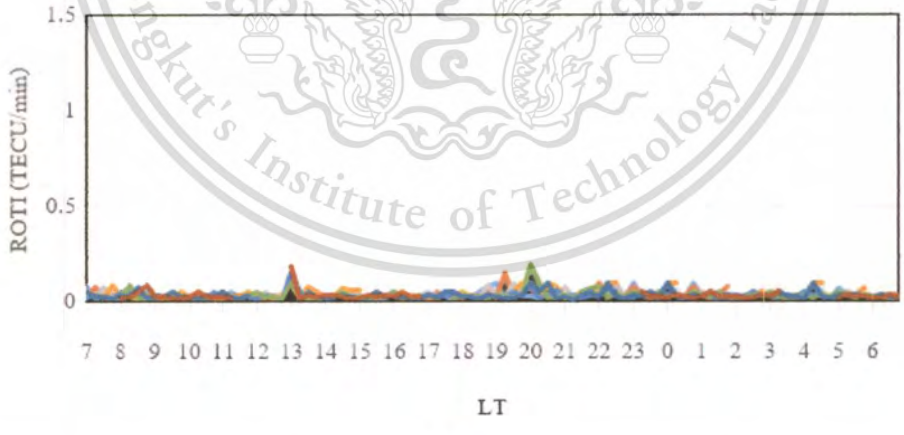

(e)

Figure 6.10 The rate of TEC index (ROTI) on the selected quiet day and the strongest geomagnetic storm day for (a) February 1, 2010, (b) May 15, 2005, (c) December 15, 2006, (d) October 25, 2011, and (e) March 17, 2013.

As a result, the ROTI can be used as the daily TEC monitoring but it cannot be used as the prediction of the geomagnetic storm day because ROTI is not more than 0.5 when the geomagnetic storm occurs. Now, let us investigate another day without the geomagnetic storm. The selected day is on March 15, 2013 as shown in Figure 6.11. Although the geomagnetic storm is not on this day, but ROTI can show the disturbance of TEC during 20 LT – 2 LT which the plasma bubble occurs.

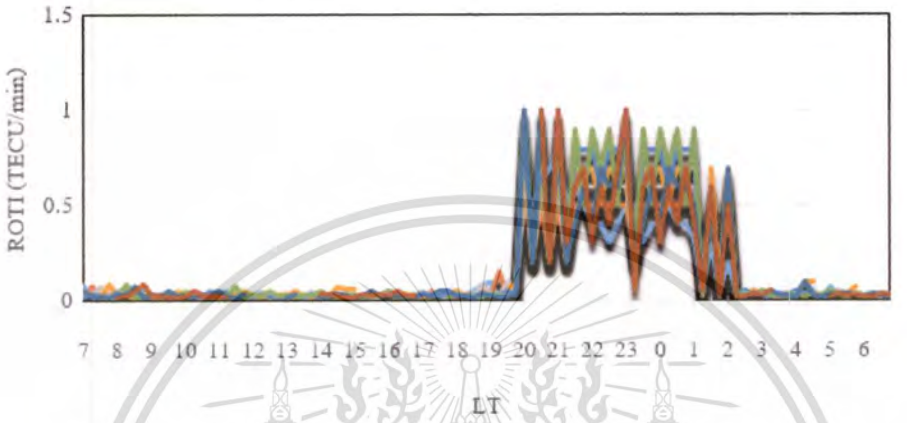

Figure 6.11 The rate of TEC index (ROTI) on the selected quiet day.

6.1.5 The variation of delay time

The variation of delay time of GPS measurements on 1 January 2004 is shown in Figure 6.12. The horizontal axis on each graph represents the hourly values at the local time, whereas the vertical axis on each graph shows the ionospheric delay time values. It can be seen that the maximum values of delay time is 25 ns occurring at 10 am to 22 pm and the minimum values of delay time is 4 ns at the period of 3-5 am. The TEC and ionospheric delay time effects on Chumphon station at the equatorial region. The GPS receiver at Chumphon station received the signal from the GPS satellite according to the ionosphere layer.

The investigation on GPS relay time based on TEC is studied to find the median of GPS delay time during 2004-2013. The results in Table 6.3 show that GPS PRN 27 transmits signal to the receiver at the maximum delay time of 21.661 ns, but GPS PRN 14 has the minimum delay time to the receiver at 7.221 ns.

Table 6.3 The median delay time for GPS satellites during the period of the year 2004-20013.

GPS (PRN)	Δt (ns)	GPS (PRN)	Δt (ns)	GPS (PRN)	Δt (ns)
1	20.662	11	18.027	21	8.664
2	18.068	12	13.158	22	9.258
3	20.693	13	16.776	23	7.593
4	19.525	14	7.221	24	18.846
5	12.386	15	10.339	25	11.312
6	13.577	16	12.332	26	16.118
7	20.877	17	17.203	27	21.661
8	21.627	18	8.5023	28	18.895
9	13.506	19	10.234	29	16.605
10	19.593	20	14.271	30	10.924

As a result, we investigate the delay frequency from 2004-2013 according to the results of GPS delay time in Table 6.3, the minimum delay frequency which transmits signal from GPS satellites to the GPS receivers at 46.166 MHz (21.661 ns) and the maximum delay frequency from GPS to the GPS receiver at 138.48 MHz (7.221 ns). This result shows that the GPS receiver should adjust the delay time and the frequency when receiver signals from the different GPS satellites.

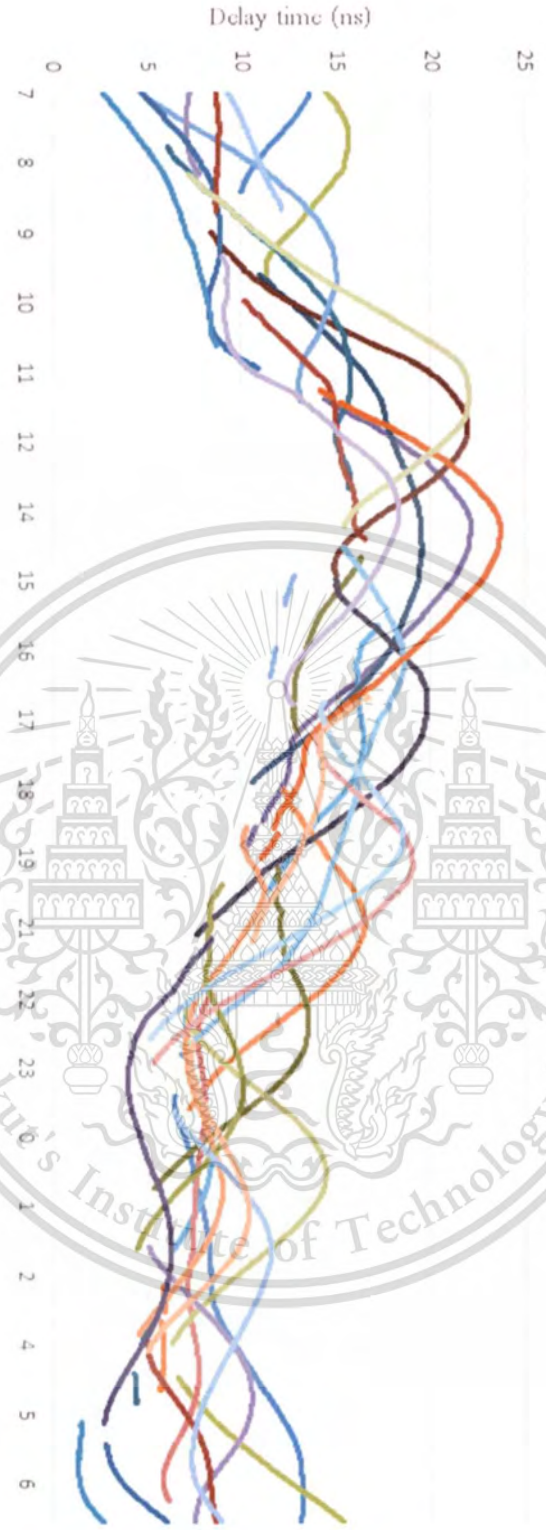

Figure 6.12 Ionospheric delay time for GPS.

6.1.6 The variation of the peak electron density in the F2-region (*Nm*F2)

In this section, we use the parameter *fo*F2 which is obtained from the ionogram recorded at Chumphon station during 2004-2009 to calculate the *Nm*F2 values following as shown in Figure 6.13. The plotting time starts at 0000 LT. It can be seen that the daytime values in 2004 are larger than those during 2005- 2009. The minimum values occur in the winter of 2008 and the maximum values are in the equinox of 2004. The minimum value of *Nm*F2 occurs between 0400 LT and 0600 LT, the pre-sunrise hours in all seasons.

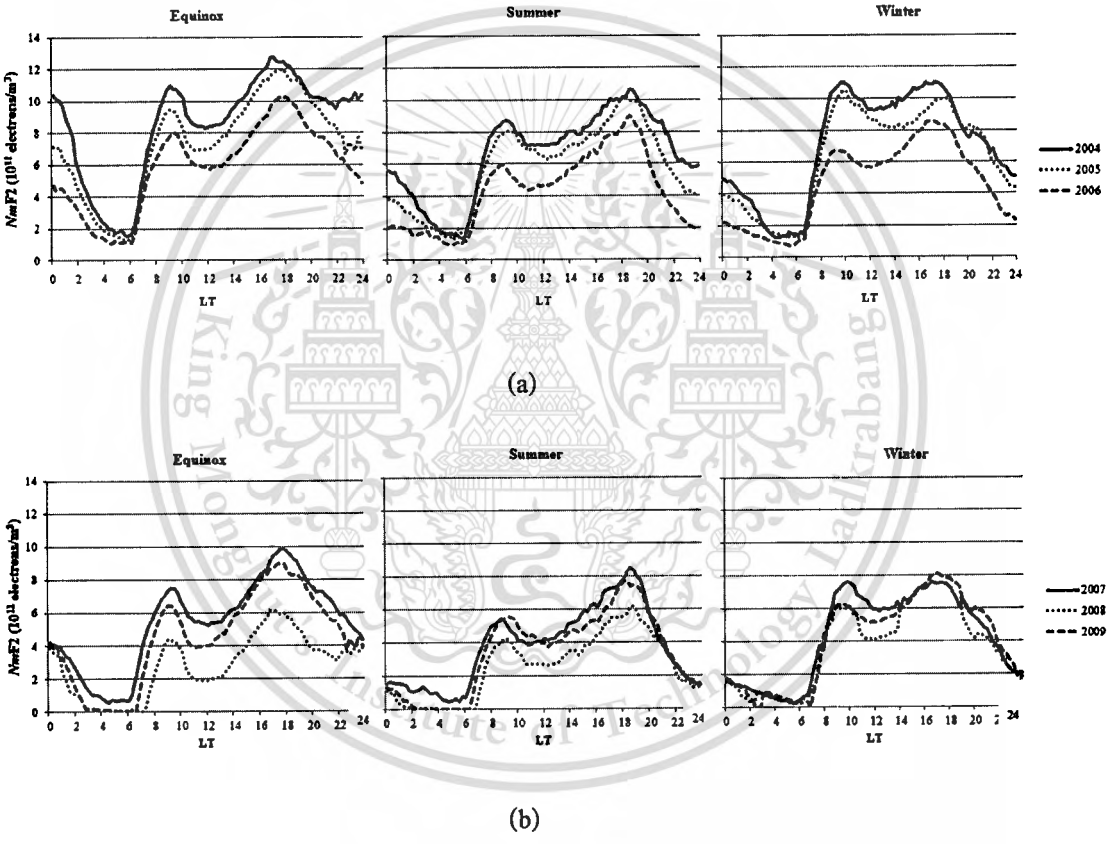

Figure 6.13 Seasonal variations of *Nm*F2 results at Chumphon station during 2004-2009.

6.1.7 The variation of ionospheric slab thickness

After calculation on NmF2 and TEC, the results of slab thickness can be found. As shown in Figure 6.14, this thesis study shows the diurnal variation of slab thickness for equinox, summer and winter seasons at Chumphon station from 2004 to 2009. It can be seen that the diurnal variation of slab thickness pattern follows similar trends during these three years. During day time, the slab thickness ranges from 200 kilometers to 580 kilometers for all seasons. During nighttime, the maximum value of slab thickness is 1250 kilometers for summer in 2004 with the maximum values occurring at pre-sunrise hours, and the minimum values occurring at nighttime hours. The maximum value of slab thickness occurs when the peak electron density in the F2 region is at the lowest level. The diurnal variation shows abnormal peaks during 0300 LT-0500 LT, the pre-sunrise hours. Furthermore, the diurnal variation shows two minima at 0900 LT and 1900 LT, during the post-sunrise and sunset hours.

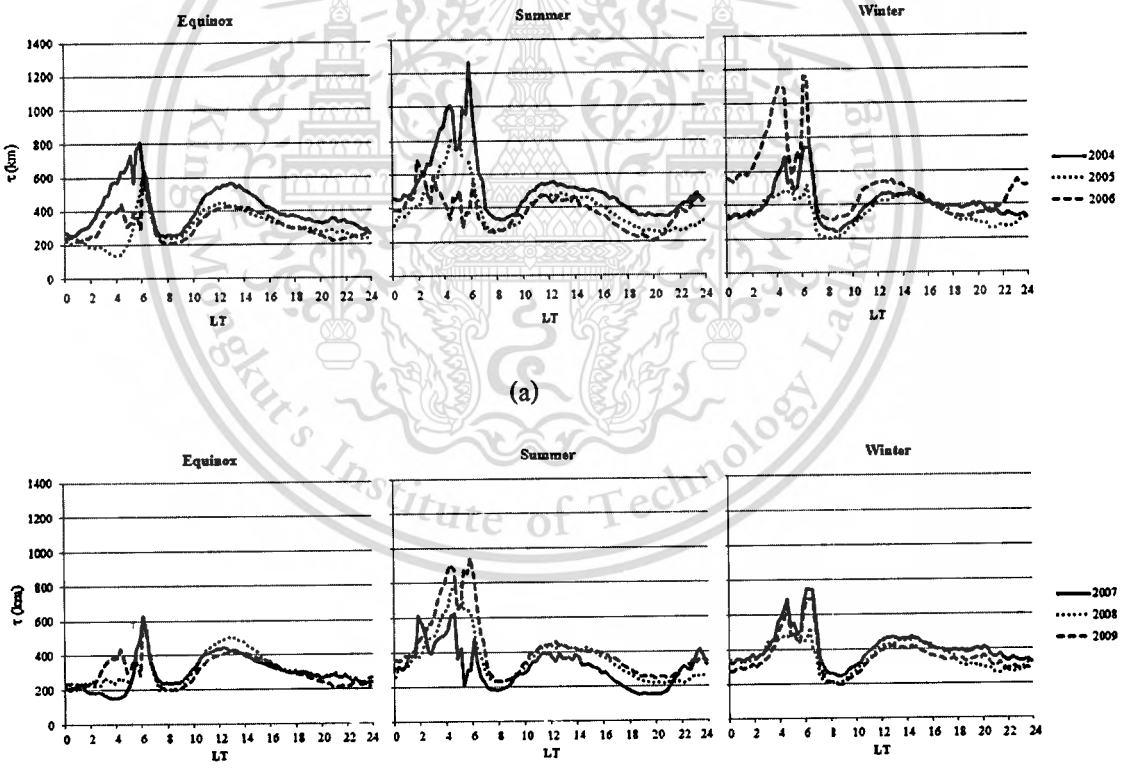

Figure 6.14 Seasonal variations of slab thickness results at Chumphon station during 2004-2009.

As a result, the average daily slab thickness is greatest during summer and the lowest value is during equinox of 2007. In addition, the slab thickness values are greater during nighttime than those during daytime for all seasons. Among all three years, the average TEC is lower as the year goes up, due to the higher solar activity in 2004 than 2005 to 2009. For all seasons from 2004-2009, our study confirms the results of Jayachandran et al. (2004) for the slab thickness variation at low, mid, and high latitudes.

This study also compared the slab thickness at Chumphon station in the equatorial latitude with Kokubunji station (35.71°N, 139.49°E) at the mid latitude. The slab thickness data at Kokubunji are given by Dr. Takuya Tsugawa from NICT, Japan. The results from Chumphon and Kokubunji stations are shown from 2004 to 2006 in Figure 6.15. In Figure 6.15, the dotted line represents the slab thickness variation at Chumphon station and the solid line is for Kokubunji station. The x axis represents the universal time (UT) and y axis is for TECU at all seasons during 2004-2006. The local times at Kokubunji station are two hours ahead of Chumphon.

As shown, the maximum slab thickness at Chumphon station is higher than that at Kokubunji station for summer during 2004-2006. During daytime, the lowest slab thickness variation is 150 kilometers at Chumphon station while the slab thickness variation reaches 1180 kilometers at Kokubunji station. However, during nighttime, the lowest slab thickness variation occurs at Kokubunji station but the highest slab thickness variation peaks, 1250 kilometers, at Chumphon station. In the equinox, the difference in the maximum slab thickness between Chumphon station and Kokubunji station is 200 kilometers. In the summer, the peak difference is as high as 850 kilometers, while, in the winter, this difference is about 450 kilometers.

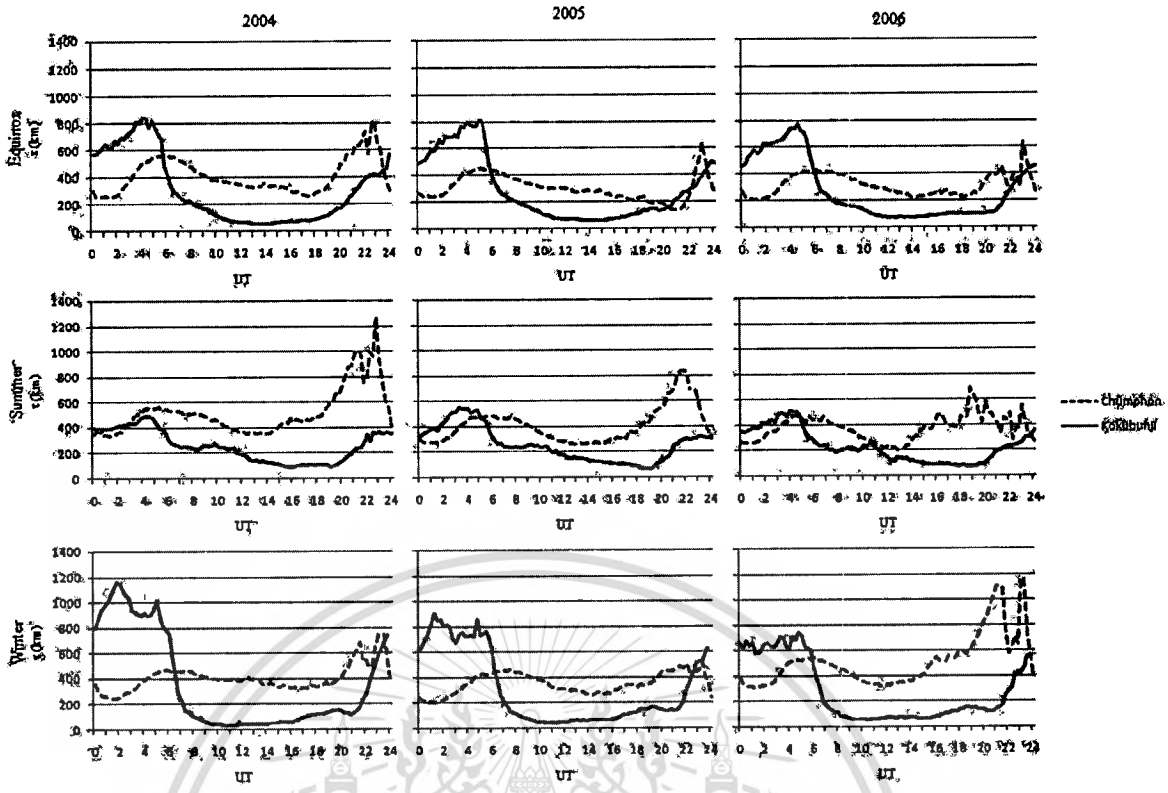

Figure 6.15 The variations of slab thickness at Chumphon and Kokubunji during 2004-2006.

6.2 Discussions

The data of TEC are obtained from Chumphon station, Thailand, located near the magnetic equator during 2004-2013. Those data are used for deriving and analyzing the diurnal, monthly, and seasonal variations. The GPS TEC derived from the TEC data at Chumpon equatorial station, Thailand is compared with the IRI TEC (IRI-2007 TEC) and the IGS TEC from 2004 to 2013. The maximum differences are about 15 TECU during daytime and about 5 TECU during nighttime. When compared with the IGS TEC, the GPS TEC measurements from the Chumphon station and the IGS model are quite similar, and both are higher than the TEC predicted from IRI-2007 model. The IRI-2007 model fits the GPS TEC data mostly in the morning hours, but generally underestimates the GPS TEC since the plasmasphere is not included in the model. The underestimation is more apparent at daytime than nighttime, particularly, during the noon bite-outs.

The ionospheric delay time effects on the Chumphon station at equatorial region. The GPS receiver receives the GPS delay signal according to the ionosphere layer by maximizing at 25 ns. The highest delay time for GPS satellites during 2004-2013 is 21.661 ns and the lowest delay time is 7.221 ns.

The study indicates that the minimum *Nm*F2 values occur in the winter of 2008 and the maximum values are in the equinox of 2004. The minimum value of *Nm*F2 occurs between 0400 LT and 0600 LT, the pre-sunrise hours in all seasons. The slab thickness variation at the equatorial latitude of Chumphon location is about 200-580 kilometers during daytime for all seasons. The highest slab thickness variation peaks at 1250 kilometers. However, at low latitude, the slab thickness variation is about 239-344 kilometers from Jayachandran et al. (2004) and about 160-300 kilometers studied by Gulyaeva et al. (2004). For mid latitude, the slab thickness variation is about 304-345 kilometers reported by Jayachandran et al. (2004) and about 153-346 kilometers studied by Gulyaeva et al. (2004). Similarly, for high latitude, slab thickness variation is about 235-351 kilometers and 143-346 kilometers from Jayachandran et al. (2004) and Gulyaeva et al. (2004), respectively. At the equatorial latitude of Chumphon station, the median diurnal variations of the seasonal slab thickness are at the highest levels during the summer. This result is also found by Chuo (2007) for low latitude and by Jayachandran et al. (2004) for mid-latitude and high latitude. However, Gulyaeva et al. (2004) shows that the highest values of slab thickness at low latitude are at equinox.

At Chumphon station, the local minimum for *fo*F2 around 1200 LT is caused by the strong eastward electric field and the resulting fountain effect. In general, lower TEC and *Nm*F2 in the summer as compared to other seasons are caused by atmospheric composition changes, generally referred to as the seasonal anomaly (Chuo, 2007). Higher *Nm*F2 values and smaller slab thickness in the equinox as compared to the other seasons around midnight are caused by the convergent wind toward the equator. A large slab thickness around 0300LT-0500 LT can be interpreted as follows: During the night, chemical recombination proceeds in the lower ionosphere. At mid-latitudes, however, plasma is supplied from the plasmasphere along magnetic field lines. The equatorial ionosphere on the other hand is not connected to the plasmasphere by magnetic field lines, and therefore no plasma replenishment is provided.

The increasing in *fo*F2 and TEC with decreasing slab thickness indicates that TEC increases lower than *Nm*F2. It is interesting to note that there is an abnormal peak (1250 km) in the slab thickness during the pre-sunrise period (0300LT - 0500 LT), particularly in summer and winter

for all the solar phases. Two major factors are associated with this peak at pre-sunrise: electric field and zonal neutral wind. Woodman (1970) reports an enhanced vertical plasma drift before the sunrise in the F-region at Jicamarca. In addition, the researchers (Krishna Murthy et al., 1990; Aggson et al., 1995; Titheridge, 1973) have suggested that the pre-sunrise peak in the slab thickness is due to the downward movement of the ionosphere, when the neutral winds maintaining the ionosphere decrease or reverse. The post-sunset increase in the slab thickness observed during different seasons at low latitudes (Bhuyan et al., 1986) could be attributed to the equatorial pre-reversal enhancement caused by the occurrence of a post-sunset strong eastward electric field existing over equatorial latitudes (Fejer et al., 1979).

As the GPS signals propagate through the ionosphere, they are refracted and slowed especially when they traverse regions of intense auroral currents. The ionosphere is used as a transmitter of radio frequency communication signals. The radio wave communication is significantly influenced by the ionospheric properties such as TEC, *fo*F2, and slab thickness. High frequency radio wave communications are most affected from the ionosphere to carry the signal to distances beyond the local horizon. At the times of high ionospheric activity, the signal can be even completely absorbed making the HF radio propagation impossible and can be degraded or even completely lost during times of high solar activity. The ionospheric delay time effects on the Chumphon station at equatorial region. The GPS receiver is received the GPS delay signal according to the ionosphere layer by the minimum delay frequency which transmits signal from GPS satellites to the GPS receivers at 46.166 MHz and the maximum delay frequency from GPS to the GPS receiver at 138.48 MHz.

CHAPTER 7

CONCLUSIONS AND SUGGESTIONS

7.1 Conclusions

In this thesis, the two proposed GPS receiver bias methods are presented for improving the TEC computation. One is the median cut method and the other is the Lagrange interpolation method. These two methods are suitable for a single GPS receiver station. The proposed methods described in the thesis are efficient and qualified for use to derive the absolute TEC, and to determine the biases of GPS receiver. Since the daily variation of GPS satellite biases is small, it is only necessary that the instrumental receiver biases be estimated or calibrated from time to time. The proposed median cut method for estimating a single receiver's bias is faster and sufficiently accurate for a receiver at the equatorial magnetic latitude. Lagrange interpolation method has the advantage to meet the requirement of being able to monitor the ionosphere in near real-time applications.

The GPS-derived TEC is mainly contributed from the electrons in the F2-region. Those data are used for deriving and analyzing the diurnal, monthly, and seasonal variations. The GPS TEC derived from the TEC data at Chumpon equatorial station, Thailand is compared with the IRI TEC (IRI-2007 TEC) and the IGS TEC from 2004 to 2013. The maximum differences are about 15 TECU during daytime and about 5 TECU during nighttime. When compared with the IGS TEC, the GPS TEC measurements from the Chumphon station and the IGS model are quite similar, and both are higher than the TEC predicted from IRI-2007 model. The IRI-2007 model fits the GPS TEC data mostly in the morning hours, but generally underestimates the GPS TEC. The underestimation is more apparent at daytime than nighttime, particularly, during the noon bite-outs.

This study shows that the slab thickness at Chumphon located near the equatorial latitude is much larger than those found at the low, mid, and high latitudes. The seasonal variations show that the largest average slab thickness appears during summer, but the lowest value occurs during the equinox. The diurnal variation shows abnormal peaks at 1250 kilometers during 0300LT - 0500 LT, the pre-sunrise hours in the summer of 2004. During daytime, the slab thickness ranges from 200 to 580 kilometers for all seasons. During nighttime, the value of slab thickness varies between 200 and 1250 kilometers. In addition, this study finds that the maximum ionospheric slab thickness

value at Chumphon is higher than the maximum value at Kokubunji. The result confirms that the slab thickness at the equatorial latitude is larger than those found at mid latitude.

Satellite navigation systems such as Global Positioning System (GPS) or the European Galileo operate by transmitting radio waves from the spacecraft to ground based receivers. Signals from several satellites are then used to calculate the observing position to high accuracy. As the signals propagate through the ionosphere, they are refracted and slowed especially when they traverse regions of intense auroral currents. The ionospheric delay time effects on the Chumphon station at equatorial region. The GPS receiver receives the GPS delay signal through the ionosphere layer by the minimum delay frequency which transmits signal from GPS satellites to the GPS receivers at 46.166 MHz and the maximum delay frequency from GPS to the GPS receiver at 138.48 MHz.

The ionosphere is utilized as a transmitter of radio frequency communication signals. As the radio amateur knows, the radio wave communication is significantly influenced by the ionospheric properties such as TEC, *fo*F2, and slab thickness. High frequency radio wave communications are most affected, as they use the reflection from the ionosphere to carry the signal to distances beyond the local horizon. At the times of high ionospheric activity, the signal can be even completely absorbed making the HF radio propagation impossible. Moreover, the telecommunication systems increasingly utilize ultra-high frequency bands to transmit signal to satellites to be relayed to other locations. Also this frequency range is vulnerable to the TEC in the ionosphere, and can be degraded or even completely lost during times of high solar activity.

7.2 Suggestions

In this thesis, the two proposed GPS receiver bias methods, the median cut method and the Lagrange interpolation method, can be used for improving the TEC computation. Those two methods are to use in a single GPS receiver station. However, those methods can probably apply to the multi GPS receiver stations by calculating the VTEC for each stations and by comparing the TEC value to each GPS receiver stations. In the median cut method, the daily median GPS receiver bias can be less than or more than 96 important points. These important points depend on what the purpose of TEC observation. For example, the median cut point can be one point for a day TEC monitor or the median cut point can be 1,440 points for one minute TEC observation. For the real time TEC monitoring, Lagrange interpolation method is significantly utilization to use the time interval less than one minute.

For the future work, the median cut method and Lagrange interpolation can certainly apply to estimate the receiver bias of other satellites which their orbits are above the ionospheric layer at 500 kilometers in any period of years. Then, the study of total electron content at equatorial region is not only by using GPS satellite, but also using other satellites with their altitudes above the ionosphere.

BIBLIOGRAPHY

Adohi, B.J.P., Vila, P.M., Amory-Mazaudier, C., Petitdidier, M. 2008. **"Equinox transition at the magnetic equator in Africa."** Ann. Geophys. 26, 1777–1792.

Aggson, T.L., Herrero, F.A., Johnson, J.A., Pfaff, R.F., Laakso, H., Maynard, N.C., Moses, J.J., 1995. **"Satellite observation of zonal electric field near sunrise in equatorial ionosphere."** J. Atmos. Terr. Phys. 57, 19–24.

Araujo-Pradere, E.A., Fuller-Rowell, T.J., Bilitza, D., 2004. **"Ionospheric variability for quiet and perturbed conditions."** Advances in Space Research 34 (9).

Appleton, E. V. 1954. **"The anomalous equatorial belt in the F2-layer."** J. Atmos. Terr. Phys., 5, 348.

Arikan, F., Erol, C. B., and Arikan, O. 2003. **"Regularized estimation of vertical total electron content from Global Positioning System data."** J. Geophys. Res., 108(A12), 1469, doi:10.1029/2002JA009605.

Bhuyan, P. K., Singh, L., Tyagi, T.R. 1986. **"Equivalent slab thickness of the ionosphere over 26°N through the ascending half of a solar cycle."** Ann. Geophys., 4, 131.

Bilitza, D., Hernandez-Pajares, M., Juan, J.M., Sanz, J. 1998. **"Comparison between IRI and GPS-IGS derived electron content during 1991-97: first results."** Physics and Chemistry of the Earth 24 (4), 311–319.

Bilitza, D. 1990. **"International Reference Ionosphere: IRI-90."** National Space Science Data Center, Rep. 90-22, Greenbelt, Maryland.

Bilitza, D. 2001. **"International Reference Ionosphere 2000."** Radio Sci. 38 (6), 261–275.

Bilitza, D., Rawer, K. 1996. **"International Reference Ionosphere, in: The Upper Atmosphere – Data Analysis and Interpretation."** Springer-Verlag, Berlin, Heidelberg, pp. 735–772.

Bilitza, D. and Reinisch, B. 2008. **"International Reference Ionosphere 2007: Improvements and new parameters."** Adv. Space Res. 42, 599–609.

Belehaki, A., Jakowski, N., Reinisch, B.W. 2003. **"Comparison of ionospheric ionization measurements over Athens using ground ionosonde and GPS derived TEC values."** Radio Sci. 38 (6), 1105.

Belehaki, A., Jakowski, N., Reinisch, B.W. 2004. **"Plasmaspheric electron content derived from GPS TEC and digisonde ionograms."** Adv. Space Res. 33, 237–833.

Blewitt, G. 1990. "**An automatic editing algorithm for GPS data.**" Geophys. Res. Lett., 17, 199-202.

Bremer, J. 2008. "**Long-term in the ionosphere E and F1 regions.**" Ann. Geophys 26 (5), 1189–1197.

Brunini, C., Meza, A., and Bosch, W. 2005. "**Temporal and spatial variability of the bias between TOPEX- and GPS derived total electron content.**" J Geod., 79, 175–188.

Brunini, C., Meza, A., Azpilicuata, F., Van zele, M.A., Gende, M. and Diaz, A. 2004. "**A new ionosphere monitoring technology based on GPS.**" Astrophys. Space Sci., 290, 415-429.

Chen, W., C. Hu, S. Gao, Y. Chen, and X. Ding. 2004. "**Absolute ionospheric delay estimation based on GPS PPP and GPS active network.**" International Symposium on GNSS/GPS, Sydney, Australia, 6–8 Dec.

Chuo, Y.J. 2007. "**The variation of ionospheric slab thickness over equatorial ionization area crest region.**" J. Atmos. Solar-Terr. Phys., 69, 947-954.

Coco, D. S., Coker, C., Dahlke, S. R., and Clynch, J. R. 1991. "**Variability of GPS satellite differential group delay biases.**" IEEE Trans. Aerosp. Electron. Syst., 27, 931–938.

Davies, K. 1980. "**Recent progress in satellite radio beacon studies with particular emphasis on the ATS 6 radio beacon experiment.**" Space Sci. Rev. 25, 357.

Dow, J.M., Neilan, R. E., and Rizos, C. 2009. "**The International GNSS Service in a changing landscape of Global Navigation Satellite Systems.**" Journal of Geodesy. 83:191–198, DOI: 10.1007/s00190-008-0300-3

Fejer, B.G., Gonzales, C.A., Farley, D.T., Kelley, M.C.1979. "**Equatorial electric fields during magnetically disturbed conditions: 1. The effect of the interplanetary magnetic field.**" J. Geophys. Res. 84, 5797–5802.

Forbes, J.M., Palo, S.E., Zhang, X. 2000. "**Variability of the ionosphere.**" J. Atmos. Solar-Terr. Phys. 62, 685–693.

Gil, A., Segura, J., Temme, N. 2007. **Numerical Methods for Special Functions**, SIAM.

Goodwin, G. L., Silby, J. H., Lynn, K. J., Breed, A. M., Essex, E. A. 1995. "**GPS satellite measurements: ionospheric slab thickness and total electron content.**" J. Atmos. Solar-Terr. Phys., 57(14), 1723-1732.

Gulyaeva, T., Huang, X., Reinisch, B. 2002. **"Plasmaspheric extension of topside electron density profiles."** Adv. Space Res. 29 (6), 825–831.

Gulyaeva, T.L., Jayachandran, B., Krishnankutty, T.N. 2004. **"Latitudinal variation of ionospheric slab thickness."** Adv. Space Res. 33, 862-865.

Gurtner, W., Beutler, G., Botton, S., Rothacher, M., Geiger, A., Kahle, H.G., Schneider, D., Wiget, A., 1989. **"The use of the Global Positioning System in mountainous areas."** Manuscripta Geodaetica. 14: 53-60

Henley, E. J. and Kumamoto, H. 1981. **Reliability Engineering and Risk Assessment.** Prentice Hall, Englewood Cliffs, NJ. (ISBN 0-13-772251-6)

Hernandez-Pajares, M., Juan, J. M., Sanz, J. and Orus, R. 2004. **"Wide area real time kinematics with Galileo and GPS signals."** ION GNSS 17th International Technical Meeting of the Satellite Division, Long Beach, Calif., 21–24 Sept.

Huang, X and Reinisch, B. 2001. **"Vertical electron content from ionograms in real time."** Radio Sci. 36 (2), 335–342.

Iwamoto, I., Katoh, H., Maruyama, T., Minakoshi, H., Watari, S., Igarashi, K. 2002. **"Latitudinal variation of solar flux dependence in the topside plasma density: comparison between IRI model and observations."** Adv. Space Res. 29 (6), 877–882.

Jakowski, N., Sardon, E., Engler, E., Jungstand, A., and Klahn, D. 1996. **"Relationships between GPS-signal propagation errors and EISCAT observations."** Ann. Geophys., 14, 1429–1436.

Jakowski, N., Sardon, E., Schlu¨ter, S. 1998. **"GPS-Based TEC observations in comparison with IRI95 and the European TEC model NTCM2."** Adv. Space Res. 22 (6), 803–806.

Jayachandran, B., Krishnankutty, T. N., Gulyaeva, T. L. 2004. **"Climatology of ionospheric slab thickness."** Ann. Geophys., 22, 25-33.

Jin, S., Cho, J., Park, J. 2007. **"Ionospheric slab thickness and its seasonal variations observed by GPS."** J. Atmos. Solar-Terr. Phys., 69, 1864-1870.

Jin, S. G. and Park, P. H. 2007. **"GPS ionospheric tomography: A comparison with the IRI-2001 model over South Korea."** Earth Planets Space, 59, 287–292.

Jodogne, J.C., Nebdi, H., Warnant, R. 2004. **"GPS TEC and ITEC from digisonde data compared with NEQUICK model."** Adv. Sapce Res. 2, 269–273.

Kee, C., and Yun, D. 2002. **"Extending coverage of DGPS by considering atmospheric models and corrections."** J. Navig., 55, 305–322, doi:10.1017/S0373463302001741.

Kenpankho, P., Supnithi, P., Tsugawa, T., and Maruyama, T. 2011. **"Variation of ionospheric slab thickness observations at Chumphon equatorial magnetic location."** Earth Planets Space, 63, 359-364.

Kenpankho, P., Watthanasangmechai, K Supnithi, P., Tsugawa, T., and Maruyama, T. 2011. **"Comparison of GPS TEC measurements with IRI TEC prediction at the equatorial latitude station, Chumphon, Thailand."** Earth Planets Space, 63, 365-370.

Komjathy, A., and Langley, R. 1996. **"An assesment of predicted and measured ionospheric total electron content using a regional GPS network."** Natl. Tech. Meet., Inst. of Navig. Santa Monica, Calif., 22–24 Jan.

Krishna Murthy, B.K., Hari, S.S., Somayajulu, V.V., 1990. **"Nighttime equatorial thermospheric meridional winds from ionospheric h'F data."** J. Geophys. Res. 95, 4307–4310.

Lanyi, G. E., and Roth,T. 1988. **"A comparison of mapped and measured total ionospheric electron content using Global Positioning System and beacon satellite observations."** Radio Sci., 23, 483–492.

Lin, L. S. 2001. **"Remote sensing of ionosphere using GPS measurements."** the 22nd Asian Conference on Remote Sensing, 5–9 Nov., Singapore.

Ma, G. and Maruyama, T. 2003. **"Derivation of TEC and estimation of instrumental biases from GEONET in Japan."** Ann. Geophys., vol. 21, 2083-2093.

Maeda, H. 1955. **Rep. Ion. Research Japan**. 9, 60.

Makela, J. J., Kelley, M. C., Sojka, J. J., Pi, X and Manucci, A. J. 2001. **"GPS normalization and preliminary modeling results of total electron content during mid latitude space weather event."** Radio Sci., 36, 356–361.

Mannucci, A.J., Wilson, B.D., Yuan, D.N., Ho, C.M., Lindqwister, U.J., Runge, T.F., 1998. **"A global mapping technique for GPS-derived ionospheric total electron content measurements."** Radio Science, 33, 3, pp. 565-582.

Maruyama, T. 2001. **Ionospheric Radio Propagations**, Science of Space Environment, pp.112-113.

Millward, G. H., I. C. F. Mu¨ ller-Wodarg, A. D. Aylward, T. J. Fuller-Rowell, A. D. Richmond, and R. J. Moffett. 2001. **"An investigation into the influence of tidal forcing on F region**

equatorial vertical ion drift using a global ionosphere-thermosphere model with coupled electrodynamics." J. Geophys. Res., 106, 24,733– 24,744.

Miyazaki, S., Saito, T., Sasaki, M., Hatanaka, Y., and Iimura, Y. 1997. **"Expansion of GSI's nationwide GPS array."** Bull. Geogr. Surv.Inst., 43, 23–34.

Mosert, M., Ezquer, R., Jadur, C., Oviedo, R. 2004. **"del V Time variation of total electron content over Tucuma´n, Argentina."** Geofisica Internacional 43 (2), 143–151.

Namgaladze, A. A., Korenko, Y. N., Klimenko, V. V., Karpov, I. V., Surotkin, V. A., and Naumova, N. M. 1991. **"Numerical modelling of the thermosphere-ionosphere-protonosphere system."** J. Atmos. Sol.-Terr. Phys., 58, 1113– 1124.

Oru´s, R., Hernandez-Pajares, M., Juan, J.M., Sanz, J., Garcia Fernandez, M. 2003. **"Validation of the GPS TEC maps with topex data."** Adv. Space Res. 31 (3), 621–627.

Otsuka, Y., Ogawa, T., Saito, A., Tsugawa, T., Fukao, S., and S. Miyazaki. 2002. **"A new technique for mapping of total electron content using GPS network in Japan."** Earth Planets Space, 54, 63–70.

Rabiu, A.B., Mamukuyomi, A.I., Joshua, E.O. 2007. **"Variability of the equatorial ionosphere inferred from geomagnetic field measurements."** Bull. Astr. Soc. India 35, 607–618.

Rastogi, R. G. 1959. **J. Geophys. Res.,** 64, 727.

Rawer, K., Bilitza, D., Ramakrishnan, S. 1978. **International Reference Ionosphere, International Union of Radio Science (URSI),** Brussels, Belgium.

Rawer, K., Bilitza, D., Ramakrishnan, S., Sheikh, M. 1978. **"Intentions and buildup of the International Reference Ionosphere, in: Operational Modeling of the Aerospace Propagation Environment, AGARD."** Conf. Proc. vol. 238, pp. 6.1–6.10.

Rawer, K., Lincoln, J.V., Conkright, R.O. 1981. **"International Reference Ionosphere – IRI 79, World Data Center A for Solar-Terrestrial Physics."** Report UAG-82, Boulder, Colorado.

Richmond, A. D., Ridley, E. C., and Roble, R. G. 1992. **"A magnetosphere thermosphere-ionosphere-electrodynamic general circulation model."** J. Geophys. Res., 103, 17,467.

Rishbeth, H. and Garriott, O.K., 1969. **Introduction to Ionospheric Physics.** Academic Press, New York and London.

Sardon, E., Rius, A., and Zarraoa, N. 1994. **"Estimation of the receiver differential biases and the ionospheric total electron content from Global Positioning System observations."** Radio Sci., 29(3), 577–586.

Schunk, R., L. Scherliess, J. Sojka, D. Thompson, and L. Zhu. 2005. **"Ionospheric weather forecasting on the horizon."** Space Weather, 3, S08007, doi:10.1029/2004SW000138.

Sethi, N.K., Pandey, V.K., Mahajan, K.K. 2001. **"Comparative study of TEC with IRI model for solar minimum period at low latitude."** Adv. Space Res. 27 (1), 45–48.

Seeber, G., 1993. **Satellite Geodesy: Foundations, Methods & Applications**. Walter de Gruyter, Berlin New York, 531.

Stenning, R. J. 1992. **"Modelling the low latitude F-region."** J. Atmos. Terr.Phys., 54(11/12), 1387 – 1412.

Stoer, J and Bulirsch, R. 2002. **Introduction to Numerical Analysis**, Third Edition, Springer.

Titheridge, J. E. 1973. **"The slab thickness of the mid-latitude Ionosphere."** Planet. Space Sci., 1, 1125.

Walker, G. O., Ma, J. H. K., and Golton, E. 1994. **"The equatorial ionospheric anomaly in electron content from solar minimum to solar maximum for South East Asia."** Ann. Geophys., 12, 195– 209.

Warnant, R. 1997. **"Reliability of the TEC computed using GPS measurements - The problem of hardware biases."** Acta Geod. Geophys. Hung., 32(3-4), 451–459.

Woodman, R.F., 1970. **"Vertical velocities and east-west electric fields at the magnetic equator."** J. Geophys. Res. 75, 6249–6259.

Zhang, Y., Wu, F., Kubo, N., and Yasuda, A. 2003. **"TEC measurement by single dual-frequency GPS receiver."** International Symposium on GPS/GNSS, Tokyo, Japan, 15–18 Nov.

APPENDIX I

LIST OF PUBLICATIONS

International journals

1. P. Kenpankho, P. Supnithi, and T. Nagatsuma, "Comparison of Observed TEC values with IRI2007 TEC and IRI-2007 TEC with Optional foF2 Measurement Predictions at An Equatorial Region, Chumphon, Thailand," Journal of Advanced Space Research, vol.52, no.10, Nov. 2013, pp. 1820-1826. DOI: 10.1016/j.asr.2013.07.041 (2011 SJR impact factor = 1.183)
2. P. Kenpankho, P. Supnithi, T. Tsugawa and T. Maruyama, "Variation of Ionospheric slab thickness observations over Chumphon equatorial magnetic latitude station," Earth Planets Space, vol. 63, pp. 359-364, June 2011. (impact factor = 2.921)
3. P. Kenpankho, P. Supnithi, T. Tsugawa and T. Maruyama, "Comparison of GPS TEC measurements with IRI TEC prediction at an equatorial latitude station, Chumphon, Thailand, " Earth Planets Space, vol. 63, pp. 365-370, June 2011. (impact factor = 2.921)

Conference proceedings

1. P. Wongcharoen, P. Kenpankho, P. Supnithi, " The Variation of Critical Frequency of E Layer over Chumphon, Thailand," ICONSpace 2013, Jul.1-3, 2013, Malacca, Malaysia.
2. P. Kenpankho, N. Wichaipanich, P. Supnithi and T. Nagatsuma,"Comparison of IRI-2007 TEC predictions with IRI-2007 TEC with optional foF2 measurements at an equatorial latitude station, Chumphon, Thailand," IRI 2011Workshop, South Africa, Oct 2011.
3. A Mongkolkachit, P. Kenpankho and P. Supnithi," GPS Data Network and Ionospheric Monitoring in Thailand," AOGS 2011, Taipei, Taiwan, Aug. 2011.
4. P. Supnithi, P. Kenpankho, T. Tsugawa and T. Maruyama, "Diurnal and Seasonal Variation of Total Electron Content (TEC) at Chumphon and Bangkok, Thailand," EIWAC 2010,Tokyo, Japan, Nov. 10-15, 2010.

5. P. Kenpankho, K. Watthanasangmechai, P. Supnithi, S. Lerkvaranyu, T. Maruyama, "The Comparison of TEC in Chumpon, Thailand with the IRI Models," AP-RASC 2010, Toyama, Japan, Sept 22-26, 2010.
6. P. Kenpankho, P. Supnithi, T. Tsugawa, and T. Maruyama, "Equatorial magnetic variation of ionospheric slab thickness observations at Chumphon", IRI 2009 Workshop, Kagoshima, Japan, October 2009.
7. P. Kenpankho, K. Watthanasangmechai, P. Supnithi, T. Tsugawa, and T. Maruyama, "Equatorial solar and latitude dependence of TEC", IRI 2009 Workshop, Kagoshima, Japan, October 2009.
8. P. Kenpankho, K. Watthanasangmechai and P. Supnithi, "Solar and Latitude Dependence of TEC inThailand," International Symposium on Antenna and Propagation (ISAP) 2009, Bangkok, Thailand, October 2009.
9. P. Kenpankho, P. Suvannasang and P. Supnithi, "Relationship between Delay Time of GPS Satellites and Total Electron Content at Chumphon Station, Thailand," International Symposium on Space Technology and Science (ISTS 2009), Tsukuba, Japan, July 6-9, 2009.

APPENDIX II

TEC COMPUTATION PROGRAM

```
% Estimate a single receiver bias and TEC computation
% By using GPS-TEC and satellite bias
% Programmed by Prasert Kenpankho

clear all;
clc;
% Define the variables for calculation
h=400000;     % the height of the ionospheric layer 400 km from Ma and Maruyama[2003]
RE=6378137;   % the mean radius of the Earth 6378.137 km  from Schaer[1999]
takenday = [70:71,80:81];
% Input Days for importing files
for filenames = takenday    % Change number of file name
%filenames = 400 ;
% Change GPS Station Here
TECfilenames = ['CPN_' num2str(filenames,'%03d') '0.TEC'];
%#====== Import and read the satellite bias file ========
% Afile = '002.txt';
Satbiasfile = [num2str(filenames,'%03d') '.txt'];
fid = fopen(Satbiasfile);
satbiasdata = textscan(fid, '%f %f','HeaderLines',1);
fclose(fid);
satprndata = satbiasdata{1};
% for testing satprn = satprndata(1,1);
satbias = satbiasdata{2};
```

```
%#===== Import and read GPS-RINEX with STEC data file ====================
format =  '%f %f %f %f %f %f %f %f %f %f %f %f %f %f %f';
fid = fopen(TECfilenames,'r');
files = filenames;
while fid == -1
   files = files + 1;
   TECfilenames = ['CPN_' num2str(files,'%03d') '0.TEC'];
   fid =fopen(TECfilenames,'r');
end
filenames = filenames + (files - filenames);
%names = textscan(fid, format,'HeaderLines',20);
names = textscan(fid,format,'HeaderLines',4); % Start reading at line #5
fclose(fid);

% ==== The original program
%Import and read GPS-TEC file
%    fid = fopen('CPN_0010.TEC');
% names = textscan(fid, '%f %f %f %f %f %f %f %f %f %f %f %f %f %f %f','HeaderLines',4); %
Start reading at line #4%
% fclose(fid);
%###### PROGRAM MUST TO START HERE ##########################
brnum = -9:0.25:2;   % set the assumed range value of br
br =[brnum]*2.853;    %     0.5 ns
brs = size(br);
brsize = brs(1,2);
brcheck = brsize +1;
%========== START finding the receiver bias ======================
% for ppoint = 1:brsize
ppoint = 1;
while ppoint ~= brcheck
% ##########################################################
% Define ymd data field
```

```
yeardata = names{1};
monthdata = names{2};
daydata = names{3};
% Let
year = yeardata(1,1);
month = monthdata(1,1);
day = daydata(1,1);

% Define HMS data field
Hdata = names{4};
Mdata = names{5};
Sdata = names{6};
% Let
hour = Hdata(1,1);
min = Mdata(1,1);
sec = Sdata(1,1);


% Calculate the zenith angle Chi
% Chi=asin((RE*cos elevangle)/RE+h))
Elevation = names{7};
% for testing Elevaangle = Elevation(2,1);

% PRN number field
PRNdata = names{1};
% for testing prnnum = PRNdata(2,1);

% Slant TEC data field
STECdata = names{12};
% VTEC data field
VTECdata = names{13};
% for testing VTEC = VTECdata(2,1);
```

```
% Define the number of PRN
NumofPRN = names{7};

nPRN = size(NumofPRN);
LinenPRN = nPRN(1,1);

Linechk = size(PRNdata);
Linecount = Linechk(1,1);

PRNnread = 1;

% Set the number of satellite bias data
m_max=size(satprndata);
mmax=m_max(1,1);

% ==========Start reading for VTEC calculationn=====================
% (24hrx60min)/15mins = 96
for nstd = 1:96

% ========= Start reading data for time interval 15 minutes ========
% It will be 30 times  ===> ((60secsx15mins)/30secs)= 30 times
   for ndatasat = 1:30

% Check for line end of data
      if PRNnread > Linecount
         PRNnread = Linecount;
      end

      numPRN = NumofPRN(PRNnread,1);
      PRNchk = numPRN+PRNnread;
      st = PRNnread+1;
```

```
% Calculate VTEC with sat bias and receiver bias
    for n = st:PRNchk
      sat(n).prn = PRNdata(n,1);
      sat(n).elevangle = Elevation(n,1);
      sat(n).VTEC = VTECdata(n,1);
      sat(n).STEC = STECdata(n,1);

  % Match satellite prn for using sat bias
      for m = 1:mmax
        if sat(n).prn == satprndata(m,1)
          sat(n).bias = satbias(m,1);
        end
      end %
      for m = 1:mmax %
        if sat(n).bias == 999999.000
          sat(n).bias = 0;
        end
      end

  % VTECadj calculation
      sat(n).Chi = asin((RE*cos(sat(n).elevangle))/(RE+h));
      sat(n).VTECadj = (sat(n).STEC*cos(sat(n).Chi)) - (sat(n).bias*cos(sat(n).Chi))-
(br(1,ppoint)*cos(sat(n).Chi));
      %if sat(n).VTECadj < 0.00
      %   sat(n).VTECadj = 0;
      % end
    end

    PRNnread = PRNchk+1;
  end
```

```
%================== End of VTEC 15 minutes loop ==========================

end
%================== End of VTEC a day loop ================================
   PRNnread1=1;
% Move cell index to array
VTECadj = [];
   VTEC =[];
   STEC =[];
   for i=1:Linecount
     VTECadj = [VTECadj sat(i).VTECadj];
     VTEC = [VTEC sat(i).VTEC];
     STEC = [STEC sat(i).STEC];
   end

   sat(ppoint).VTECbs = VTECadj;
% Read the number of PRN for finding the end line steps

   chkline = size(VTECadj);
   chklinemax = chkline(1,2);

   nnpend = Linecount-chklinemax; % (25973-23166=2807)

   for nn = 1:nnpend

% Check for line end of data
      if PRNnread1 > Linecount
        PRNnread1 = Linecount;
      end

   numPRN1 = NumofPRN(PRNnread1,1);
   PRNchk1 = numPRN1+PRNnread1;
```

```
st1 = PRNnread1+1;

% Calculate VTEC with sat bias and receiver bias
sat(nn).numprn = numPRN1;

PRNnread1 = PRNchk1+1;
end

% Move cell index to cell array for number of PRN
SatnumPRN=[];
for ii=1:nnpend
   SatnumPRN =[SatnumPRN sat(ii).numprn];
end

chkline1 = size(SatnumPRN);
chklinemax1 = chkline1(1,2);

% Find Standard Deviation for each, 15 minutes, interval
pttime= 0;
npp = 1;
npt = 0;
upt = 30;
nssEnd = fix((Linecount-chklinemax)/30);

for nss = 1:nssEnd
   pttime = pttime+sum(SatnumPRN(npp:(npt+upt)))-30;
   if (npt+upt) > chklinemax1
      npp = nssEnd*30;
      xxp = (Linecount-chklinemax)-(nssEnd*30);
      pttime = pttime+sum(SatnumPRN(npp:(npp+xxp)))-30;
   end
sat(nss).VTECstd = std(sat(ppoint).VTECbs(npp:pttime));
```

```
  %  sat(nss).VTECstd = std(VTECadj(npp:pttime));
  nummean = pttime-npp;
  nnck = npp;
  nbb = nummean;
    for nck = 1:nummean
     % sat(nss).TECcheck = sat(ppoint).VTECbs(nnck);
      if sat(ppoint).VTECbs(nnck) == 0  % sat(nss).TECcheck == 0
         nbb = nbb-1;
      end

    end
    if nbb == 0
    sat(nss).VTECday = mean(sat(ppoint).VTECbs(npp:pttime));
    else
    sat(nss).VTECday = sum(sat(ppoint).VTECbs(npp:pttime))/nbb;
    end
  npp = npt+upt;
  npt = npp;

  end

VTECday = [];
  for i=1:nss
    VTECday = [VTECday sat(i).VTECday];
  end

% Find the sum of Standard Deviation for a day
% Check ppoint value

  STD15min = [];
  for iii = 1:nssEnd
    STD15min = [STD15min sat(iii).VTECstd];
```

```
  end
  VTECsumSTD(1,ppoint) = sum(STD15min);

filenames   % For Date checking
ppoint = ppoint+1 % For time checking
end

%##### Find the minimum VTEC sum STD ##########

[sortedX idx] = sort(VTECsumSTD);
minVals = sortedX(1:6);   % For checking the 6 minimum valules
minIdx = idx(1:6);        % For checking the 7 minimum localtion
minTECstd = sortedX(1);
minbr = idx(1);
showbr = br(1,minbr)/2.853;
% days(filenames,1) = filenames;
% CPNRecb(filenames,1) = showbr;
% VTEC15min = VTECday';

%======= Save a receiver bias file ==============
% save Br_('files').txt CPNRecb -ascii;
Rbsfiles = ['BrV_' num2str(filenames,'%03d') '.txt'];
fid = fopen(Rbsfiles, 'w');
fprintf(fid,'%f %f \n',showbr,minTECstd); % Write file must be in Cell array NOT Cell index
fclose(fid);
clear all;
clc;
% Define the variables for calculation
h=400000;     % the height of the ionospheric layer 400 km from Ma and Maruyama[2003]
RE=6378137;   % the mean radius of the Earth 6378.137 km  from Schaer[1999]
end
```

AUTHOR BIOGRAPHY

Full name	Prasert Kenpankho
Birthdate	13 October 1972
Address	596/25 Soi Ladpao 87, Ladpao road, Klongjan, Bangkapi
	Bangkok, Thailand 10240
Education background	
1996	Bachelor's degree in Telecommunication Engineering
	King Mongkut's Institute of Technology Ladkrabang, Thailand
2001	Master's degree in Industrial Technology
	Utah State University, The United States of America
2003	Master's degree in Electrical Engineering
	University of Massachusetts, The United States of America
Specific expertise	1. GPS devised TEC
	2. Ionosphere and space
	3. Satellite orbit design
Work experience	
1997 - 1998	a coordinator for satellite redundancy system at Samart Comtech
1998 – 2001	a research assistant at Utah State University
2001 – 2003	a research assistant at University of Massachusetts
1998 – present	an assistant professor at Department of Engineering Education,
	King Mongkut's Institute of Technology Ladkrabang